Exploration of the microbiome-derived factors impacting human Langerhans cell function

Doctoral thesis

to obtain a doctorate (MD/PhD)

from the Faculty of Medicine

of the University of Bonn

Yi Pan

from Hubei, China

2023

Written with authorization of

the Faculty of Medicine of the University of Bonn

First reviewer: Prof. Dr. Dr. Prof. h. c. Thomas Bieber

Second reviewer: Prof. Dr. Waldemar Kolanus

Day of oral examination: 21.04.2023

From the Department of Dermatology and Allergy and Christine Kühne-Center for Allergy Research and Education, University Hospital Bonn

Director: Prof. Thomas Bieber, MD, PhD, MDRA

Table of Contents

List of abbreviations

7AAD	7-aminoactinomycin D
AHR	Aryl hydrocarbon receptor
ANOVA	Analysis of Variance
-APC	-Allophycocyanin
APC	Antigen presenting cell
BSA	Bovine serum albumin
CCL	C-C Motif Chemokine Ligand
CCR	Chemokine receptor
CD	Cluster of differentiation
cDNA	Complementary DNA
DC	Dendritic cell
DMSO	Dimethyl sulfoxide
DMSZ	Deutsche Sammlung von Mikroorganismen und Zellkulturen
DNA	Deoxyribonucleic acid
dNTP	Deoxynucleoside triphosphate
DTT	Dithiothreitol
e.g.	*Exempli gratia*, for example
ELISA	Enzyme-linked immunosorbent assay
et al.	*Et alii*, and others
FACS	Fluorescence activated cell sorting
FBS	Fetal bovine serum
FITC	Fluorescein isothiocyanate
FLT3L	Fms like tyrosine kinase 3 ligand
Gam	Goat anti-mouse
GM-CSF	Granulocyte-macrophage colony-stimulating factor
h	Hours
HLA	Human leukocyte antigen
HSC-LCs	$CD34^+$ hematopoietic stem cell derived Langerhans cells
IFN-γ	Interferon γ
Ig	Immunoglobulin

IL	Interleukin
ITAM	Immunoreceptor tyrosine-based activation motif
L	Liter
LC	Langerhans cell
LPS	Lipopolysaccharides
M	Mole
mAb	Monoclonal antibody
MACS	Magnetic activated cell sorter
Max	Maximum
MFI	Mean fluorescence intensity
MHC	Major histocompatibility complex
min	minutes
mRNA	Messenger RNA
ns	Not significant
P2C	Pam_2Cys-SKKKK
P3C	Pam_3Cys-SKKKK
PBMC	Peripheral blood mononuclear cells
PBS	Phosphate-buffered saline
PCR	Polymerase chain reaction
PE	Phycoerythrin
PerCP	Peridinin-chlorophyll-protein
RNA	Ribonucleic acid
RT	Room temperature
S.a.	*Staphylococcus aureus*
S.e.	*Staphylococcus epidermidis*
SCF	Stem cell factor
SD	Standard deviation
sec	seconds
TGFβ	Transforming growth factor beta
Th	T helper cell
TNFα	Tumor necrosis factor α
T_{reg}	Regulatory T cell

1. Introduction

1.1 Atopic dermatitis (AD)

Atopic dermatitis (AD) is the most common chronic inflammatory skin disease worldwide. Approximately 80 % of cases typically begin in infancy or childhood, with the remainder developing in adulthood. While the point prevalence in children varies from 2.7 % to 20.1 % in different countries, it ranges from 2.1 % to 4.9 % in adults (Bieber 2022). AD causes not only a clinical, but also a humanistic economic burden (Luger et al., 2022; Weil et al., 2022). Gender, education, and preventive measures implemented are important cost determinants in AD, the main cost driver being treatment with systemic therapies such as biologics or JAK inhibitors. However, incremental patient-relevant benefits of high-cost therapy are reflected by the significantly better clinical outcomes in the group treated with biologics (Mohr et al., 2022).

With increasing concern about environmental exposures as risk factors in AD, studies have shown that exposure to lower temperatures, lower humidity, and higher levels of air pollutants is significantly associated with an increased risk of developing AD. These effects were more pronounced in children younger than 7 years and in women (Ye et al., 2022). Opioidergic signaling might also be a neglected but potentially important player in AD (Adam et al., 2022). While suspected, maternal serum levels of polychlorinated biphenyls (PCBs) showed no association with asthma, allergic rhinitis, or AD (Berlin et al., 2022).

Clinical manifestations are characterized by sensitive and dry skin, localized or disseminated eczematous lesions, usually accompanied by severe pruritus (Silverberg 2017). AD belongs to the spectrum of atopic diseases, which also includes food allergies, allergic asthma and allergic rhinoconjunctivitis, cardiovascular and neuropsychiatric disorders, which are relevant comorbidities (Bieber 2008, 2017, 2022). Patients with AD have a significantly increased risk alopecia areata but not other autoimmune diseases (de Lusignan et al., 2022). AD is a very heterogeneous disease that can be divided into different phenotypes and clinical presentations defined by ethnicity, disease onset,

disease severity, chronic vs. acute, IgE level, pediatric vs. adult, and inflammatory signature (Hülpüsch et al., 2021).

Eczema Area and Severity Index (EASI), SCORing Atopic Dermatitis (SCORAD), Patient Oriented Eczema Measure (POEM), Dermatology Life Quality Index (DLQI), Numeric Rating Scale (NRS), and the validated Investigator Global Assessment for Atopic Dermatitis (vIGA-AD™) are standardized assessment tools for use in clinical trials and registries (Simpson et al., 2022; Thyssen et al., 2020). A recently reported noninvasive method that comprehensively analyses RNA present in sebum using a next-generation sequencing may be a useful tool for understanding the molecular pathology of pediatric AD (Shima et al., 2022).

The pathophysiological mechanisms of AD are very complicated and multifactorial. Among them are genetic defects of the epidermal barrier, dysregulations of the innate and adaptive immune systems and the role of microbes (Magnifico et al., 2020; Yoshida et al., 2022). Biomarkers such as CCL17/TARC, IgE, eosinophils, CCL22/MDC, CCL26/Eotaxin-3, CCL27/CTACK, CCL18/PARC, IL-13 and IL-22 (Renert-Yuval et al., 2021) are correlating with the severity of the disease. Lesional AD skin contains significantly higher levels of mast cells, dendritic cells, and T cells (Peng et al., 2022; Peng et al., 2020), eosinophils and macrophages (Koh et al., 2022). AD is associated with a Th2-response with high expression of IL-13 and its receptors in the skin, as well as IL-17 and IL-22 in more chronic courses, and the involvement of IL-31 in triggering itch (Ring 2022). The random-effects model of the meta-analysis showed that patients with AD had an increased proportion of Th22 cells, Th17 cells, and IL-17, whereas Tregs in peripheral blood were found to be reduced (Zhang et al., 2022b).

1.2 Human skin microbiome

Human skin consists of a physical, chemical, immunological and neurological barrier, but the microbiological barrier has also been recently highlighted. Compared to the microbiomes seen in the human intestine and respiratory tract, the skin harbors the most diverse commensal communities in the body, with more than 1000 different bacterial species from 19 different phyla (Paller et al., 2019). It is estimated that human skin is inhabited by about one million bacteria/cm^2. Molecular approaches have shown that in healthy individuals, the most common skin bacterial phyla are *Actinobacteria, Firmicutes, Proteobacteria* and *Bacteroidetes*, which are arranged in different proportions depending on the skin areas and layers. At the level of genus, the cutaneous microbiota is mainly formed by *Staphylococcus, Propionibacterium, Corynebacterium,* and *Streptococcus*. In the sebaceous sites dominate *Staphylococci* and *Propionibacteria*, while *Corynebacteria* mainly colonize moist sites such as the antecubital fossa and interdigital spaces (Di Domenico et al., 2019). See Figure 1.1.

This microbiome can vary from person to person and in different anatomical sites of the skin throughout an individual´s lifespan. Human skin provides several different niches in which microbes are exposed to variable ecological pressures such as UV exposure, humidity, temperature, pH, and composition of antimicrobial peptides and lipids secreted by other microbes through interactions or metabolism. In addition, skin structures such as hair follicles, sebaceous glands, eccrine and apocrine glands form discrete niches that harbor unique microbiota (Balato et al., 2019). Temporal stability of the skin microbiome in healthy individuals suggests strong selective control of the microbial constituents (Koh et al., 2022).

Human microbes interact with different anatomical niches and alter the state of immune activation, the status of the skin barrier, microbe-host and microbe-microbe interactions, creating a continuous interplay that is important for the establishment and maintenance of host homeostasis. The skin microbiota plays a key role in health and disease by maintaining the immune homeostasis and preventing the growth of pathogenic bacteria.

Alterations in the composition of the microbiome can lead to a shift in immune system reactivity and subsequently the development of inflammatory diseases.

It is known that commensal bacteria inhibit pathogen colonization. However, due to complex host–microbe and microbe–microbe interactions, it is difficult to understand in detail the mechanisms involved in the inhibition of colonization (Iwase et al., 2010). Apart from directly competing for host nutrients and adhesion sites, commensal bacteria produce specific metabolites and antimicrobial peptides to inhibit pathogenic colonization. The realization that commensal microorganisms are not simple “passengers” onto our bodies, but instead play key roles in our physiology, including adaptive immune responses and metabolism, as well as in disease, is one of the most exciting scientific advances in recent years.

Skin commensal-related factors play a key role in regulating the homeostasis of skin microbiota and may directly affect the ability of *Staphylococcus aureus* (*S.a.)* to adhere to and proliferate on skin epithelia. The interaction of immune cells with commensal bacteria is crucial for the maturation and stability of the skin immune system (Folster-Holst 2022). A diverse community of skin commensals is therefore important to train the immune system and allow the host to develop tolerance and respond appropriately to environmental stimuli (Koh et al., 2022)

Previous studies of microbial communities on humans relied on culture-based techniques and thus were quite limited. The advent of next-generation sequencing technologies has revolutionized methods for characterizing the human microbiome and introduced the concept of “precision manipulation of the microbiome”.

1.2.1 The role of skin microbiome in AD

Microbes coexist with humans and play an important role in regulating health and disease. The skin microbiome is an interactive ecosystem, including pathogenic and commensal bacteria, fungi and viruses. All microbes in the body fall somewhere on the spectrum of potentially pathogenic (aggressive) and mutualistic (passive), where some microbes are generally beneficial to the host, but can become invasive under certain circumstances, while some microbes can be primarily virulent (Koh et al., 2022).

The skin of AD patients is characterized by microbial dysbiosis, with a reduction in microbial diversity and an overrepresentation of pathogenic *S.a.*, especially in lesional skin sites (Koh et al., 2022)(see Figure 1.1). Dysbiosis is one of the most important features determining disease severity and propensity to relapse. The complexity of the AD skin microbiome includes species, such as *Staphylococcus, Streptococcus spp*, *Stenotrophomonas*, *Corynebacterium spp, Cutibacterium*, *Malassezia*, *M. globose, Roseomonas* strains (Flores et al., 2014; Koh et al., 2022). While they represent only a minority of the bacterial communities in the skin of healthy individuals, in untreated AD flares the predominant species are *S.a.* and *S.e.* In healthy human skin, the acidic pH limits the growth of harmful skin bacteria such as *S.a.* and promotes the growth of the commensal *S.e*.

Possible mechanisms underlying microbial dysbiosis in AD are skin barrier dysfunction and inflammation. Mutations in tight junctions, epidermal differentiation complex proteins and endogenous proteases have all been reported to aggravate the immune dysregulation in AD (Blicharz et al., 2021). Skin barrier disruption can be caused by filaggrin mutations or an elevated skin pH. This facilitates penetration of allergens and irritants, which can lead to food allergy, allergic rhinitis, and/or allergic asthma (Hülpüsch et al., 2021). Interestingly, AD microenvironment predisposed to certain microorganisms corresponds to host gene expression, which in turn is influenced by the microbiota (Bay et al., 2021). Loss of anaerobic bacteria such as *Lactobacillus spp.* and *Finegoldia spp.* shifts AD microbiota toward more aerobic metabolism. These microorganisms are involved in

stimulating the antimicrobial peptide (AMP) response in keratinocytes and are decreased in filaggrin mutant skin (Fyhrquist et al., 2019). Therefore, a deficiency of anaerobic microorganisms may weaken the vital skin barrier functions and favor potential pathogens. Changes of the microbiota profoundly affect the changes of filaggrin deficiency (Clausen et al., 2018) and epidermal lipid composition and vice versa (Baurecht et al., 2018).

Disruption of the epidermal barrier leads to increased permeability of the epidermis, pathological inflammation in the skin and percutaneous sensitization to allergens (Tsakok et al., 2019). Conversely, Inflammation aggravates skin barrier dysfunction. One part of all inflammatory reactions is migration of immune cells. Whether antigen presenting cells leave the tissue towards the next draining lymph node or effector cells arrive at the site of inflammation, all immune cells need to move through tissues. In order to accomplish this, immune cells secrete a wide variety of proteases to digest extracellular matrix or cell-cell-adhesion molecules. In this way, the simple fact of massed migration of immune cells can already damage tissues (Verollet et al., 2011). Furthermore, several immune cells actively secrete proteases as chemical weapons against pathogens, causing collateral damage to the surrounding tissue in the process (Jung et al., 2022). One elegant study investigated the skin inflammation in EGFR-delta-EP mice (Klufa et al., 2019). These mice develop severe skin inflammation at p5 and most of them do not survive until adulthood. The onset of this inflammation coincides with the hair eruption through the epidermis. Interestingly, the same mice under germ free conditions do not show any skin inflammation. Klufa et. al. could demonstrate that hair eruption opens the epidermal barrier, which in WT mice closes again quickly. In EGFR-delta-EP mice, reconstitution of the barrier is impaired, allowing bacterial infiltration into the skin and leading to skin inflammation. This leads to a vicious circle: the barrier is disturbed, bacteria invade, the skin is inflamed. Inflammation leads to further disruption of the barrier; further disruption of the barrier leads to more bacteria entering. The skin inflammation and lethality of EGFR-delta-EP mice can be completely rescued with high doses of broad-spectrum antibiotics, demonstrating that the source of the inflammation is the opportunistic skin microbiome.

Formation of biofilm is another mechanism involved in microbial dysbiosis in AD. Biofilm is the dominant growth form of the skin microbiota that promotes adhesion and

persistence in the cutaneous microenvironment, contributing to epidermal barrier function and local immunomodulation. The local immunological microenvironment in turn plays a role in shaping the composition of skin microbiota. Chronic production of inflammatory cytokines in the skin of AD supports overgrowth of the *S.a.* biofilm at the expense of other microbial commensals, thereby further de-regulating the composition of the skin microbiome. The close relationship between the host and the skin microbial biofilm has profound implications for human health and makes skin microbiota an attractive target for therapeutic treatment of various skin diseases (Bay et al., 2021; Blicharz et al., 2021; Di Domenico et al., 2019; Iwase et al., 2010; Vandecandelaere et al., 2014). Gonzalez et al found that strain-level variations in *Staphylococcal* isolates determine interactions between *S.e.* and *S.a.* and that the balance between these two species and their propensity to form biofilms has important implications for AD. Their group reported that the skin of children with AD contains *Staphylococcal* biofilms. *S.a.* strains with higher relative biofilm propensity (compared with *S.e.* from the same patient) are associated with increased AD severity and increased lesional and non-lesional transepidermal water loss. (Gonzalez et al., 2021).

Different *Staphylococcus* species may play distinct roles in AD development; for example, *S.e.* and *S. hominis*, which are predominantly found on healthy human skin, contribute to skin homeostasis (Nakatsuji et al., 2018). Specially, selected *Staphylococcus* strains can promote cutaneous antimicrobial activity. Other strains however can trigger inflammation in AD. Patients with milder disease showed higher amounts of *S.e.* in flares while patients with severe disease were colonized by dominant clonal *S.a.* strains (Byrd et al., 2017).

Microbial diversity during AD flares changed with the presence of recent AD treatments, with even intermittent treatment linked to greater bacterial diversity than no current treatment. In AD treatments, diversification of skin bacteria precedes amelioration of the disease (Kong et al., 2012). One attempt at treating AD is the use of antibiotics to inhibit *S.a*. However, their efficacy on skin is limited and has disadvantages of killing beneficial strains and breaking mutualistic interactions between skin and microbial communities (Nakatsuji et al., 2019).

Natural AMP are not only produced by the skin itself but also by microbes. Patients suffering from AD showed reduced expression of specific AMPs, indicating an increased susceptibility to pathogenic microbes such as *S.a.* (Nakatsuji et al., 2017). They also showed the reduced expression of dermcidin (Tokura et al., 2022). Alteration of the commensal microbiota is accompanied by decreased production of antimicrobial proteins, which is normally induced by Coagulase-negative *Staphylococcus* (CoNS), such as *S.e.*. The AD-typical strains were characterized by a reduced or complete lack of ability to synthesize potent AMPs specifically target *S.a.* (Nakatsuji et al., 2017).

A recent study showed that a microbial index of skin health (MiSH) based on 25 bacterial genera can diagnose AD with 83 to ∼95% accuracy. MiSH is expected to contribute, in conjunction with SCORAD, to AD diagnosis and treatment in the clinical setting, where the state of skin microbiota is also taken into consideration (Sun et al., 2019).

Neutrophils, γδ T cells, DC, keratinocytes and adipocytes are all involved in the host immune response to skin microbes (Koh et al., 2022). Bacteria shape essential biological functions such as the development of a tolerogenic immune response to commensals. Compared to healthy skin, non-lesional AD skin showed decreased hydration, impaired lipid synthesis, altered expression of differentiation markers and an increased presence of inflammatory T cells. Non-lesional AD skin expressed less immune-mediated inflammation compared with lesional skin.

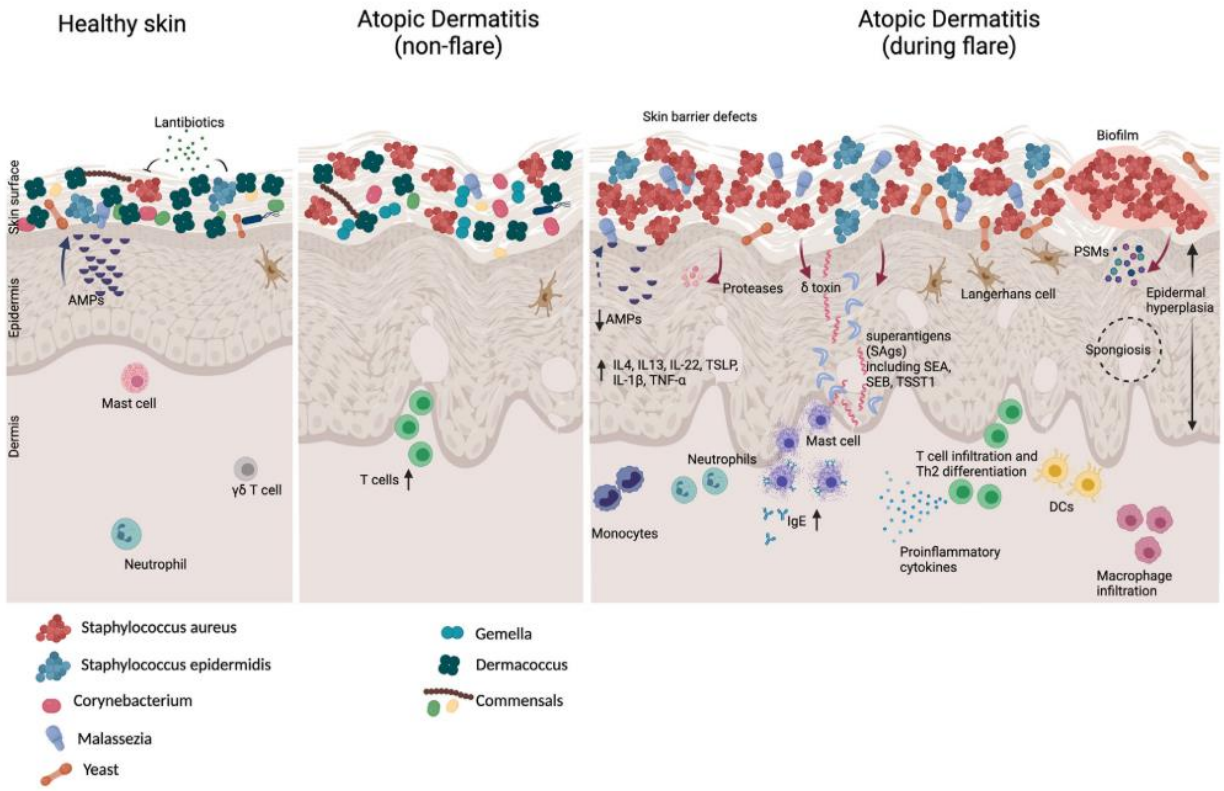

Figure 1.1 Crosstalk between skin and microbiome in healthy and AD conditions. Adapted from (Koh et al., 2022). Commensals on the skin interact with the host to establish a functional immune response and prevent the overgrowth of pathogenic microbes. On healthy skin (left), there is a high microbial diversity, which includes *Dermacoccus* and *Corynebacterium* as well as other commensals. Secretion of AMPs and production of lantibiotics by commensals shape the microbial community on healthy skin to prevent colonization of pathogens like *S.a*. AD skin in a non-flare state (middle) displays microbial dysbiosis with a reduction of *Dermacoccus* and an increased abundance of *Streptococcus* and *Gemella* species. The skin of AD patients during flares (right) is characterized by an overgrowth of pathogenic microbes such as *S.a.* and reduced microbial diversity. Biofilm production by *S.a.* promotes its colonization and drives pathogenesis. Commensals including *Dermacoccus* are depleted.

1.2.2 Staphylococcus aureus

Staphylococcus aureus (S.a.) is a gram-positive, round-shaped bacterium that belongs to the *Bacillota*. It is a common member of the body's microbiota and is often found in the upper respiratory tract and on the skin. It is often positive for catalase and nitrate reduction and is a facultative anaerobe that can grow without oxygen. Although *S.a.* normally acts as a commensal of the human microbiota, it can also become an opportunistic pathogen.

Already in 1974, *S.a.* was described as the dominant organism not only in the lesions but also in nearby clinically normal skin in AD patients (Leyden et al., 1974). Meanwhile, *S.a.* has also been found in active cutaneous lupus erythematosus (SLE) lesions (Sirobhushanam et al., 2020).

Adult AD patients colonized with *S.a.* have more severe disease, type 2 immune deviation, allergen sensitization, barrier disruption, and LDH level elevation than noncolonized patients with AD (Simpson et al., 2018). Interestingly, *S.a.* colonization precedes clinical onset of AD (Meylan et al., 2017). *S.a.* occurs in 70% of lesional versus 39% of nonlesional or healthy skin (Geoghegan et al., 2018). 50% of *S.a.* colonizing AD skin is toxin producing. With regard to AD heterogeneity, skin colonization of *S.a.* is more frequently observed in extrinsic AD than in intrinsic AD. Not only the presence of *S.a.* but also its capability to produce biofilm and toxins is associated with AD severity (Di Domenico et al., 2019). While no single virulence factor correlates with AD prevalence or severity, AD exacerbations correlate with different combinations of virulence factors in certain lineages of *S.a.* (called clonal complexes) (Gough et al., 2022).

Classical *S.a.*-eradicating treatments included topical antibiotic therapy with fusidic acid, sulmycin and mupirocin, antiseptics such as chlorhexidine, potassium permanganate ($KMnO_4$), and gentian violet, acid electrolyte water spraying and balneotherapy with acidic hot spring water. Such treatments led to the comprehensive eradication of both *S.a.* and commensal bacteria. However, *S.a.* replicates and recolonizes AD skin more quickly than commensals, which leads to microenvironment even more dominated by *S.a.* than before, exacerbating AD (Hwang et al., 2020).

The first step in colonization and infection is bacterial adhesion to the cornified envelope of corneocytes in the outermost layer of the epidermis, the stratum corneum. To facilitate adhesion, *S.a.* expresses clumping factor B, which binds ligands at the corneocyte surface (Feuillie et al., 2018; Fleury et al., 2017; Geoghegan et al., 2018). Decreased levels of natural moisturizing factor (NMF) in the stratum corneum have been shown to be associated with more severe AD symptoms. *S.a.* isolated from AD skin bind much more strongly to corneocytes when the NMF level is reduced. *S.a.* exploits the reduced expression of AMPs, the decreased presence of filaggrin filaments, the resulting structurally altered corneocytes, and an IL-4/IL-13-induced increased expression of fibronectin and fibrinogen for enhanced adhesion to corneocytes (Folster-Holst 2022).

The next step is our immune system reaction to the infection. *S.a.* colonization modulates innate and adaptive immune responses, predisposing the organism to allergic sensitization and disrupting immune tolerance. *S.a.* proteins include proteases, toxins, superantigens and other virulence factors (see table 1.1). Protein A induces human Tregs, leads to the release of soluble Treg-inducing factors, and might be relevant for the establishment of colonization (Uebele et al., 2020). δ-toxin stimulates mast cells, α-toxin damages keratinocytes, phenol-soluble modulins stimulate cytokine release by keratinocytes, protein A triggers inflammatory responses from keratinocytes, superantigens trigger B cell expansion and cytokine release, and proinflammatory lipoproteins. Bacterial proteases contribute to disruption of the epidermal barrier. Serine protease-like proteins initiate a type 2 response and contribute to the IL-33/ST2 signaling axis in allergic reactions induced by bacterial allergens (Krysko et al., 2019).

Loss of the epidermal barrier function in AD can alter the balance of *S.a.* penetration into the dermis, and dermal dysbiosis leads to increased inflammatory cytokines and exacerbation of the disease (Nakatsuji et al., 2016). *S.a.*-AD accumulates in the lysosome of keratinocytes with the help of bacterial cell wall proteins and induces IL-1α via TLR9 (Moriwaki et al., 2019). Another study demonstrated that normal human skin microbiome can contribute to epithelial barrier homeostasis by using quorum sensing to inhibit toxin production of *S.a.* (Williams et al., 2019).

Table 1.1 *S.a.* proteins that contribute to AD. Adapted from (Geoghegan et al., 2018)

S. aureus proteins	Possible role in AD
Clumping factor B	Adhesion to corneocytes in stratum corneum via loricrin or other ligands
Fibronectin-binding proteins	Adhesion to fibronectin that is present at high levels in the upper strata of epidermis and stratum corneum of AD skin
Protein A	Proinflammatory. Binds to TNFR-1 on keratinocytes
Lipoproteins	Proinflammatory. Activate TLR-2 on keratinocytes
α-Toxin	Membrane damage/lysis of keratinocytes
δ-Toxin	Mast cell degranulation. Synergy with IgE. Allergic skin inflammation
Phenol-soluble modulins	Trigger proinflammatory responses associated with AD in keratinocytes at sublytic concentrations
Enterotoxins and TSST-1	Excessive T cell cytokine production and toxicity. Allergens. Enterotoxins might trigger mast cell degranulation directly
Staphopain Aureolysin	Inactivation of antimicrobial peptides
V8 serine protease	Epidermal barrier dysfunction in hairless mice
Serine protease-like proteins	Potent allergens in idiopathic asthma following *S. aureus* colonization. Similar role in AD?

1.2.3 *Staphylococcus epidermidis*

Like *S.a.*, *Staphylococcus epidermidis* (*S.e.*) is a gram-positive, facultative anaerobe bacterium. As a commensal bacterium, it is found ubiquitously on human skin and mucous membranes of the respiratory tract and intestines.

Coagulase-negative *Staphylococci* (CoNS) such as *S.e.*, *S. hominis*, and *S. lugdunensis* are commensals and are important players in immunity of healthy skin (Koh et al., 2022). Specially *S.e.* has been reported to modulate the host immune system and to shape the development of the skin and nasal microbiome by preventing host colonization by more virulent bacteria, fungi and viruses.

Biofilm formation is considered a central factor in the homeostatic control of CoNS in the skin. It allows colonization and persistence on almost all body surfaces, especially moist areas such as the nostrils, axillae, inguinal, and perineal areas. CoNS successfully adapt to their life as microbial biofilm communities colonizing the skin surface by activating numerous quorum-sensing genes encoding adhesion, biofilm production and AMP secretion.

S.e. and *S. hominis* are the predominant CoNS species that colonize normal human skin. They have the potential to suppress inflammation, stimulate the adaptive and innate immune system, and produce molecules with antimicrobial activity against infectious pathogens. Within the skin microbiota, CoNS are the major colonizers competing with *S.a.* for the same ecological niche. Changes in the homeostasis of the skin microbiota associated with a reduction in beneficial commensal microbes significantly increase the risk of *S.a.* colonization (Di Domenico et al., 2019).

S.a. and *S.e.* are the most abundant bacteria found on the skin of patients with AD. The harmful *S.a.* is known to aggravate AD, while *S.e.* is considered a beneficial commensal organism. On the other hand, the excessive amount of *S.e.* found in some atopic patients can act similarly to *S.a.* and damage the skin by expressing a cysteine protease (Cau et al., 2020). Recent investigations suggest an association with flares and AD severity (Kong

et al., 2012), which may be due to S100A8/A9-dependent changes of the skin barrier proteins (Kim et al., 2019). However, it is still controversial whether *S.e.* is pathogenic or beneficial in AD. The fundamental mechanisms underlying immune-commensal crosstalk are only beginning to unfold (Paller et al., 2019).

The neonatal period is a time of active adaptive immunosuppression when Tregs are abundant in neonatal skin and peripheral tissue. A specialized subset of Tregs induces tolerance to *S.e.* colonization during neonatal skin development, but not in adulthood. *S.e.* triggers specific T-cell responses that are different from the immune response to pathogens and thus influence immunomodulatory and barrier-stabilizing processes (Linehan et al., 2018). Leech et al. demonstrated an early childhood capacity to distinguish between commensal and pathogenic skin bacteria that preferentially promotes the accumulation of commensal specific Tregs and immune tolerance (Leech et al., 2019). It inhibits colonization by pathogenic bacteria, protects the growth of resident bacteria and induces immune tolerance by Tregs (Scharschmidt 2017). One example is the use of *S.e.* by DCs to calibrate the skin´s immunity (Naik et al., 2015).

S.e. has been found to be the most common producer of antimicrobials (Janek et al., 2016), including high levels of extracellular serine proteases that prevent adhesion of *S.a.* to the epithelial surface (Iwase et al., 2010). *S.e.* can also produce a mixture of serine, cysteine, and metalloproteases that specifically inhibit and destroy *S.a* biofilm (Nguyen et al., 2017; Vandecandelaere et al., 2014). It was first postulated that *S.e.* supports the production of vitamin D in the host through basal activation of TLR2. In addition, *S.e.* induces host ceramides through the production of sphingomyelinase and directly inhibits *S.a.* growth and colonization through the induction of host antimicrobial peptides such as cathelicidin, the production of biofilm inhibitory serine proteases, and the production of autoinducing peptides that disrupt quorum sensing (Gough et al., 2022). Glycerol fermentation of *S.e.* resulted in the production of butyric acid and effectively inhibited the growth of a *S.a.* strain isolated from skin lesions of patients with AD (Traisaeng et al., 2019). Known Phenol-soluble modulins (PSMs) produced by *S.e.*, which are thought to have a number of functions, including biofilm formation and spread, evasion of host immunity, and interspecies competition (Joubert et al., 2022).

1.3 Human epidermal Langerhans cells (LCs)

In 1868, Paul Langerhans discovered a dendrite-shaped cell in the human epidermis. Based on their alternating number of dendrites, he assumed that these cells were cells of the nervous system (Langerhans 1868). Later LCs were definitively recognized as immune cells, specifically as a member of the dendritic cell (DC) system (Schuler et al., 1985; Steinman et al., 1973).

LCs are unique among other DCs in their distribution, phenotype, ontogeny, and function. Human LCs are found in the basal or suprabasal layer of the epidermis, extending their dendrites through tight junctions toward the stratum corneum to recognize antigens also on the skin surface. LCs can also be found in various mucous membranes of the body such as the nasal, oral, and cervical mucosa, in other epithelial linings such as the foreskin, tonsils, tongue, upper respiratory tract, or intestine (Allam et al., 2006; Iijima et al., 2008). In addition, a considerable number of LCs have been found in the skin draining lymph nodes but not in the mesenteric nodes (Stoitzner et al., 2003). In steady-state, LCs account for 2-5% of the epidermal cells in human adults and 5–7% in mouse skin, making them by far the most abundant population of immune cells in healthy human skin.

One hallmark of LCs is the expression of Birbeck granules, tennis-racket-shaped organelles composed of superimposed and zippered membranes (Birbeck et al., 1961). The induction of Birbeck granules is a consequence of the antigen-capturing function of Langerin (CD207), which allows for transduction into these organelles and provides access to a nonclassical antigen-processing pathway (Valladeau et al., 2000). LCs were mainly recognized on the basis of their expression of human leukocyte antigen (HLA)-DR, CD1a and CD207 in humans or the major histocompatibility complex class II (MHC-II) in mice (Romani et al., 2010). Notably, human and murine LCs show several key differences which should be kept in mind when trying to apply research data from mouse models to the human system.

1.3.1 LCs phenotype and heterogeneity

Epidermal residency of LCs is maintained by their expression of various adhesion molecules (Borek et al., 2020; Clausen et al., 2020), e.g., E-cadherin ($CD324^+$), EpCAM (Trop1), Trop2 (TACSTD2), Axl receptor tyrosine kinase, and tight junction proteins such as claudin, occluding, and zonula occludens-1 (ZO-1) (Koch et al., 2006; Kohl et al., 2004; Kohl et al., 2007).

LCs are characterized by a unique set of surface markers that allow their clear distinction from other DCs. They express high levels of CD207 and CD1a (de Jong et al., 2021). In contrast to mouse LCs, human LCs express low levels of CD11c and no F4/80, but high levels of CD1a and CD1c, two MHCI-related molecules involved in lipid antigen presentation (Kashem et al., 2017). Human and mouse LCs express SIRPα (CD172α), CD11b and CX3CR1, which is also expressed by most type 2 classical DCs (Deckers et al., 2018). Human epidermal LCs also express CD69 and indoleamine 2,3-dioxygenase (IDO) (Bieber et al., 1992b; von Bubnoff et al., 2004).

In inflammatory skin lesions, LCs express FcεR1 (Bieber et al., 1992a; Bieber et al., 1992c). $FceR1^+$LC is controlled by the TGF-β1 concentration in the microenvironment and may be particularly important in the context of atopic disease (Allam et al., 2004). In normal human epidermal LCs, expression of the low affinity receptor for IgE (FcεR2/CD23) can be induced by addition of recombinant IL-4 and IFN-γ (Bieber et al., 1989b).

LCs can be generated *in vitro* and are phenotypically similar to LCs in AD skin lesions *in vivo* (Novak et al., 2004). However, several protocols exist to generate LCs *in vitro*, which all generate slightly different phenotypes. Furthermore, LCs generated from stem cells or from monocytes are quite different. Several studies have already shown detailed phenotypes in terms of antigen recognition, expression of interleukins and their receptors, signaling molecules, CD antigens, chemokines and receptors, maturation/presentation, adhesion, etc. This data is vital for the selection of an appropriate model for *in vitro* testing

and support the development of DC subsets-based immunotherapy (Alcantara-Hernandez et al., 2017; Collin et al., 2018; Lundberg et al., 2013; Otsuka et al., 2018).

The heterogeneity of LCs has long been investigated in relation to other subsets of skin DCs in mice and human. Liu et al. (2021) have identified four subpopulations of primary and HSC-derived LCs in human that differ phenotypically and functionally and require distinct developmental regulations. They identified two steady-state (LC1 and LC2) and two activated LC subsets, *i.e.,* activated LCs (aLC) (CD83, $CCR7^{lo}$) and migratory LCs (migLC) ($CCR7^{hi}$) in human skin epidermis and in LCs derived from $CD34^{+}$ hemopoietic stem cells (HSC-LCs) by utilizing single-cell RNA sequencing and mass cytominetry. LC1 ($CD207^{hi}$, CD1a) were characterized as classical LCs, mainly associated with innate immunity and antigen processing. LC2 ($CD207^{lo}$, CD1c, CD1b) resembled monocytes or myeloid DCs and were involved in immune responses and leukocyte activation. LC1 remained stable under inflammatory microenvironment, whereas LC2 tended to be activated and showed increased expression of immunosuppressive molecules (Liu et al., 2021). The phenotypical and functional heterogeneity of LCs may provide an explanation for the controversial roles of LCs in skin inflammatory diseases.

1.3.2 LCs ontogeny and homeostasis

LCs are a self-renewing, bone-marrow-independent population of embryonically derived macrophages (Anderson et al., 2021; Hoeffel et al., 2012). Lineage tracing studies in mice have shown that LCs express both Zbtb46 and Mafb, giving them a dual identity of DCs and macrophage (Wu et al., 2016). Interestingly, LCs have thus recently been described as ‘‘macrophage in dendritic cell clothing’’ (Doebel et al., 2017). Patients with GATA2 or IRF8 mutation have a normal number of LCs, showing that epidermal LCs development differ from pDCs and cDCs (Collin et al., 2011).

During a human´s life, the LC network faces several different processes of development. First, the LC network is established in the epidermis by populating the pre-natal skin with monocyte-derived precursors, which differentiate to LCs after birth. Second, despite constant low-grade activation and emigration of LCs, the LC network needs to be maintained at a stable density in the healthy adult epidermis. Third, in case of inflammation, the LCs leave the epidermis to migrate towards the draining lymph nodes. The same applies to dermal langerin^{+} cells as well (Romani et al., 2010). Most DCs are ablated by UV irradiation and can be reconstituted from donor bone marrow. LCs, on the other hand, are resistant to radiation, and are only replenished from bone marrow under highly inflammatory conditions (Kaplan 2010a, b, 2017; Kaplan et al., 2005; Kaplan et al., 2008).

In a steady-state, LCs are long-lived cells that can self-renew. LCs derived from the donor are still present in the skin of patient allografts over a period of 4.5 years (Kanitakis et al., 2004). LCs have an estimated half-life of 2 months and exhibit a slow proliferation rate under homeostatic conditions to replace dying and migrating cells. In this respect, LCs resemble tissue-resident macrophages rather than classical DCs, which are derived from bone-marrow precursors and depend on circulating progenitors to retain their high turnover rate (Deckers et al., 2018).

The murine LC network arises from fetal liver and yolk sack precursors early during embryogenesis and shares its origin with macrophages, microglia and Kupffer cells (Hoeffel et al., 2012). In the first described DC network in the epidermis of the human

prenatal skin study, $CD45^{+}HLA\text{-}DR^{high}CD1c^{+}$ DCs are already present in the epidermis and dermis at an estimated gestational age of 9 week. Interestingly, this correlated with TGF-β expression in the epidermis (Schuster et al., 2009).

LCs development required FLT3L, TGF-β1, GM-CSF, IL-4, Notch ligand (Delta-1 Jagged2) (Anselmi et al., 2020; Lutz et al., 2017). The interaction of CSF1R with IL-34 has been also reported for LCs differentiation (Kaplan 2017). Knock-out of the TGF-β1 downstream transcription factors PU.1, Id2 and Runx3 abolished LC development (Romani et al., 2010).

For a long time, it was believed that TGF-β was absolutely necessary for development of LCs (Strobl et al., 2019). However, recent studies by the group of Herbert Strobl showed that also the TGF-β-superfamily proteins of the bone morphogenetic protein (BMP) superfamily are involved. LCs in prenatal epidermis already start to express BMP before it expresses TGF-β. LCs can also be generated *in vitro* with BMP7 instead of TGF-β (Yasmin et al., 2013). However, BMP-generated LCs show a slightly different phenotype than TGF-β generated LCs, marked by different expression of some receptors, lack of Birbeck granules and increased proliferation. Such LCs can be observed *in vivo* in human psoriatic lesions, where the epidermis shows high amounts of BMP signaling. In healthy human skin, the basal layers of the epidermis also express BMPs, but no active TGF-β. TGF-β is restricted to the higher levels of the epidermis. Interestingly, all proliferating LCs in healthy human epidermis are located on the BMP-zone of the skin (Borek et al., 2020). Still, the full scope of ontogeny and differentiation regulation of LCs is far from being entirely understood.

During severe injury or inflammation, activated LCs mobilize through chemokine receptor 7 (CCR7)-dependent migration to draining lymph nodes, where they present antigen to T cells and are eventually cleared through apoptosis and other mechanisms. LCs express L-selectin, integrins, platelet endothelial cell adhesion molecule-1, E-cadherin and CCR6, making them suitable for transendothelial migration and immigration to the dermis. Under inflammatory conditions, monocytes in the peripheral blood have the potential to migrate to the epidermis and differentiate into LC-like cells (Allen et al., 2018).

1.3.3 LCs function

LCs are myeloid immune cells; their primary function is the recognition and presentation of antigen. All antigen-presenting cells (APCs) express an extensive repertoire of pattern-recognition receptors (PRRs) to detect non-self-signals.

C-type lectin receptors (CLRs) comprise a subfamily of PRRs dedicated to sensing glycans, including those expressed by commensal and pathogenic bacteria. LCs express C-type lectin receptors, which include DC-SIGN (CD209), langerin (CD207) and mannose receptor (MR, CD206). Their respective binding sites and bacteria recognition has been nicely reviewed recently (Mnich et al., 2020).

Toll-like receptors (TLRs) are also PRRs composed of an extracellular part, which allow binding of pathogen-associated molecular patterns. To date, 13 mammalian TLRs have been identified and characterized, with TLR1 to TLR11 appearing in humans. TLR1, TLR2, TLR4, TLR6 and TLR10 detect extracellular pathogen-associated molecular patterns, while TLR3, TLR7, TLR8 and TLR9 are expressed on endosomal membranes and recognize nucleosides, nucleotides and oligo- and polynucleotides derived from intracellular viral and bacterial pathogens. (Novak et al., 2011; Novak et al., 2010; Sun 2019).

Skin´s DCs in AD are equipped with a particular set of intra- and extracellular TLRs (Novak et al., 2010). TLR2 is expressed by epidermal LCs as well as dermal DCs. For ligand binding, TLR2 forms heterodimers with TLR1 and TLR6. TLR1/2 heterodimers recognize triacylated lipopeptide like Pam3Cys-SKKKK (P3C) while TLR2/6 heterodimers interact with diacylated lipopeptides such as Pam2Cys-SKKKK (P2C). In contrast, TLR4 represents the main structure in recognizing lipopolysaccharides (LPS) of gram-negative bacteria.

Antigen uptake and internalization is often accompanied by LCs maturation. During this process, LCs undergo a series of phenotypical and functional alterations such as the upregulation of surface MHC class II molecules and the co-stimulatory molecules CD40,

CD80, CD86 and CD83 (Von Bubnoff et al., 2011). Additionally, migratory capacities increase due to the upregulation of the CCR7 and downregulation of the CCR6 (Barbaroux et al., 2006). During their maturation, LCs almost lose their phagocytic properties, but gain their T cell priming capabilities.

Upon the capture of the antigen LCs mature and lose their connection with the surrounding epithelium by downregulation of E-cadherin. They become highly motile, egress from the skin, and migrate to the skin-draining lymph nodes, where they present antigens to T lymphocytes.

As professional APCs, LCs can present antigen via MHC-I and MHC-II. Intracellular antigens including self-proteins are normally degraded proteasomally and assemble with MHC class I molecules in the endoplasmic reticulum before the complex is transported to the cell surface for recognition by $CD8^+$ T cells. In contrast, extracellular antigens are processed and loaded on MHC class II molecules in late endosomal compartments. MHC class II complexed are recognized by $CD4^+$ T cells. Exogenous antigens can also be presented by MHC class I complexes. This so called cross-presentation enables APCs to present exogenous antigens to $CD8^+$ T cells and include either immunity or tolerance against self-antigens by peripheral deletion of autoreactive $CD8^+$ T cells (Clausen et al., 2015).

The question whether LCs are pro-or anti-inflammatory has been debated for many decades. Nowadays we know that LCs can, dependent on the context, act both ways. On one hand, in steady-state skin, they prevent harmful immune activation by maintenance of Tregs and induction of tolerance to self-antigens and commensals in skin microbiome. One mice study has shown that $CD4^+CD25^+$ T cells from germ-free mice showed a lower relative gene expression of fork head box p3 gene (Foxp3) and were not as potent suppressors *in vitro* as $CD4^+CD25^+$ T cells from conventional (conv) NMRI mice (Ostman et al., 2006).

1.3.4 The role of LCs in AD

The epidermis is constantly surveyed by LCs, $CD8^+$ resident memory T cells (T_{RMs}), innate lymphoid cells (ILCs), and, in mouse skin, dendritic epidermal γδ T cells (DETCs) (Naik 2022). The dendrites of LCs penetrate the tight junctions that separate the stratum corneum from the stratum granulosum. Langerin accumulates at dendrite tips and Birkbeck granule formation is detected at the cell surface, suggesting that the LCs can take up antigens outside the tight-junction barrier, in addition to having the capacity to capture penetrated antigens. Since this also happens in AD lesions, some researchers have suggested that the tight-junction-penetration of LCs may contribute to formation of lesions (Yoshida et al., 2014; Yoshida et al., 2022).

Clinically unaffected skin is in fact “abnormal” in AD patients as compared to non-AD subjects. This has been shown at the functional (i.e., TEWL and skin irritation) and molecular level. Of note, in addition to skin barrier abnormalities, non-lesional (NL) skin also is characterized by subclinical inflammation, representing both innate and adaptive pathways (mostly skewed toward Th2, Th17/Th22). As discussed above, another important feature of NL AD skin barrier disruption is the association with microbial dysbiosis and more specifically, *S.a.* colonization. LCs, the most prominent professional APCs in the epidermis, are among the first responders upon invasion of *S.a.* into the skin, contributing to early initiation of proinflammatory responses and recruitment of neutrophils. Langerin binding increases bacterial uptake, LC maturation, and the production of pro-inflammatory cytokines such as neutrophil chemoattractant IL-8 (Hendriks et al., 2021). *S.a.* strain isolated from AD skin can skew T cell responses towards imbalanced Th1/Th2 skin immunity in an LC-dependent manner (Iwamoto et al., 2017).

Previous findings from our group show that in human LCs, ligation of TLR2 by *S.a.*-derived products down-regulates FcεRI and its transcription factor PU.1. TLR2-mediated sensing of *S.a.*-derived signals is strongly impaired in LCs from AD skin. This phenomenon may partly contribute to the immune deviation in AD and the lack of *S.a.* clearance (Herrmann et al., 2013; Iwamoto et al., 2018; Leib et al., 2018).

A recent focus of research is the large number of IgE molecules bound to the cell surface of APCs in AD. This occurs specifically in patients who develop either an increased production of IgE with allergic asthma or rhinitis, or an APC-T-cell-mediated chronic inflammatory skin disease (Bieber et al., 1989a). While the low affinity receptor for IgE, FcεRII/CD23 (Bieber et al., 1989b), and the IgE binding lectin galectin-3 have been described on the surface of epidermal LCs in AD patients, it appeared that the relevant structure for IgE binding on these cells is the high affinity receptor IgE FcεRI, which belongs to the multichain immune recognition receptors family (Bieber et al., 1992a; Bieber et al., 1992c). FcεRI expression on CD1a cells correlated significantly with the serum IgE level of the patients (Wollenberg et al., 1996). Unlike LCs, which are present in healthy and infected skin, inflammatory dendritic epidermal cells (IDECs) appear only in inflamed skin. Both IDECs and LCs, but not pDC, express CD1a which mediated the presentation of lipid antigens to T cells. Of note, investigation of these structures are not possible in animal models, since only human express FcεRI on APCs. Intriguingly, narrow-band UVB phototherapy of patients with AD reduced the number of $FcεRI^{+}$ DC in lesional skin. This effect may at least contribute to the inflammation-ameliorating effect of phototherapy (Koch et al., 2017).

Taken together, LCs can exert different functions during AD depending on the stimuli they receive from the microenvironment. This explains why, despite many efforts, researchers have been so far unable to ascribe a specific role to LCs in AD.

1.4 The aim of the study

The aim of this thesis is to explore the impact of the microbiome on the phenotype and function of human epidermal LCs *in vitro*. The working hypothesis is that *S.a.* and *S.e.* as representatives of pathogens and commensals, respectively, have differing impacts on the biology of epidermal LCs. The lessons learned from this project may have significant translational consequences, potentially in the management of AD. The use of topical therapies containing bacterial products may be able to redirect the cutaneous immune response in a way that more tolerance could be achieved towards environmental allergens known to be provocative factors for this disease.

To investigate the impact of these bacteria on the migration, phenotype, and function (including cytokine production and antigen-presentation) of epidermal LCs, methods such as laser confocal microscopy, flow cytometry, beads-based ELISA and quantitative real time PCR (qRT-PCR) are applied.

2. Material and methods

2.1 Materials

2.1.1 **Table 2.1.1**: Antibodies for flow cytometry analysis.

Antibody	Source	Clone	Identifier #
Biotin anti-human CD281 (TLR1) Antibody	Biolegend	TLR1.136	334504
Brilliant Violet 605™ Mouse IgG1	Biolegend	MOPC-21	400161
CCR5 APC	Miltenyi Biotec	REA245	130-123-057
CCR6 PE	Miltenyi Biotec	REA190	130-120-458
CCR7 PE	Miltenyi Biotec	REA546	130-119-583
CD11b Percpvio700	Miltenyi Biotec	REA713	130-110-557
CD11c Viobright515	Miltenyi Biotec	REA618	130-127-207
CD14 APC	Miltenyi Biotec	TÜK4	130-113-705
CD14 Percpvio700	Miltenyi Biotec	REA599	130-110-523
CD1a RD1	Beckman Coulter	SCFI19Thy1A8	6603185
CD1a VioBlue	Miltenyi Biotec	REA736	130-111-875
CD1b PEvio770	Miltenyi Biotec	SN13	130-101-578
CD1c PEvio615	Miltenyi Biotec	REA618	130-126-883
CD206 Percpvio700	Miltenyi Biotec	DCN228	130-104-129
CD207	Beckman Coulter	DCGM4	PN IM3449
CD207 APC-Vio770	Miltenyi Biotec	REA770	130-112-214
CD209 Percpvio700	Miltenyi Biotec	REA617	130-109-593
CD324 PEvio615	Miltenyi Biotec	REA811	130-125-732
CD34 PE	Becton Dickinson	581 (RUO)	555822
CD36 PE	Miltenyi Biotec	REA760	130-110-740
CD40 PEvio770	Miltenyi Biotec	REA733	130-110-948
CD80 PE	Miltenyi Biotec	REA661	130-123-253

Antibody	Source	Clone	Identifier #
CD83	Santa Cruz Biotechnology	HB15a	sc-19677
CD83 APC	Miltenyi Biotec	REA714	130-110-504
CD86 Viobright515	Miltenyi Biotec	REA968	130-116-165
CX3CR1 APC	Miltenyi Biotec	REA385	130-122-912
CXCR1 PEvio770	Miltenyi Biotec	REA958	130-115-881
FceR1a	eBioscience	AER-37	16-5899-025
FceRIa FITC	Miltenyi Biotec	REA758	130-110-726
Gam FITC	Jackson ImmunoResearch	Polyclonal	115-095-003
HLA-DR PEvio615	Miltenyi Biotec	REA805	130-111-797
IgG1 PE	Becton Dickinson	X40	340761
IgG1 RD1	Beckman Coulter	2T8-2F5	6602884
IgG2a APC	Miltenyi Biotec	S43.10	130-113-831
IgG2b	Sigma-Aldrich	MOPC-141	M5534
mouse IgG1κ Percpvio700	Miltenyi Biotec	IS5-21F5	130-113-776
mouse IgG1κ PEvio770	Miltenyi Biotec	IS5-21F5	130-113-764
Recombinant human IgG1 APC	Miltenyi Biotec	REA293	130-113-446
Recombinant human IgG1 APC-Vio770	Miltenyi Biotec	REA293	130-113-447
Recombinant human IgG1 FITC	Miltenyi Biotec	REA293	130-113-449
Recombinant human IgG1 PE	Miltenyi Biotec	REA293	130-113-450
Recombinant human IgG1 Percpvio700	Miltenyi Biotec	REA293	130-113-453
Recombinant human IgG1 PEvio615	Miltenyi Biotec	REA293	130-113-451
Recombinant human IgG1 PEvio770	Miltenyi Biotec	REA293	130-113-452
Recombinant human IgG1 VioBlue	Miltenyi Biotec	REA293	130-113-454

Antibody	Source	Clone	Identifier #
Recombinant human IgG1 Viobright515	Miltenyi Biotec	REA293	130-113-457
TLR2	Imgenex	1030A5.138	MAB0066
TLR2 PEvio615	Miltenyi Biotec	REA109	130-107-462
TLR6 PE-Vio770	Miltenyi Biotec	REA382	130-106-590
Trop1 FITC	Miltenyi Biotec	REA764	130-110-998
Trop2 APC	Miltenyi Biotec	REA916	130-115-056

2.1.2 **Table 2.1.2**: Antibodies for live imaging analysis.

Antibody	Source	Clone	Identifier #
Goat anti-Mouse IgG (H+L) Cross-Adsorbed Secondary Antibody, Alexa Fluor 488	Invitrogen	Polyclonal	A-11001
Goat anti-Rabbit IgG (H+L) Highly Cross-Adsorbed Secondary Antibody, Alexa Fluor 546	Invitrogen	Polyclonal	A-11035
Staphylococcus aureus Polyclonal Antibody	Invitrogen	Polyclonal	PA1-7246
Staphylococcus epidermidis Monoclonal Antibody	Invitrogen	17-5	MA1-35788

2.1.3 **Table 2.1.3**: Chemical, reagents, and enzymes.

Product	Source	Identifier #
2-Mercaptoethanol (50 mM)	Gibco	31350010
2-Propanol	Sigma-Aldrich	67-63-0
7AAD	Biolegend	420404
Brilliant Violet 605™ Streptavidin	Biolegend	405229
BSA	Roth	8076.2
CD207 MicroBead Kit, human	Miltenyi Biotec	130-097-898
CD34 MicroBead Kit, human	Miltenyi Biotec	130-046-701
$CD4^+$ T Cell Isolation Kit, human	Miltenyi Biotec	130-096-533
CellGenix® GMP DC Medium	CellGenix	20805-0500
CellTracker™ Blue CMHC Dye	Invitrogen	C2111
Chloroform	Sigma-Aldrich	67-66-3
Compensation Beads	Invitrogen	01-2222-42
Distilled water	Thermo Scientific	15230097
DMSO	Roth	A994.2
dNTP	Sigma-Aldrich	71004-3
DTT	Roche	3483-12-3
Ethanol	Roth	K928.4
FACS clean	BD Biosciences	340345
FACS flow	BD Biosciences	342003
FACS rinse	BD Biosciences	340346
FACS shutdown	BD Biosciences	334224
FBS	Gibco	A3840401
FcR Blocking Reagent human	Miltenyi Biotec	130-059-901
Ficoll® Paque Premium	GE healthcare Bio-Sciences AB	GE17-5442-02
FLT3L	R&D systems	308-FKE-010
Glycogen, RNA grade	Thermo Scientific	R0551
GM-CSF	R&D systems	215-GMP-010

Product	Source	Identifier #
Human IgE, Myeloma	Merck	US1401152-100UG
LEGENDplex™ HU Proinflam. Chemokine Panel 1 (13-plex) w/VbP	Biolegend	740985
LEGENDplex™ HU Th Cytokine Panel (12-plex) w/ VbP V02	Biolegend	741028
LEGENDplex™ Human Inflammation Panel 1 (13-plex) with V-bottom Plate	Biolegend	740809
Live/dead Viobility 405/520 Fixable Dye	Miltenyi Biotec	130-109-814
Normal mouse serum	Jackson ImmunoResearch	015-000-120
PBS	Pan-biotech	P04-36500
Penicillin-Streptomycin	Gibco	15140-122
RPMI Medium 1640 + GlutaMAX	Gibco	61870036
SCF	R&D systems	255B-GMP-010
SYBR® Green Supermix with ROX™	Bio-Rad Laboratories	1708886
Tandem Signal Enhancer, human	Miltenyi Biotec	130-099-888
Temperierbad Additiv	Invicon	200 001
TGF-beta	R&D systems	240-B-002/CF
Thrombopoietin	R&D systems	288-TP-005/CF
TNF-a	R&D systems	210-TA-005/CF
TRIzol®	Life technologies	15596
Trypan blue	Thermo Scientific	15250061
UltraPure™ 0.5M EDTA, pH 8.0	Invitrogen	15575020

2.1.4 **Table 2.1.4**: Equipment, consumables and software.

Name	Manufacturer
Autoclave varioclav 500	Labortechnik
AutoMACS Pro® separator	Miltenyi Biotec
BioPhotometer	Eppendorf
Cellstar™ polypropylene tube, 15/50ml	Greiner Bio-One
Cellstar™ serological pipet, 10ml, sterile	Greiner Bio-One
Centrifuge 5417R	Eppendorf
Costar® 24well clear TC-treated plates	Corning
Costar® serological pipet, 5ml/10ml, sterile	Corning
Counting slides, dual chamber for cell counter	Bio-Rad laboratories
Disposable cuvettes, 1.5ml	Brand
FACSDiva software	BD Bioscience
Flow cytometry CytoFLEX LX	Beckman Coulter
Flow cytometry FACSCanto™	BD Bioscience
FlowJo V10.6 software	BD Bioscience
GraphPad Prism V8	GraphPad Prism
IBM SPSS statistics	IBM Deutschland
Image J software	Open source
Incubator Heracell	Thermo Fisher Scientific
Incubator shaker innova 4000	New Brunswick Scientific
LS columns	Miltenyi Biotec
MicroAMP® fast optical 96-well reaction plate, 0.1ml	Applied Biosytem
Microsoft office 2010	Microsoft corporation
Millex® syringe-driven filter unit (0.22µm)	Merck
Milli-Q reference water purification system	Merck
Mr. Frosty™ freezing container	Thermo Fisher Scientific
Multitron Standard Incubator shaker	INFORS HT
NanoDrop™ 2000/2000c Spectrophotometers	Thermo Fisher Scientific
Neubauer chamber	Sigma
Nikon A1R confocal microscope	Nikon

Name	Manufacturer
Nikon Eclipse Ti2-E inverted microscope	Nikon
Nikon Nis-elements viewer	Nikon
Nunc™ biobanking and cell culture cryogenic tubes, 1.8ml	Thermo Fisher Scientific
Opti-seal optical disposable adhesive	BIOplastics
Pipettors	Eppendorf
Pre-separation filters (20µm)	Miltenyi Biotec
Primer Express 3.0.1	Applied Biosytem
R studio v4.0.2	Open source
Safe lock tubes, PCR clean, 1.5ml	Eppendorf
StepOne™ plus qPCR machine	Applied Biosytem
StepOne™ plus sofrware	Applied Biosytem
Synergy™ Milti-Mode microplate reader	BioTek
TC20 Automated cell counter	Bio-Rad laboratories
Thermomixer 5436	Eppendorf
Water bath	Memmert
WillCo-dish® glass bottom dish, 50mm diameter	Willco Wells

2.1.5 **Table 2.1.5**: qRT-PCR Primer list.

Gene	Forward sequence	Reverse sequence
ACTB	AGCGCGGCTACAGCTTCA	TCCTTAATGTCACGCACGATTT
CCL13	GTGCCTGCTGCTCATGACA	TGCATCTGGCTGAGCAAGTC
CCL17	GAAGACGTGGTACCAGACATCTGA	CCCTGCACAGTTACAAAAACGA
CCL22	CGGCGCCAACATGGAA	CAGACGGTAACGGACGTAATCA
CCR6	CCATTCTGGGCAGTGAGTCA	GCACGTGGCATTGCTGAA
CCR7	GCTGCGTCAACCCTTTCTTG	AAGAGATCGTTGCGGAACTTG
CD83	GCCTCGAAAACCATCACATGA	GGTGGCCATGGAGAAGCA
Elf.1	TGCCCCAGTCACCCATGT	ACCCGGTGAGTCTGCATATT
FceRIa	GGCAGCTGGACTATGAGTCTGA	CTTCTCACGCGGAGCTTTTATT
FceRIg	GATGCCATCCTGTTTCTGTATGG	CACTTGGATCTTCAGTCGACAGTAG
HMGB1	GATCCTAAGAAGCCGAGAGGC	CTTATGCTCCTCCCGACAAGT
HMGB2	CCCGGACTCTTCCGTCAATT	TCTTCCATCTCTCCGAACACTTC
IL-13Ra1	AAGCGCAATTCCACACTCTACA	TGCACCTGCGACGATGACT
IL-2Rg	TGTCTAAGGGACTGGCTGAGAGT	TGACGAGGCAGAGTCGTTCA
IL-4Ra	CCTGGAGCAACCCGTATCC	CAAATGTTGACTGCATAGGTGAGAT
Jak1	CGAGATCCCCTTGAAAGACAAG	TGCACCGGCTTTCATAGAATC
Jak2	TGCTCCAGAATCACTGACAGAGA	ACCACTCCAAAGCTCCAAACA
Jak3	TGCCATCAACAAGCTCAAGACT	TGCCATCAACAAGCTCAAGACT
MY88	TCACTGTCTGCGACTACACCAA	GGCAAGGCGAGTCCAGAAC
PU.1	GGAGAGCCATAGCGACCATT	GGAGCTCCGTGAAGTTGTTC
SP1	GGACTACCTGGAGTGATGCCTAA	CCCATCAACGGTCTGGAACT
TLR1	TGTGCTGCCAATTGCTCATT	TTTTCCCCATAAGTCTCTCCTAAGAC
TLR2	CCAAGGAAGAATCCTCCAATCA	GCTGCCCTTGCAGATACCA
TLR4	CCTCGGCGGCAACTTCATAA	AGAGCGGATCTGGTTGTACTG
TLR6	GGGACTCAGCATGGTAGAAGGTA	CTCCTGTTACTCTGCAAGCTTTCA
Tyk2	TTCTCTCTGCGTCGCTGTTG	CCGCATGATGATGAGATTGG
YY.1	GTTCAGGGATAACTCGGCCA	TTCTGCACAGACGTGGACTC

2.2 Methods

2.2.1 Isolation of peripheral blood mononuclear cells (PBMCs) from human cord blood

Human cord blood was collected during healthy and full-term deliveries by the Johanniter Hospital Bonn and the St. Marien Hospital Bonn, Germany. The local ethics committee of the University of Bonn approved the use of human cord blood following the declaration of the Helsinki principles. Some additional $CD34^+$ hematopoietic stem cells from donors´ cord blood was kindly provided by Prof. Herbert Strobl´s lab in the Medical University of Graz, Austria. Ethics approval (26-520) was given by the Medical University of Graz Institutional Review Board. Informed consent was obtained from all patients as required by the Declaration of Helsinki. Blood samples were collected in 50 ml tubes prepared with 250 µl heparin and stored at 4 ℃ until processing on the same day. PBMCs were isolated using Ficoll® Paque Premium (GE Healthcare Bio-Sciences AB, Uppsala, Sweden) density gradient medium. Cord blood was mixed 1:2 with PBS, layered on 20 ml Ficoll® Paque Premium (GE Healthcare Bio-Sciences AB, Uppsala, Sweden) in a 50 ml tube and centrifuged (800 xg, 20 ℃, 28 min, break off). The PBMC-containing interphase was collected, washed, and subjected to magnetic activated cell sorting (MACS®) for the enrichment of $CD34^+$ hematopoietic stem cells.

2.2.2 Isolation of $CD34^+$ hematopoietic stem cells (HSCs)

HSC-LCs were isolated using a CD34 microbead kit (Miltenyi Biotec, Bergisch Gladbach, Germany), according to the manufacturer´s instructions and an AutoMACS Pro® Separator (Miltenyi Biotec, Bergisch Gladbach, Germany). In brief, isolated PBMCs (see 2.2.1) were washed first with 15 ml PBS (300 xg, 20 ℃, 10 min) and then with 25 ml 4℃ MACS buffer (137 mM NaCl; 2.7 mM KCl; 8.5 mM Na_2HPO_4; 1.47 mM KH_2PO_4; 0.5 % (w/v) BSA; 1 % (v/v) 0.5 M EDTA) (300 xg, 4 ℃, 10 min). Cells were resuspended in 1ml 4 ℃ MACS buffer and were magnetically labeled with CD34 MicroBeads. Then, the cell suspension is loaded onto a MACS® Column which is placed in the magnetic field of a MACS Separator. The magnetically labeled $CD34^+$ cells are retained within the column. The unlabeled cells run through; this cell fraction is thus depleted of $CD34^+$ cells. After removing the column from the magnetic field, the magnetically retained $CD34^+$ cells can

be eluted as the positively selected cell fraction. HSCs were either saved for cryopreservation in liquid nitrogen or were freshly differentiated into $CD34^+$ hematopoietic stem cell derived Langerhans cells (HSC-LCs). The purity of each batch of enriched cell was confirmed by flow cytometry. For further experiments, only isolates with a purity of > 95 % were used.

2.2.3 Generation of $CD34^+$ hematopoietic stem cells derived Langerhans cell.

Freshly isolated or thawed $CD34^+$ hematopoietic stem cells were adjusted to 60.000 cells/ml RPMI medium 1640 GlutaMAX™ supplemented with 50 µM 2-mercaptoethanol, 10 % FBS and 1 % Penicillin-Streptomycin. Cells were cultured in a 24-well plate at 37 ℃ and 5 % CO_2 for 8 days. Culture conditions are summarized in Table 1.

Table 2.2.1 Culture conditions for HSC-LCs. Final concentrations are listed.

Reagent	Day 0	Day 2	Day 4	Day 6	Day 8
GM-CSF	300 IU/ml		300 IU/ml		300 IU/ml
mIgE	1 µg/ml	1 µg/ml	1 µg/ml	1 µg/ml	1 µg/ml
FLT3L	10 ng/ml				
SCF	10 ng/ml				
TGF-β	0.5 ng/ml		0.5 ng/ml		0.5 ng/ml
TNF-α	20 U/ml				
Culture volume / well	0.5 ml	0.5 ml	0.75 ml	0.75 ml	1 ml

2.2.4 *In vitro* stimulation of LCs

After 8 days of differentiation, LCs were collected and centrifuged (300 xg, 4 ℃, 10 min). The cell pellet was resuspended in sterile MACS buffer. $CD207^+$ LCs were enriched following the manufacturer´s protocol of the CD207 Microbeads Kit from Miltenyi Biotec. In principle, the technique resembles the magnetic isolation of HSCs (see 2.2.2). The purity of enriched LCs was confirmed by flow cytometry. For further experiments, only isolates with a purity of > 90 % were used. $CD207^+$ LC were adjusted to 10^6 cells/ml in freshly prepared medium (see 2.2.3) and were distributed in 24-well plates with 1ml per well. Cells were left untreated or treated with specific stimulants (see Table 2) and were

incubated at 37 ℃, 5 % CO_2 for different time course experiments. Stimulation effects were analyzed by flow cytometry of all $CD207^+$ LC.

Table 2.2.2 Stimulants of LCs.

Stimulant	Derived from	Final conc.	Used as ligand for	Source
LPS	*E.coli* 0111:B4	0.1 µg/ml	TLR4	InvivoGen, San Diego, USA
P3C	Synthetic triacylated lipopeptide	1 µg/ml	TLR1/2	EMC microcollections GmbH, Tübingen, Germany
P2C	Synthetic diacylated lipoproteins	1 µg/ml	TLR2/6	EMC microcollections GmbH, Tübingen, Germany
Heat-killed *S.a.*	DSM 20372	10 µl suspension/ml	TLR	Leibniz Institute DSMZ-German Collection of Microorganisms and Cell Cultures GmbH
Heat-killed *S.e.*	DSM 1798	10 µl suspension/ml	TLR	Leibniz Institute DSMZ-German Collection of Microorganisms and Cell Cultures GmbH
Live *S.a.*	DSM 20372	100 µl suspension/ml	TLR	Leibniz Institute DSMZ-German Collection of Microorganisms and Cell Cultures GmbH
Live *S.e.*	DSM 1798	100 µl suspension/ml	TLR	Leibniz Institute DSMZ-German Collection of Microorganisms and Cell Cultures GmbH
unstimulated	-	Equal volume of medium	-	

2.2.5 Flow cytometry analysis

Surface and intracellular immunofluorescence staining was employed in order to analyze $CD34^+$ hematopoietic stem cell and $CD207^+$ cell enrichment as well as LC phenotype and treatment effects. Staining antibodies used in this study are summarized in Table 1. Viability of the cells was examined by 7-AAD (Biolegend, USA) staining in Bonn Lab or

Viobility 405/520 Fixable Dye (Miltenyi Biotec, Germany) in Graz lab. Intracellular staining was performed according to the BD Cytofix/Cytoperm Kit protocol (Beckton Dickinson, Germany). 50.000 cells per FACS tube for surface staining were stained successively with the indicated antibodies in a total volume of 100 µl FACS buffer at 4 ℃ for 20 min. Washing steps were executed in 1 ml FACS buffer (PBS supplemented with 2 mM EDTA and 0.5 % BSA, 400 xg, 4 ℃, 5 min). Cells were measured and analyzed utilizing a FACSCanto™ flow cytometer and FACSDiva™ software (Beckton Dickinson, Germany) or FlowJo v10 software (FlowJo, USA) in Bonn Lab. CytoFlex LX (Beckman Coulter, Germany) was used in Graz lab. For statistics, mean fluorescence intensity (MFI) was calculated.

2.2.6 Phenotypic characterization of LCs

In Bonn lab, expression of specific surface molecules was assessed by staining with unconjugated mouse monoclonal antibodies- against Langerin (CD207), FcεR1α, TLR2, CD80, CD83, CD86 and MHC II. Unspecific mouse IgG2b was used as an Isotype control antibody. FITC-conjugated goat-anti-mouse IgG polyclonal antibody was used as a secondary antibody. Free antigen-binding sites were blocked with 2.5 mg/ml mouse serum for 15 min at 4 ℃. Finally, an antibody mix containing IgG2a-APC, IgG1-RD1 and 7-AAD or CD14-APC, CD1a-RD1 and 7-AAD was added. In Graz lab, expression of specific surface molecules was examined by conjugated REAfinity antibody (listed in Table 1).

2.2.7 RNA isolation

RNA of $CD207^+$ enriched cells was extracted via the phenol/chloroform method utilizing TRIzol® reagent in accordance with the manufacturer´s protocol. In brief, after complete dissociation of nucleoprotein complexes. Centrifuge at full speed for 15 minutes at 4 ℃. Following centrifugation, the mixture separates into 3 layers: Lower red phenol chloroform phase, middle interphase, and colorless upper aqueous phase. Carefully transfer the upper aqueous phase to fresh 1.5 ml tube. Add 0.5 ml of isopropanol. Vortex briefly. Incubate at room temperature for 10 min followed by centrifugation at 4 °C for 8 min. The RNA precipitates can be visualized as a small palette. Carefully remove the supernatant. Wash the palette with 1 ml of 75 % ethanol. Mix by brief vortexing and centrifuge at full speed at 4 °C for 5 min. Discard the supernatant while watching the pallet. Airdry the pallet.

RNA was resuspended in 25 µl nuclease-free water. DNA contaminations were removed using DNA-free™ DNA Removal Kit (Ambion®, Life Technologies GmbH, Darmstadt, Germany) following the manufacturer´s instructions. RNA concentration and purity were evaluated. RNA was reverse transcribed to cDNA for gene expression experiments or stored at – 80 ℃.

2.2.8 Determination of RNA and DNA concentration and purity

In Bonn lab, concentrations and purity of nucleic acids were determined by using the spectrophotometer SynergyTM HT Multi-Mode Microplate Reader (BioTek, Bad Friedrichshall, Germany). Concentrations were calculated by measuring RNA and DNA at the wavelength λ = 260 nm. Purity was assessed by a λ 260/280 ratio. Value was calculated with Gen5™ software (BioTek, Bad Friedrichshall, Germany). 2 µl of each nucleic acid and of nuclease-free water for RNA reference were measured. In Graz lab, NanoDrop™ Spectrophotometers (Thermo Fisher Scientific, MA, USA) was used for RNA measurement.

2.2.9 Reverse transcription for gene expression experiments

RNA was reverse transcribed into complementary DNA (cDNA). 1 µg RNA in 15.5 µl nuclease-free water was denatured at 65 ℃ for 3 min and was then transferred directly on ice. 34.5 µl of a reverse transcription reaction mix (see table 2.2.3) was added to RNA and incubated at 37 ℃ for 1 hour. The reaction was stopped at 95 ℃ for 3 min. The cDNA volume was adjusted to 100 µl with nuclease-free water. cDNA was kept on ice for immediate use in qPCR or were stored at - 20 ℃.

Table 2.2.3 Components of reverse transcriptions reaction mix.

Reagents	Final concentration
5 x reverse transcription buffer	1x
dNTP	4 µM (each)
DTT	100 µM
Random primer	2.4 ng/µl
RNAsin	1 U/µl
SuperScript™ Reverse Transcriptase	4 U/µl
Final Volume	34.5 µl

2.2.10 Quantitative real-time PCR (qRT-PCR) for gene express experiment

In this study, iTag™ SYBR® Green Supermix with ROX™ was used. The mix includes SYBR® Green (DNA-dye-complex absorption λ_{max} = 497 nm; emission λ_{max} = 520 nm) and ROX™, a passive reference dye to normalize non-PCR-related fluctuations in fluorescence. StepOnePlus™ qRT-PCR devices and StepOne™ software v2.2.2 (Applied Biosystem, Life Technologies GmbH, Darmstadt, Germany) were used to execute qRT-PCR and to analyze the results. Primers (see table 2.1.5) were designed using Primer Express 3.0.1 software (Applied Biosystem, Life Technologies GmbH, Darmstadt, Germany). Absolute quantification of the gene expression transcripts was achieved by using standard curves with a defined number of molecules of an amplicon calculated by its nanomolar quantity as follows:

$$\text{Molecules} = x \text{ mole} * 6.022 * 10^{23}$$

Amplicon stock solutions were adjusted to 3 x 10^{13} molecules/µl in nuclease-free water and stored at 4 ℃. A standard dilution series was prepared in six concentrations reaching from 3 x 10^{8} molecules/µl to 3 x 10^{3} molecules/µl. Six standard curves of each primer pair were prepared. The mean CT values were plotted against the concentrations.

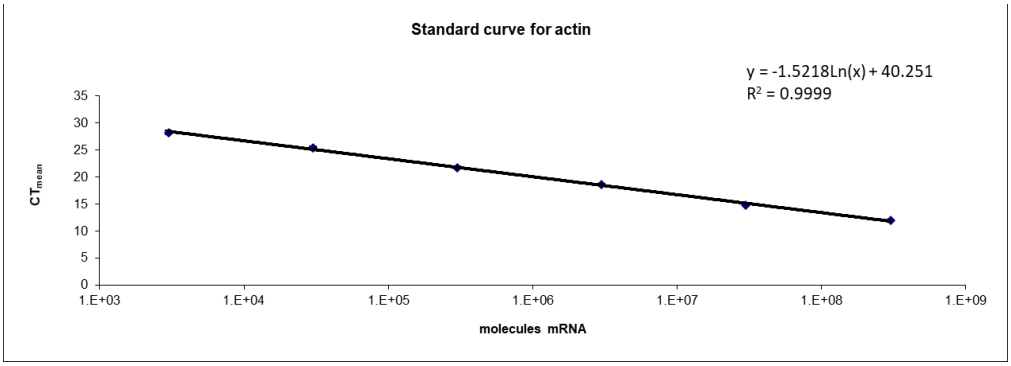

Figure 2.1 Standard curve for actin. Dilution series of the amplicon for actin were prepared as described in the text. Mean CT values of n=6 experiments were used to generate the regression line.

The linear function of the regression line was used to calculate the amounts of molecules in cDNA samples:

$$y = -1.5218\ln(x) + 40.251$$

$$x = \exp((y-40.251) / (-1.5218))$$

Results were normalized to 10^3 molecules actin. The efficiency of primers was greater than 80 %.

The PCR master mix (see table 2.2.4) was prepared in a volume of 9 µl and distributed into 96-well plates. Forward and reverse primers were mixed (1:1). 1 µl of target cDNA, standard dilution series or nuclease-free water for a non-template control was added to the corresponding qRT-PCR master mix. Samples and controls were measured in triplicates. Cycling conditions are summarized in Table 2.2.5.

Table 2.2.4 Components of qRT-PCR reaction mix.

Reagent	Volume	Final concentration
SYBR® Green Supermix with ROX™ (2x)	5 µl	1 x
Primer Mix (5 µM)	0.4 µl	0.2 µM
cDNA / standard dilution / nuclease-free water	1 µl	10 %
Nuclease-free water	3.6 µl	-
Final volume	10 µl	

Table 2.2.5 Thermal cycling conditions for qRT-PCR (40 cycles).

Step	Duration	Temperature
Initial denaturation	10 min	95 ℃
Denaturation	15 s	95 ℃
Annealing and elongation	1 min	60 ℃
Melting curve	15 s	+ 0.3 ℃ （until 95 ℃）

2.2.11 Eclipse Ti2 Nikon live imaging

Eclipse Ti2-E inverted microscope equipped with six LEDs and standard filter sets. C2 confocal system (laser lines at 405 nm, 488 nm, 561 nm, 630 nm). OKOLAB CAGE incubator with 37 ℃ temperature, 90 % humidity, and 5 % CO_2 controller. In this study, unstimulated 1 mio. HSC-LCs were stained with 5 µM CellTracker™ Blue CMHC Dye in 1ml clear serum free medium (CellGenix® GMP DC Medium, CellGenix, Germany), incubate 30 min in 37 ℃, 5 % CO_2 incubator. Harvest cells and centrifuge 300 xg, 5 min, Room temperature (RT). Discard the supernatant and resuspend the cell pallet in 5 ml serum free medium in 50 mm diameter WillCo-dish® glass bottom dish (Willco Wells B.V., Amsterdam, Netherlands). Live *S.a.* from 1 ml stock (OD600=0.5) was stained with 5 µg/ml *S.a.* polyclonal antibody for 20 min in the dark, RT. Then add 5 µg/ml goat anti-rabbit IgG secondary antibody Alexa Fluor 546, incubate for another 20 min in the dark, RT. Live *S.e.* was stained from 1 ml stock (OD600=0.5) was stained with 5 µg/ml *S.e.* monoclonal antibody for 20 min in the dark, RT. Then add 5 µg/ml goat anti-mouse IgG secondary antibody Alexa Fluor 488, incubate for another 20 min in the dark, RT. Detailed antibody information is listed in table Table 2.1.2. Each stained *S.a./S.e.* will be applied 100 µl cell suspension into original 5 ml serum free medium containing unstimulated HSC-LCs for live imaging. During imaging, every 10 min time lapse was taken for the image acquisition. NIS-Elements C software was used for later image analysis.

2.2.12 Bacteria culture

Staphylococcus aureus (DSM 20372) and *Staphylococcus epidermidis* (DSM 1798) were bought from Leibniz Institute, DSMZ-German Collection of Microorganisms and Cell Cultures GmbH DSMZ, Germany.

For generation of heat-killed bacteria the bacteria were grown on tryptic soy agar overnight. One to two colonies from tryptic soy agar were used to inoculate in 250 mL tryptic soy broth (TSB) and incubate at 37 ℃, 180 rpm in a water bath. Bacteria were harvested at an OD600 of 0.6 by centrifugation for 10 min at 8000 g at RT. Bacteria were washed 2 x with 20 mL PBS-azide (10 min, 8000 xg, RT). The pellet was weighed and resuspended in 10 % PBS-azide (w / v). Bacteria were fixated by addition of formalin (final concentration 1.5 %) stirred for 1 h at RT (magnetic stirrer). Bacteria were washed with 20 mL PBS-azide (10 min, 8000 xg, RT). The pellet was weighed and resuspended in 10 % (w / v) PBS-acidic. Bacteria were heat-inactivated by shaking in a water bath for 10 min at 80 ℃ with immediate cool down in an ice water bath. Bacteria were washed twice with 20 mL PBS-azide (10 min, 8000 xg, RT) and resuspended in 10 % (w / v) PBS-acidic.

For live bacterial culture, frozen stocks were streaked on tryptic soy agar plates and grown overnight at 37 ℃. A single colony was picked to inoculate 10 mL TSB and grown overnight at 37 ℃ with shaking at 180 rpm. The overnight culture was used to inoculate fresh room-temperature TSB in an Erlenmeyer flask at a dilution of 1:200. Bacteria for infections were harvested typically after 8 h culture at 37 ℃ shaked at 180 rpm when an OD600 of 0.5 was reached. Cells were pelleted by centrifugation for 5 min at 1800 g at 4 ℃. Pellets were washed once with endotoxin-free PBS. Before infections, serial dilutions of the inoculum were plated on tryptic soy agar in order to quantify the titer (viable bacteria).

2.2.13 Flow cytometry bead-based immunoassays

BioLegend’s LEGENDplexTM assays are bead-based immunoassays using the same basic principle as sandwich immunoassays. Beads are differentiated by size and internal fluorescence intensities. Each bead set is conjugated with a specific antibody on its surface and serves as the capture beads for that analyte. When a selected panel of

capture beads is mixed and incubated with a sample containing target analytes specific to the capture antibodies, each analyte will bind to its specific capture beads. After washing, a biotinylated detection antibody cocktail is added, and each detection antibody in the cocktail will bind to its specific analyte bound on the capture beads, thus forming capture bead-analyte-detection antibody sandwiches. Streptavidin-phycoerythrin (*SA*-PE) is subsequently added, which will bind to the biotinylated detection antibodies, providing fluorescent signal intensities in proportion to the amount of bound analytes. Since the beads are differentiated by size and internal fluorescence intensity on a flow cytometer, analyte-specific populations can be segregated and PE fluorescent signal quantified. The concentration of a particular analyte is determined using a standard curve generated in the same assay. Consequently, the concentration of each cytokine could be calculated using LEGENDplex™ 7.0 data analysis software provided by BioLegend. Secreted cytokines and chemokines were analyzed via flow cytometry bead-based immunoassays, using the following kits:

LEGENDplex™ Human Proinflammatory Chemokine Panel 1 (13-plex)
This kit measures the concentrations of 13 human chemokines, including MCP-1 (CCL2), RANTES (CCL5), IP-10 (CXCL10), Eotaxin (CCL11), TARC (CCL17), MIP-1α (CCL3), MIP-1β (CCL4), MIG (CXCL9), MIP-3α (CCL20), ENA-78 (CXCL5), GROα (CXCL1), I-TAC (CXCL11) and IL-8 (CXCL8).

LEGENDplex™ Human Inflammation Panel 1 (13-plex)
This kit measures the concentrations of 13 human inflammatory cytokines/chemokines, including IL-1β, IFN-α2, IFN-γ, TNF-α, MCP-1 (CCL2), IL-6, IL-8 (CXCL8), IL-10, IL-12p70, IL-17A, IL-18, IL-23, and IL-33.

LEGENDplex™ Human Th Cytokine Panel (12-plex)
This kit measures the concentrations of 12 human cytokines, including IL-2, 4, 5, 6, 9, 10, 13, 17A, 17F, 22, IFN-γ and TNF-α.

2.2.14 Isolation of naïve $CD4^+$ T cells

PBMCs were incubated with $CD4^+$ T Cell Biotin-Antibody Cocktail against CD8a, CD14, CD15, CD16, CD19, CD36, CD56, CD123, TcRγ/δ, and CD235a (Glycophorin A) for 5 min on ice. Then added $CD4^+$ T Cell MicroBead Cocktail conjugated to monoclonal anti-biotin antibody (isotype: mouse IgG1) and monoclonal anti-CD61 antibody (isotype: mouse IgG1) for 10 min on ice. Proceeded to subsequent magnetic cell separation and collected flow-through containing unlabeled cells, representing the enriched CD4+ T cells. The purity of sorted cells was assessed by flow cytometry. For further experiments, only isolations with cell purity ≥ 95 % were used. Freshly isolated naïve $CD4^+$ T cells were stored in liquid nitrogen for further mixed lymphocyte reaction experiments at later time points.

2.2.15 Mixed lymphocyte reaction (MLR)

Allogeneic naïve $CD4^+$ T cells were isolated and stored as described above. Unstimulated HSC-LCs were exposured to either live *S.a.* or live *S.e.* for 1 hour in 37 ℃, 5 % CO_2 incubator. Harvested all three conditions, i.e., unstimulated LCs, *S.a.* primed LCs and *Se* primed LCs. Washed cells thoroughly three times with RMPI 1640 supplemented with 5 % Penicillin-Streptomycin. Unstimulated LCs and *S.a./S.e.* primed LCs were seeded in graded numbers with constant number ($5x10^5$) of purified allogenic naïve $CD4^+$ T cells in 96-well round bottom tissue culture plates in RMPI 1640 (Sigma-Aldrich, USA) supplemented with 10 % FBS, 5 % Penicillin-Streptomycin (in case there is live bacteria grown). The proliferation of T-cells was analyzed by CellTracker™ Blue Dye. On day 5, all cells were harvested for flow cytometry analysis and supernatants were collected for Th human cytokine measurement (see 2.2.13). Assays were performed in duplicates and the mean was used for the statistical analyses.

2.2.16 Statistical analysis

The gene expression experiments data and cytokine detection experiments were visualized and analyzed with R (R Core Team, 2020) (v4.0.2, packages stringr, dplyr, readxl, pheatmap, ggplot2, dendsort and Tibco Spotfire (v11.6.0). Normality and scedasticity was tested by Kolmogorov-Smirnov test with *stats::ks.test()* and by Bartlett test with *stats::bartlett.test()*, applying Benjamini-Hochberg (BH) multiple test adjustment

with *stats::p.adjust()*. Data distribution improved sufficiently after log_{10}-transformation and only transformed data was used for subsequent statistical analysis. Genes with an absolute log10 (fold change) and an adjusted p-value ≤ 0.05 were considered as differentially expressed. Hierarchical clustering analysis was performed centred and scaled to unit variance *base::scale()* over parameters and over samples. Dendrograms were calculated with standard clustering *stats::hclust(dist())* (Lance-Williams dissimilarity update with complete linkage) and sorted *dendsort::dendsort()* according to the average distance of subtrees at every merging point. Heatmaps were plotted using *pheatmap::pheatmap()*. All other statistical analysis were performed using GraphPad Prism V8 software (GraphPad Software). Differences between the two groups were calculated with a two-tailed Student's t-test. Multiple groups were compared by one-way analysis of variance (ANOVA), corrected with the Tukey multiple comparison test. P-values < 0.05 were considered significant differences and are marked: * < 0.05; ** < 0.01; *** < 0.001**** < 0.0001; ns = not significant.

3. Results

3.1 Study 1: LCs stimulated with heat-killed *S.a.* and heat-killed *S.e.*

AD skin is heavily colonized with *S.a.* and showed reduced levels of *S.e.* (Koh et al., 2022). LCs as sentinel cells in the epidermis can sense those pathogens or commensals via TLRs or FcεRI. However, LCs only present 2-5% of the epidermis cells. This presents a practical challenge for research: human skin samples are limited, and LCs isolation procedure can easily activate these sensitive cells. Therefore, a human cell model of *in vitro* generated HSC-LCs was established to investigate bateria-host cell interaction (see Figure 3.1 A).

3.1.1 *In vitro* generated HSC-LCs resemble LCs found in AD skin

Expression of CD207 and CD1a marks our *in vitro* generated cells as fully differentiated LCs. A prerequisite for stimulation experiments is that the LCs are of an immature (non-activated) phenotype, resembling LCs in the steady state epidermis. Cell surface staining and flow cytometry analysis was performed to characterize LCs phenotype and maturation state. Cells were gated by morphology, singlets, 7-AAD viability staining and by CD1a expression. $CD1a^+$ cells were further analyzed for CD207, CD83, TLR2, FcεRI expression. As shown in Figure 3.1 B, *in vitro* LCs were $CD207^+CD1a^+TLR2^+FcεRI^+$, and ideally correspond to LCs in AD skin. The immature phenotype of the cells was confirmed by low or absent CD83 surface expression.

3.1.2 LCs strongly respond to heat-killed bacteria stimulation

To investigate the microbiome-LC interaction, LCs were stimulated with heat-killed bacteria. *In vitro* LCs, purified via CD207 magnetic microbeads, were exposed to heat-killed *S.a.* or heat-killed *S.e.* for 24h in 37°C, 5% CO_2. The stimulated cells were harvested for flow cytometry and qRT-PCR analysis. Supernatants were collected for ELISA (see Figure 3.2 A). For the gene expression experiments, 33 genes related to AD pathogenesis

were checked. As expected, LCs strongly responded to heat-killed bacteria stimulation (see heatmap in Figure 3.2 B). LCs stimulated with both heat-killed *S.a.* as well as heat-killed *S.e.* show increased expression of CCL22, CCR7, IL-6, JAK1 (upper block), and decreased expression of TGFβ, TNFα, FcεRIα, FcεRIγ, AHR(Aryl hydrocarbon receptor), CCR6, TLR1, TLR2, TLR4, TLR6, TLR10, CCL17 (lower block). Heat-killed *S.a.*, but not heat-killed *S.e.,* led to increased expression of IL-10, IL4-Rα and CCL13.

3.1.3 Heat-killed bacteria stimulation induces LCs maturation

At day 9, stimulated LCs were harvested for gene expression experiments. Relative expression level of CD83, CCR6, CCR7 were determined via qRT-PCR. Values were normalized to per 10^3 actin. CD83 is marker for LC maturation. CCR6 is typically expressed in immature LCs and is involved in the recruitment of LCs to inflammation sites. CCR7 is upregulated in activated LCs and facilitates the migration to the lymph nodes. Upon heat-killed bacteria stimulation, LCs matured and activated as evidenced by upregulation of CD83 and CCR7 and downregulation of CCR6 (see Figure 3.3 A). Upregulation of CD83 was also evaluated on the protein level via flow cytometry (see Figure 3.3 B and C). These findings show that both heat-killed *S.a.* and *S.e.* can induce LC maturation.

3.1.4 Heat-killed bacteria stimulation downregulates TLRs on LCs

In order to investigate the involvement of TLRs, stimulated LCs were harvested for gene expression experiments. Relative expression level of TLR1, TLR2, TLR4, TLR6 and TLR10 were determined via qRT-PCR. Values were normalized to per 10^3 actin. Both heat-killed *S.a.* and *S.e.* stimulation downregulated TLR1, TLR2, TLR6, TLR10 (see Figure 3.4 A), but no significance was observed in downregulatory capacity between these two heat-killed bacteria. Downregulation of TLR2 was also detectable via flow cytometry (see Figure 3.4 B and C). These findings demonstrate that TLRs were functional on LCs upon heat-killed bacteria stimulation.

3.1.5 Heat-killed bacteria stimulation downregulates FcεRI on LCs

Human LCs FcεRI builds a trimeric complex which is composed of one α- and two γ-chains. Surface expression validation of the γ-chains by flow cytometry analysis was not practical because of the deficient epitopes of the almost exclusively intracellularly assembled chains. Expression of FcεRI was detected and analyzed by flow cytometry. Next, qRT-PCR of FcεR1α, FcεR1γ and their related transcription factors PU1, YY1, HMGB1, HMGB2, SP1 and ELF1 were performed. FcεRI expression was severely downregulated on protein and on transcriptional levels upon heat-killed bacteria stimulation. Furthermore, its related transcription factors PU1 and YY1 were also significantly downregulated, but again no difference was found between *S.e.* and *S.a.* (see Figure 3.5).

3.1.6 Heat-killed bacteria stimulation upregulates JAK1 and JAK3 on LCs

As in other atopic diseases, the acute inflammatory reaction in AD is dominated by a Th2 immune response and its associated cytokines IL-4 and IL-13. Both cytokines decrease the production of skin barrier proteins such as filaggrin and thereby contribute to skin barrier dysfunction. The JAK family of cytoplasmatic tyrosine kinases contains JAK1, JAK2, JAK3, and TYK2, which all can associate to type I and type II cytokine receptors. Recently developed JAK-inhibitors show significant amelioration of moderate-to-severe AD (Alves de Medeiros et al., 2016; Bieber et al., 2021; Kim et al., 2020; Klaeschen et al., 2020; Peng et al., 2022). However, the connection between skin microbiome and the JAK family in LCs was unknown till now. Here, the expression levels of JAK1, JAK2, JAK3, TYK2, IL-4Rα, IL-13Rα1 and IL-2Rγ via qRT-PCR were investigated. Heat-killed bacteria upregulated JAK1, JAK3 and IL-4Rα on LCs (see Figure 3.6 A). However, flow cytometry analysis did not show significant changes of IL-4Rα, IL-13Rα1 and IL-2R. This shows that heat-killed bacteria only influence JAK family but not type I or type II cytokine receptors.

3.1.7 LCs release proinflammatory chemokines and inflammatory cytokines upon heat-killed bacteria stimulation

To investigate the cytokine or chemokines production of LCs upon heat-killed bacteria stimulation, qRT-PCR on *S.a.* and *S.e.* stimulated LCs was performed to check expression of CCL13, CCL17, CCL22, IL-6, IL-10, IL-23, TNFα, TGFβ, IFN-γ and AHR. Both heat-killed bacteria instructed LCs to release large amounts of CCL22, IL-6 and IL-23, as well as considerable amounts of TNFα, TGFβ and AHR. Compared to heat-killed *S.e., S.a.* led to higher secretion of CCL13, IL-23, IL-10 and IFN-γ (see Figure 3.7).

To validate our findings at the protein level, flow cytometry bead-based ELISA in the supernatants after 24h stimulation was performed. The heat map in Figure 3.8 A visualizes differentially expressed protein level in the supernatants released by unstimulated LCs, heat-killed *S.a.*- and *S.e.*-stimulated LCs. Our ELISA data shows that both heat-killed *S.a.* and *S.e.* stimulated LCs secrete high levels of proinflammatory chemokines such as CXCL1, CXCL5, CXCL9, IP-10 (CXCL10), CXCL11, CCL2, CCL4, CCL5, CCL11 and CCL20 as well as inflammatory cytokines such as IFN-α2, IL-1β, IL-10, IL-12p70, IL-18 and TNF-α. Interestingly, heat-killed *S.a.*-stimulated LCs release even higher amounts of chemokines and cytokines than *S.e.*-stimulated LCs except for CXCL5, IL-10 and IL-18. Heat-killed *S.e.*-, but not *S.a.*-stimulated LCs showed a moderate secretion of CCL17 (see Figure 3.8 B). The levels of CCL3, IFN-γ, IL-6, IL-8, IL-17A, IL-23 and IL-33 were investigated, but they were below the detection limit of the method (data not shown). In summary, both heat-killed *S.a.*- and heat-killed *S.e.*-stimulated LCs secreted high levels of proinflammatory chemokines and inflammatory cytokines, with only subtle differences.

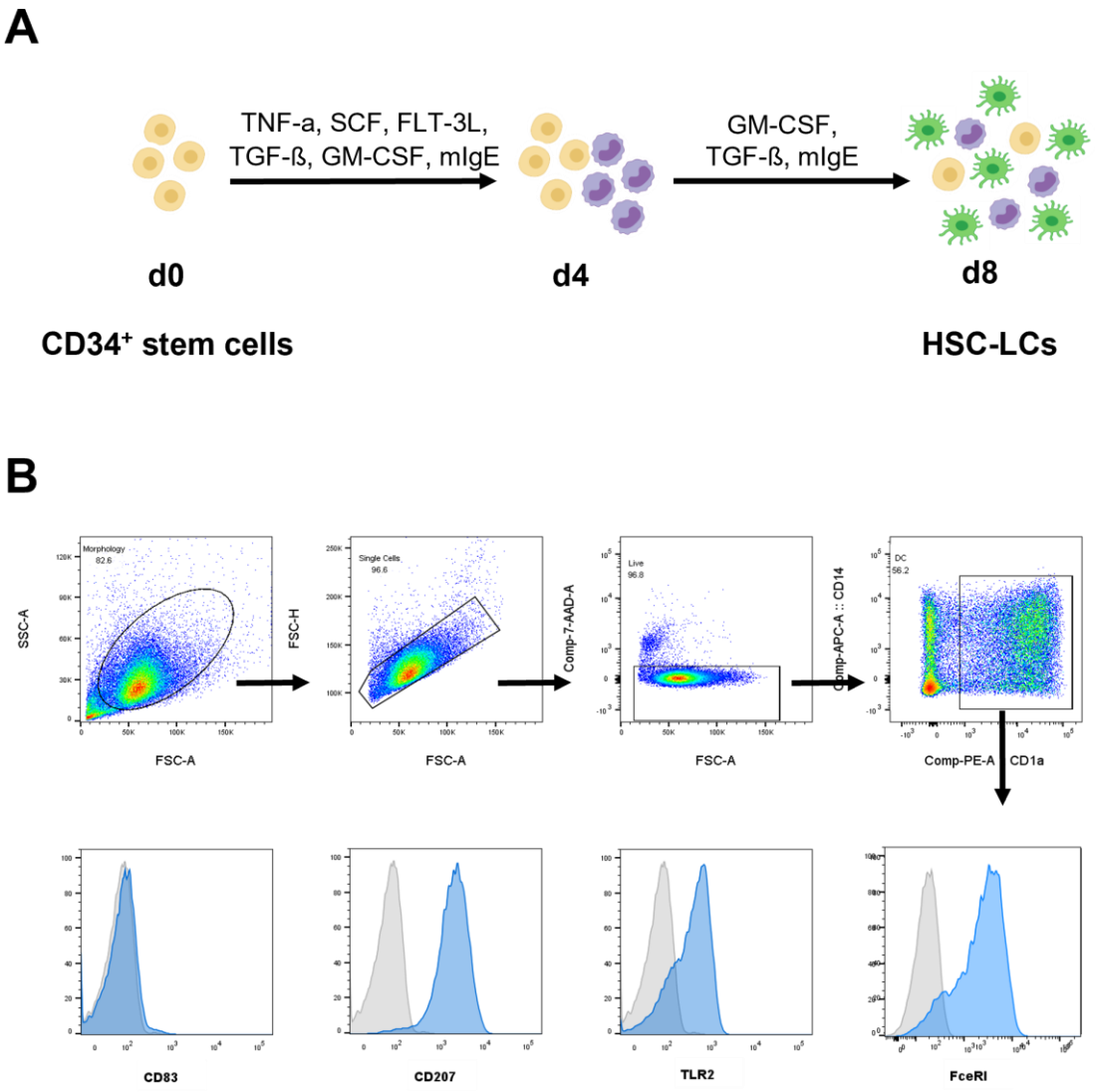

Figure 3.1 *In vitro* generated LCs are CD207$^+$CD1a$^+$TLR2$^+$FcεRI$^+$LCs with immature phenotype.
(A) CD34$^+$ HSCs were differentiated into HSC-LCs during 8 days in culture. (B) Viable cells were stained with anti-CD83 (blue), anti-CD207 (blue), anti-TLR2 (blue), anti-FcεRI (blue), anti-IgG2b (grey) as isotype control and were counterstained with FITC-labeled goat anti-mouse IgG.

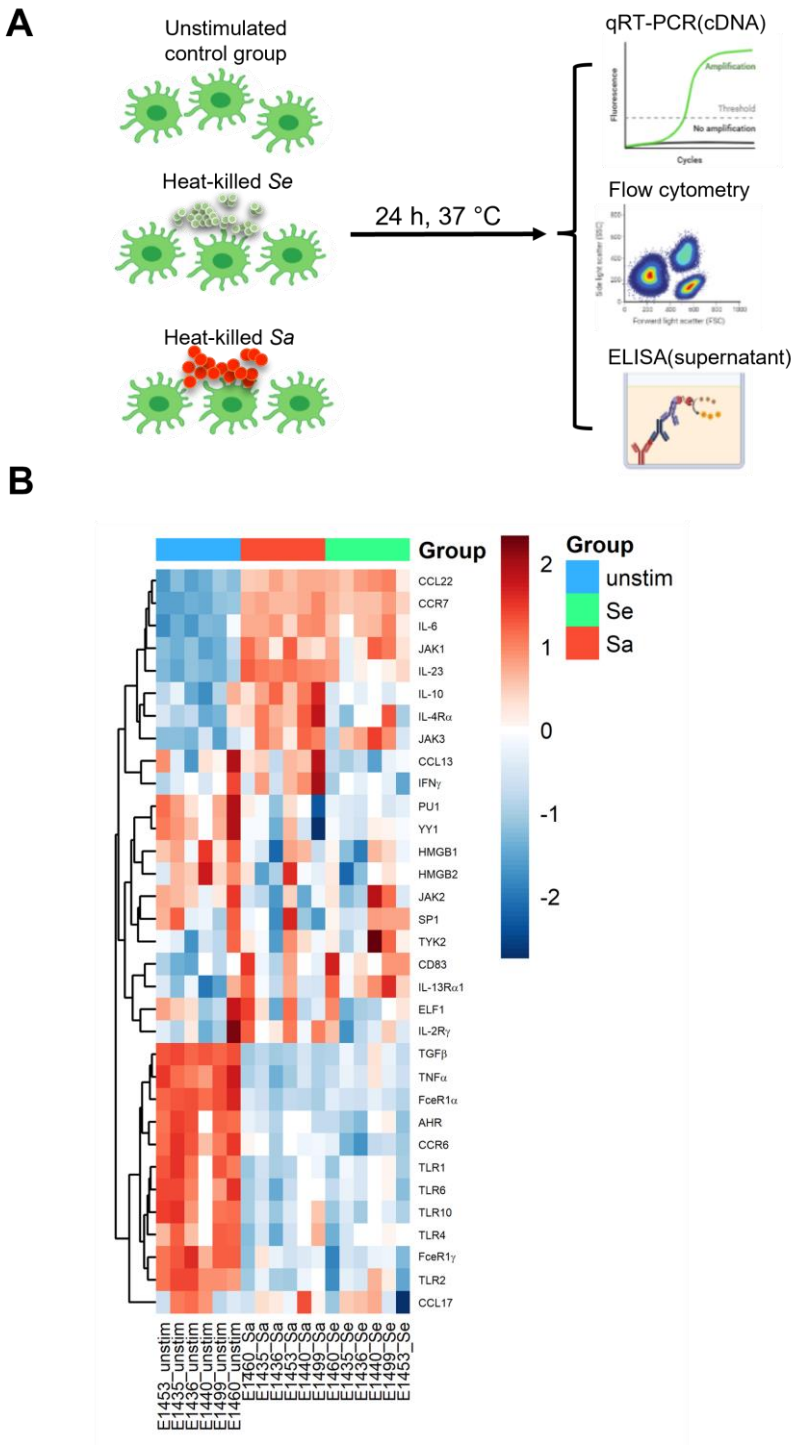

Figure 3.2 LCs strongly respond to heat-killed bacteria stimulation.
(A) Workflow of Study 1. *In vitro* generated day-8 LCs were exposed to heat-killed *S.e.*, heat-killed *S.a.* or sham-treated. Day-9 LCs were harvested for analysis via qRT-PCR or flow cytometry. Supernatants from each condition were collected for ELISA. (B) After 24h heat-killed bateria stimulation, cells were analyzed via cDNA microarray. Heat map visualizes differentially expressed genes among unstimulated LCs (blue), heat-killed *S.a.* stimulated LCs (red) and heat-killed *S.e.* stimulated LCs (green). Colors represent high (red) and low (blue) expression intensity (n=6).

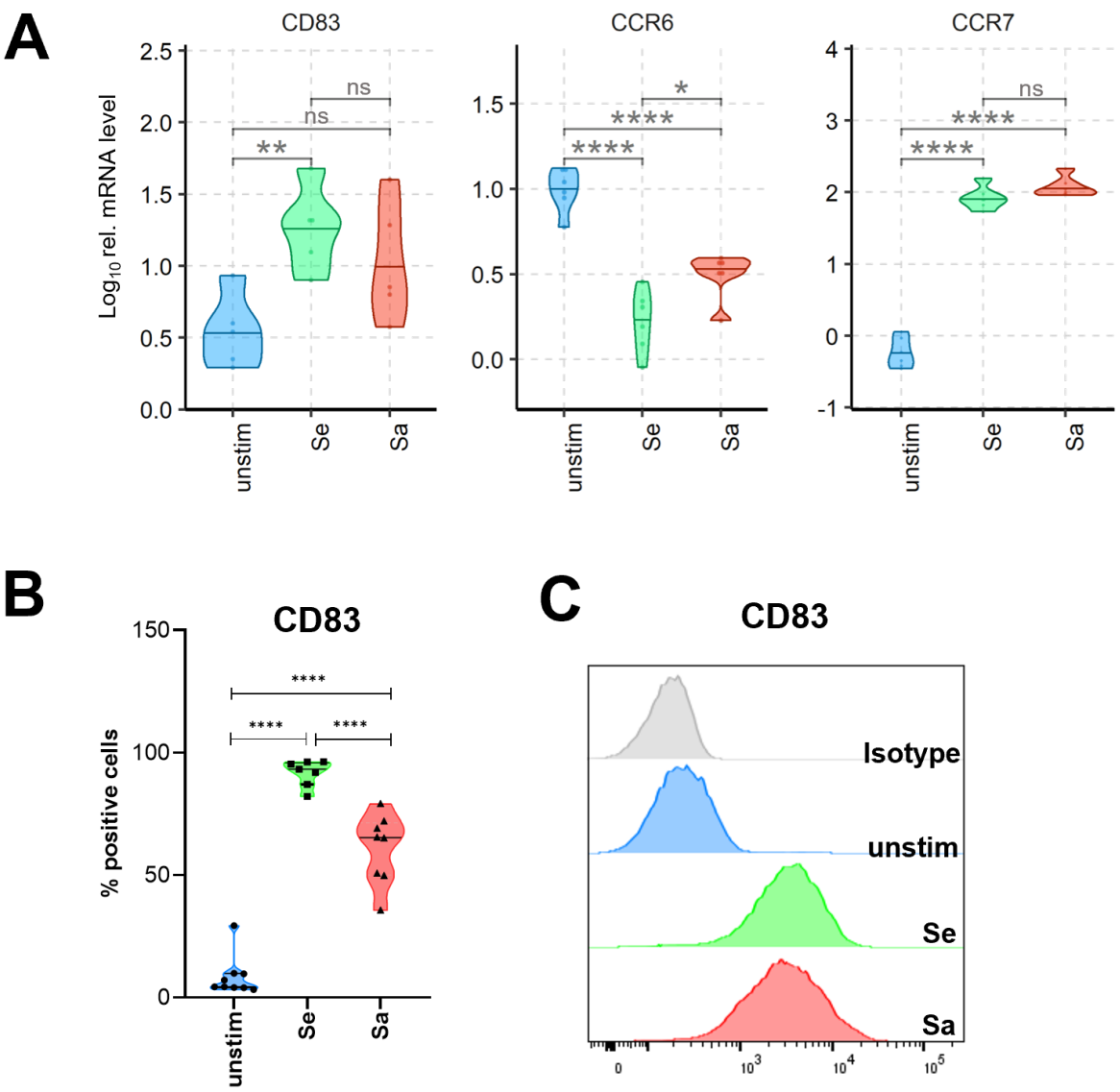

Figure 3.3 Heat-killed bacteria stimulation induces LC maturation.
(A) Day-9-stimulated LCs were harvested for qRT-PCR. Values were normalized to per 10^3 actin (n=6, ±SD). (B) CD83 surface expression of day-9-stimulated LCs were analyzed via flow cytometry. Violin plots shows percentage of CD83 positive cells gated on $CD1a^+CD207^+$LCs and median. Heat-killed *S.a.* (red), heat-killed *S.e.* (green) or unstimulated (blue). One-way-ANOVA, N=7-9, each dot represents one donor. (C) Result of one representative experiment is shown for CD83 of flow cytometry offset histograms.

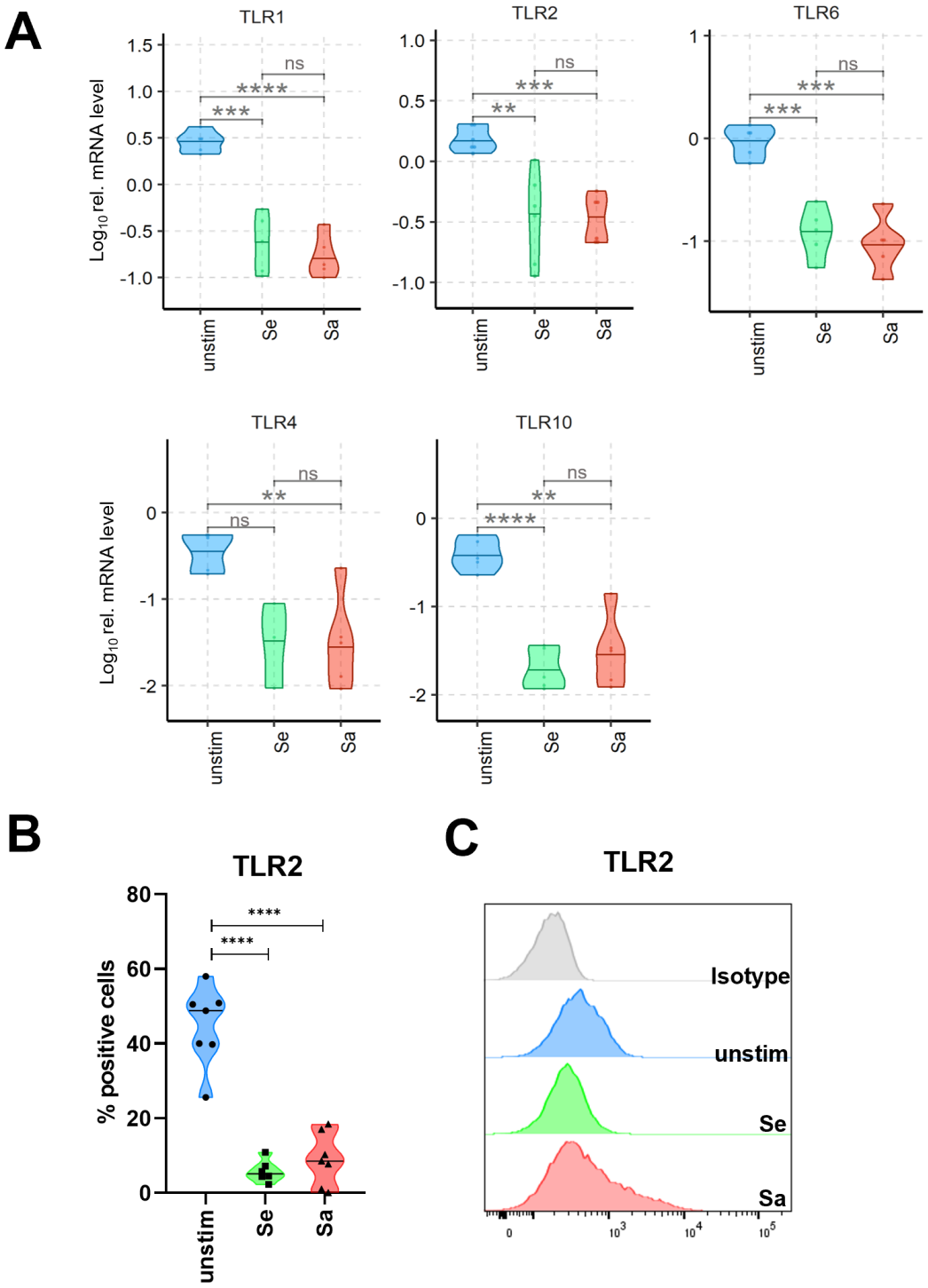

Figure 3.4 Heat-killed bacteria stimulation downregulates TLRs on LCs.
(A) Day-9-stimulated LCs were harvested for qRT-PCR. Values were normalized to per 10^3 actin (n=6, ±SD). (B) TLR2 surface expression of day-9 stimulated LCs was analyzed by flow cytometry. Violin plots show percentage of TLR2 positive cells gated on $CD1a^+CD207^+$LCs, stimulated by either heat-killed *S.a.* (red), heat-killed *S.e.* (green) or were sham-treated (blue). One-way-ANOVA, N=7-9, each dot represents one donor, line is median. (C) Representative histogram of TLR2 expression.

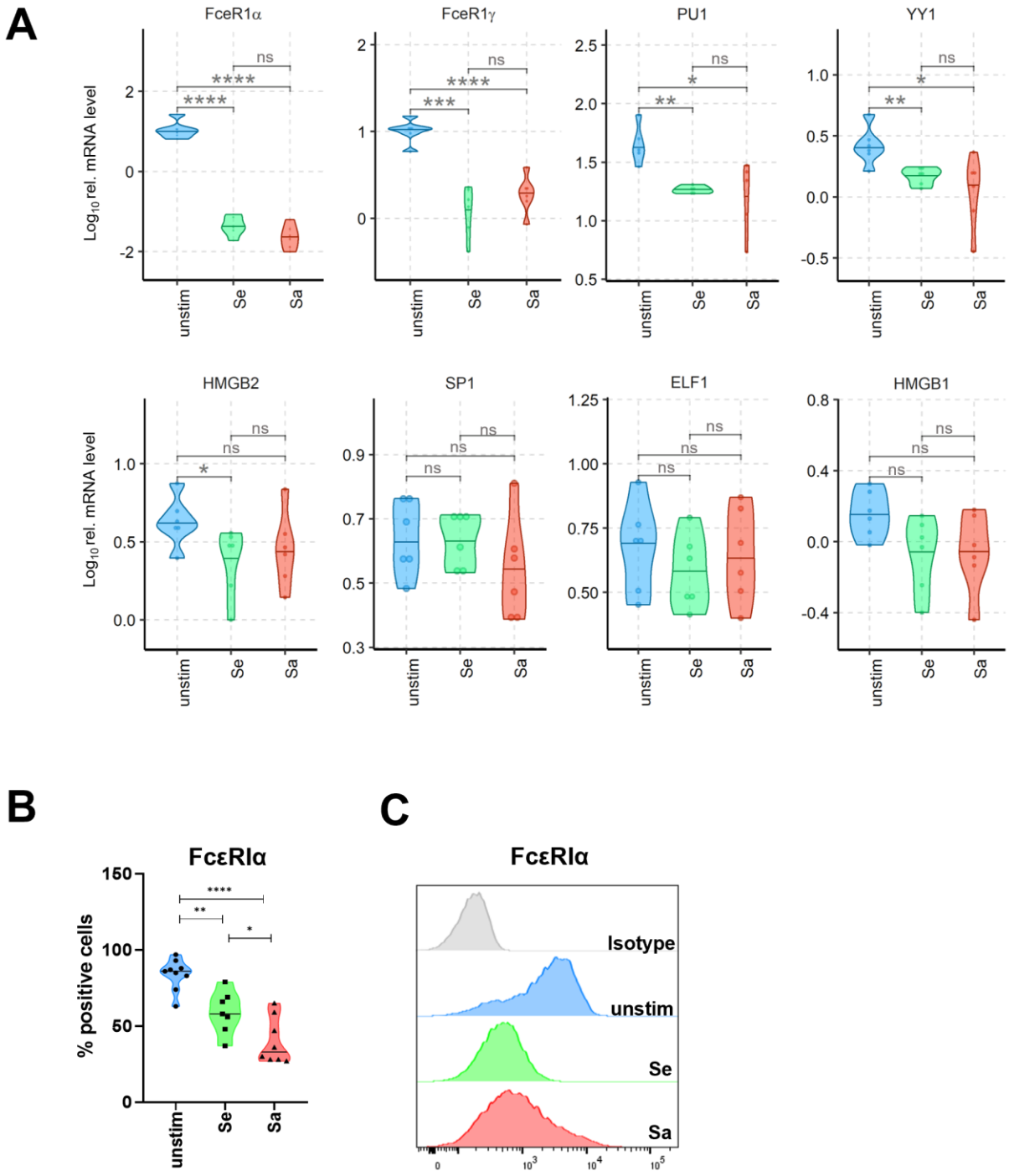

Figure 3.5 Heat-killed bacteria stimulation downregulates FcεRI on LCs.
(A) Day-9-stimulated LCs were harvested for qRT-PCR. Values were normalized to per 10^3 actin (n=6, ±SD). (B) FcεR1α surface expression of day-9-stimulated LCs was analyzed by flow cytometry. Violin plots show percentage of FcεR1α positive cells, gated on $CD1a^+CD207^+$LCs, stimulated by either heat-killed *S.a.* (red), heat-killed *S.e.* (green) or were sham-treated (blue). One-way-ANOVA, N=7-9, each dot represents one donor, line is median. (C)Representative histogram of FcεR1α expression.

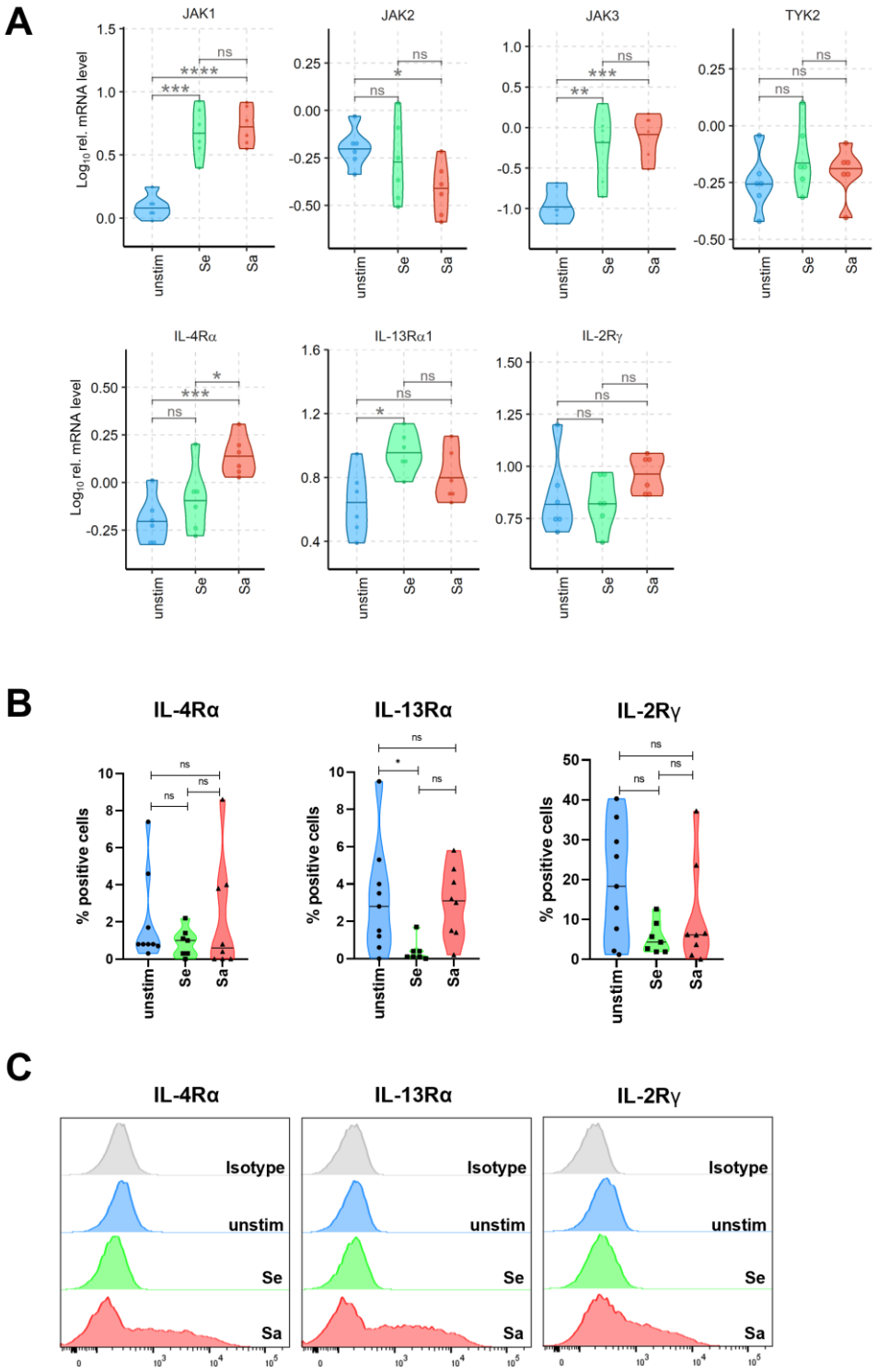

Figure 3.6 Heat-killed bacteria stimulation upregulates JAK1 and JAK3 on LCs. (A) Day-9-stimulated LCs were harvested for qRT-PCR. Values were normalized to per 10^3 actin (n=6, ±SD). (B) IL-4Rα, IL-13Rα1 and IL-2Rγ surface expression of day-9-stimulated LCs was analyzed by flow cytometry. Violin plots show percentage of positive cells, gated on $CD1a^+CD207^+$LCs, stimulated by either heat-killed *S.a.* (red), heat-killed *S.e.* (green) or were sham-treated (blue). One-way-ANOVA, N=7-9, each dot represents one donor, line is median. (C) Representative histograms corresponding to (B).

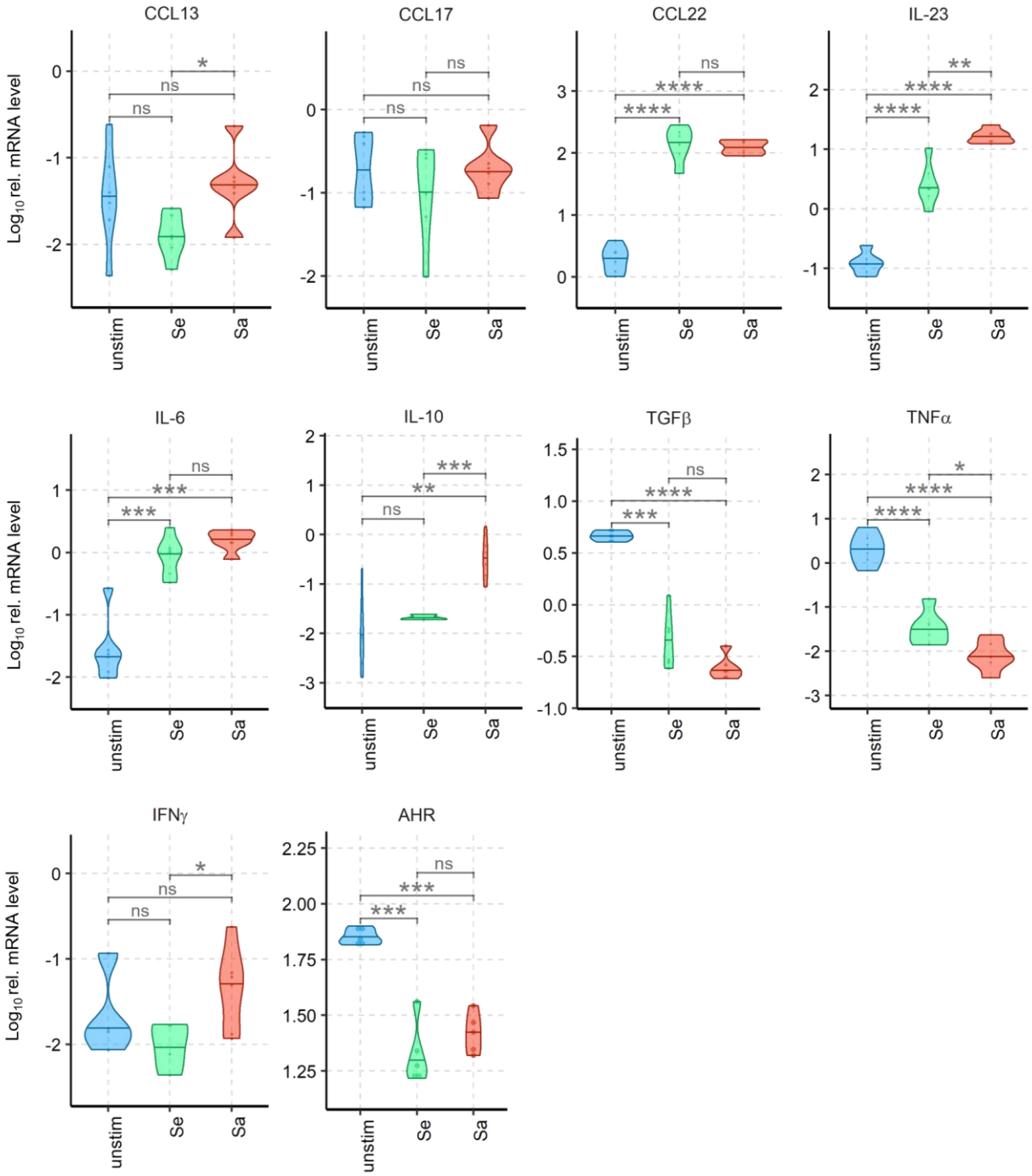

Figure 3.7 Heat-killed bacteria stimulation instructs LCs with inflammatory gene expression profile.
Day-9-stimulated LCs were harvested for qRT-PCR. Values were normalized to per 10^3 actin (n=6, ±SD). LCs were stimulated by either heat-killed *S.a.* (red), heat-killed *S.e.* (green) or were sham-treated (blue). One-way-ANOVA, N=6, each dot represents one donor, line is median.

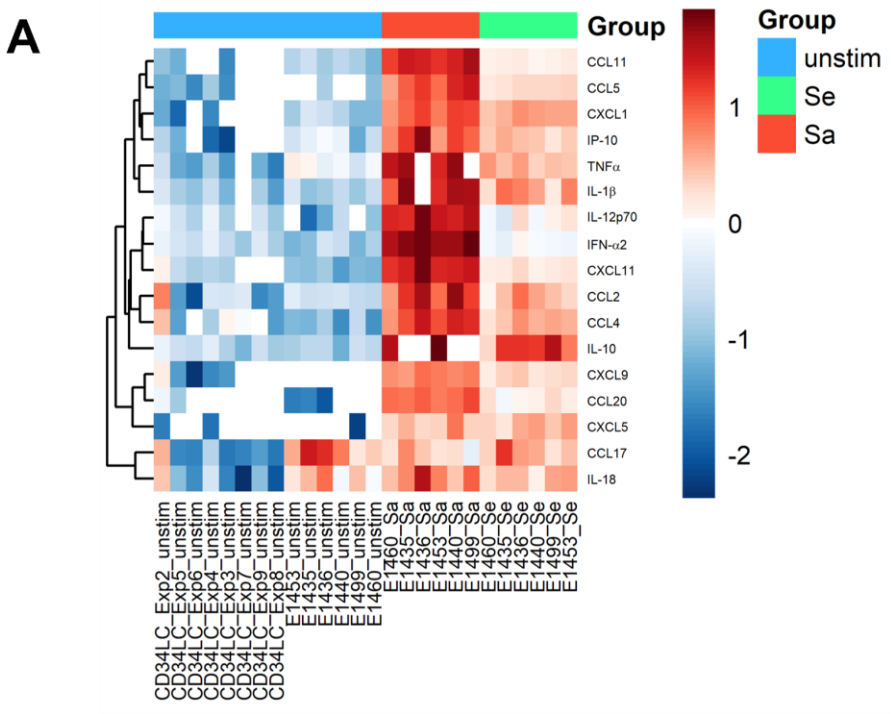
A
Group
unstim
Se
Sa
1
0
-1
-2
CCL11
CCL5
CXCL1
IP-10
TNFα
IL-1β
IL-12p70
IFN-α2
CXCL11
CCL2
CCL4
IL-10
CXCL9
CCL20
CXCL5
CCL17
IL-18
CD34LC_Exp2_unstim
CD34LC_Exp5_unstim
CD34LC_Exp6_unstim
CD34LC_Exp4_unstim
CD34LC_Exp3_unstim
CD34LC_Exp7_unstim
CD34LC_Exp9_unstim
CD34LC_Exp8_unstim
E1453_unstim
E1435_unstim
E1436_unstim
E1440_unstim
E1499_unstim
E1460_unstim
E1460_Sa
E1435_Sa
E1436_Sa
E1453_Sa
E1440_Sa
E1499_Sa
E1460_Se
E1435_Se
E1436_Se
E1440_Se
E1499_Se
E1453_Se

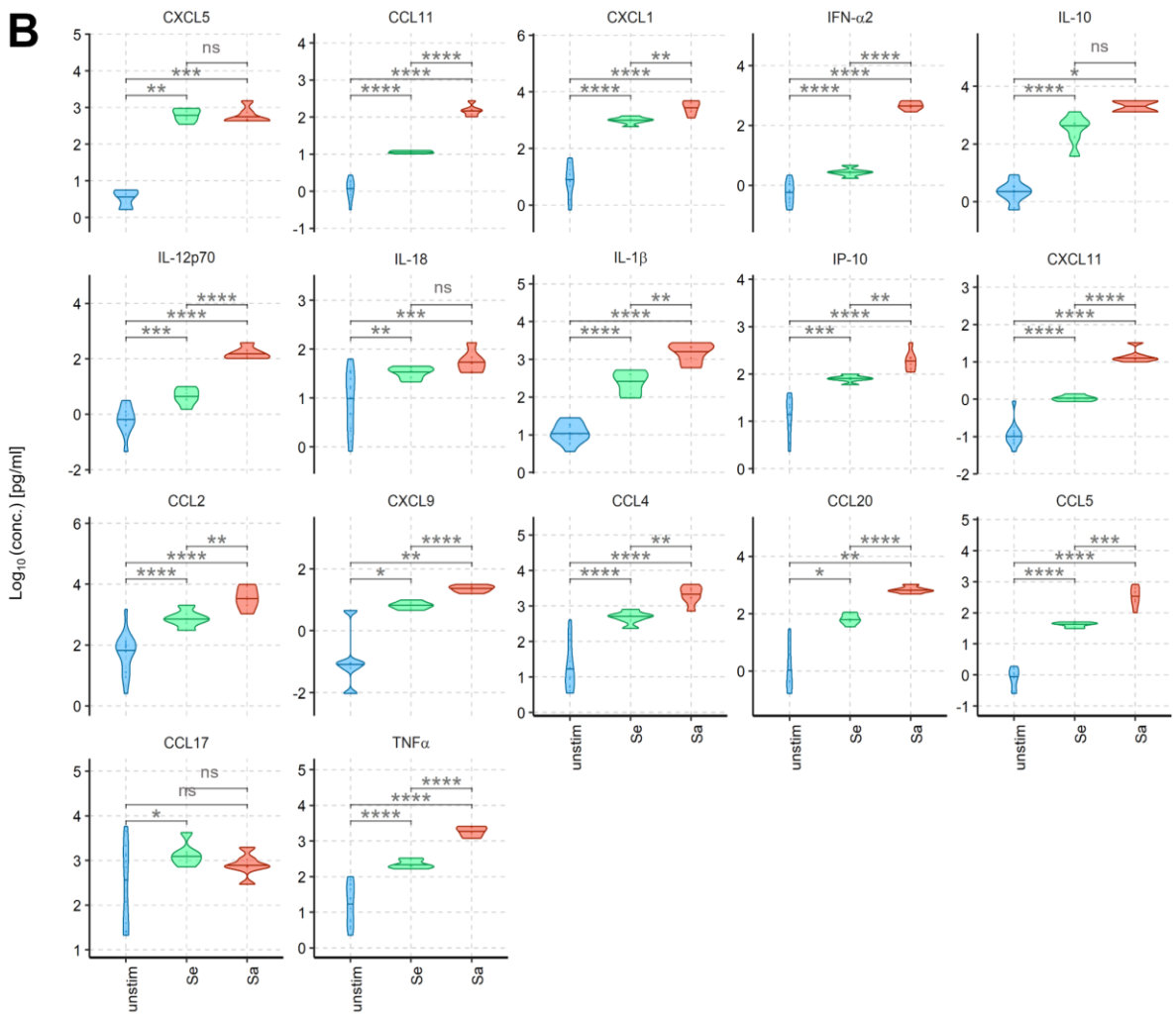
B
Log10 (conc.) [pg/ml]
CXCL5
CCL11
CXCL1
IFN-α2
IL-10
IL-12p70
IL-18
IL-1β
IP-10
CXCL11
CCL2
CXCL9
CCL4
CCL20
CCL5
CCL17
TNFα
unstim
Se
Sa
ns

Figure 3.8 LCs release proinflammatory chemokines and inflammatory cytokines upon heat-killed bacteria stimulation.
After 24h heat-killed bateria stimulation, supernatants were collected for flow cytometry bead-based ELISA. CCL3, IFN-γ, IL-6, IL-8, IL-17A, IL-23 and IL-33 were analyzed but below detection limit, data are not shown here. (A) Differentially expressed proteins in the supernatants released by unstimulated LCs (blue), heat-killed *S.a.* stimulated LCs (red) and heat-killed *S.e.* stimulated LCs (green). Colors represent high (red) and low (blue) expression intensity (n=6). (B) LCs were stimulated by either heat-killed *S.a.* (red), heat-killed *S.e.* (green) or were sham-treated (blue). One-way-ANOVA, N=6, each dot represents one donor, line is median.

3.2 Study 2: LCs stimulated with TLR ligands, LPS, P2C, and P3C

TLRs are PRRs, containing an extracellular part with leucin-rich repeats, which allow binding of pathogen-associated molecular patterns. To date, 13 mammalian TLRs have been identified and characterized, namely, TLR1 to TLR13, including TLR1 to TLR11 in human. TLR1, TLR2, TLR4, TLR6 and TLR10 detect extracellular pathogen-associated molecular patterns, while TLR3, TLR7, TLR8 and TLR9 are expressed on endosomal membranes and recognize nucleosides, nucleotides and oligo- and polynucleotides derived from intracellular viral and bacterial pathogens. LCs express those TLRs upon heat-killed bacteria stimulation as shown in Study 1. For ligand binding, TLR2 forms heterodimers with TLR1 and TLR6. TLR1/2 heterodimers recognize triacylated lipopeptide like Pam_3Cys-SKKKK (P3C) while TLR2/6 heterodimers interact with diacylated lipopeptides such as Pam_2Cys-SKKKK (P2C). TLR4 represents the main structure in recognizing LPS from gram-negative bacteria. While synthetic peptides to mimic bacteria in different models have been used and published, the results are controversial. After investigating the effect of heat-killed bacteria, the effect of purified synthetic TLRs ligands was examined on our $CD207^+CD1a^+TLR2^+Fc\varepsilon RI^+$ *in vitro* LCs. In study 2, the same *in vitro* generated LCs were stimulated with different TLRs ligands in order to compare these two models of stimulation.

3.2.1 LCs strongly respond to TLRs ligation

To investigate the synthetic peptide-LC interaction, LCs were stimulated with TLR ligands, i.e., LPS (TLR4 ligand), P2C (TLR2/6 ligand), P3C (TLR1/2 ligand), for 24h in 37°C, 5% CO_2 incubator. Cells from different conditions were harvested for flow cytometry and qRT-PCR analysis. Supernatants were collected for ELISA. (Experimental workflow shown in Figure 3.9 A). For the gene expression experiments, the same 33 genes (as in Study 1) related to AD pathogenesis were checked so that the data was comparable. As expected, LCs strongly responded to TLR ligations as shown in the heatmap in Figure 3.9 B. LPS, P2C and P3C stimulated LCs showed increased expression of CCL22, CCR7, JAK1, JAK3, CD83, IL-6 (upper block), but reduced expression of FcεRIα, TGFβ, CCR6, TNFα, FcεRIγ, TLR1, TLR2, PU1 and YY1 (lower block).

3.2.2 TLRs ligation induces LCs maturation

Day-9-stimulated LCs were harvested for gene expression experiments. Relative expression level of CD83, CCR6, CCR7 were determined with qRT-PCR. Values were normalized to per 10^3 actin. Upon TLRs ligation, LCs matured/activated as shown by upregulation of CD83, CCR7 and downregulation of CCR6 (see Figure 3.10 A). CD83 upregulation was confirmed by flow cytometry (see Figure 3.10 B and C). Interestingly, P2C- and P3C-stimulated LCs displayed on protein level significantly higher CD83 expression than LPS-stimulated LCs. This finding shows that all these purified and synthesized TLRs ligands induced LC maturation, activation, and migration.

3.2.3 TLRs ligation downregulates TLRs on LCs

To further investigate TLRs, day-9-stimulated LCs were harvested for gene expression experiments. Relative expression level of TLR1, TLR2, TLR4, TLR6 and TLR10 was determined with qRT-PCR. Values were normalized to per 10^3 actin. All TLRs ligands induced downregulation of TLR4, but only P2C- and P3C-stimulated LCs led to a decrease expression of TLR1, TLR2, TLR6. No significance was found for TLR10 (see Figure 3.11 A). TLR2 downregulation was confirmed by flow cytometry (see Figure 3.11 B and C). These findings show that synthetic peptides are sufficient to ligate TLRs and induce LC response.

3.2.4 TLRs ligation downregulates FcεRI on LCs

As in Study 1, qRT-PCR analysis of FcεR1α, FcεR1γ and their related transcription factors PU1, YY1, HMGB1, HMGB2, SP1, ELF1 was performed in day-9-TLR ligands-stimulated *in vitro* LCs. FcεRI expression was significantly downregulated on transcriptional levels upon TLR ligation. Only P2C- and P3C-stimulated LCs showed decreased expression of PU1 and YY1. Only P3C-stimulated LCs displayed a reduced expression of ELF1. No significance in gene expression was observed for HMGB1, HMGB2 and SP1 (see Figure

3.12 A). FcεR1α surface expression was only downregulated in P3C-stimulated LCs. This finding shows that FcεR1α is functional upon TLR ligation, especially P3C.

3.2.5 TLRs ligation upregulates JAKs on LCs

To investigate the effect of TLR ligation on the JAK family in LCs, qRT-PCR on JAK1, JAK2, JAK3, TYK2, IL-4Rα, IL-13Rα1 and IL-2Rγ was performed. All TLR ligations upregulated JAK1, JAK 2, JAK3. Both P2C- and P3C-stimulated LCs displayed increased expression of TYK2. Only P3C-stimulated LCs showed increased expression of IL-13Rα1 (see Figure 3.13 A). Flow cytometry analysis did not show significant changes of IL-4Rα, IL-13Rα1 and IL-2Rγ. This indicates that TLR ligands only influence JAK family but not type I or type II cytokine receptors.

3.2.6 LCs release proinflammatory chemokines and inflammatory cytokines upon TLRs ligation

To investigate the cytokine and chemokines production of LCs upon TLR ligation, the gene expression of day-9-stimulated LCs was checked. Relative expression level of CCL13, CCL17, CCL22, IL-6, IL-10, IL-23, TNFα, TGFβ, IFN-γ, AHR were determined with qRT-PCR. All three TLR-ligands-instructed LCs released a high amount of CCL22. Both P2C- and P3C-stimulated LCs showed increased secretion of IL-6, TNFα, TGFβ and AHR (see Figure 3.14). To validate findings at the protein level, flow cytometry bead-based ELISA in supernatants after 24h stimulation was performed. The heat map visualizes differentially expressed proteins in supernatants released by LPS-, P2C- and P3C-stimulated LCs (see Figure 3.15 A). All stimulated LCs secreted high levels of proinflammatory chemokines such as CXCL1, IP-10 (CXCL10), CCL2, CCL3, CCL4, CCL5, CCL17 as well as inflammatory cytokines such as IL-1β, IL-10, IL-6, IL-8, IL-18, IL-23 TNF-α. P2C- and P3C-stimulated LCs, but not LPS-stimulated LCs, showed increased secretion of CCL20. Of note, CXCL5, CXCL9, CXCL11, CCL11, IFN-α2, IFN-γ, IL-12p70, IL-17A, and IL-33 were analyzed, but found to be below the detection limit of the assay (data not shown). In summary, TLR ligation through synthetic peptides causes LCs to secrete high levels of proinflammatory chemokines and inflammatory cytokines.

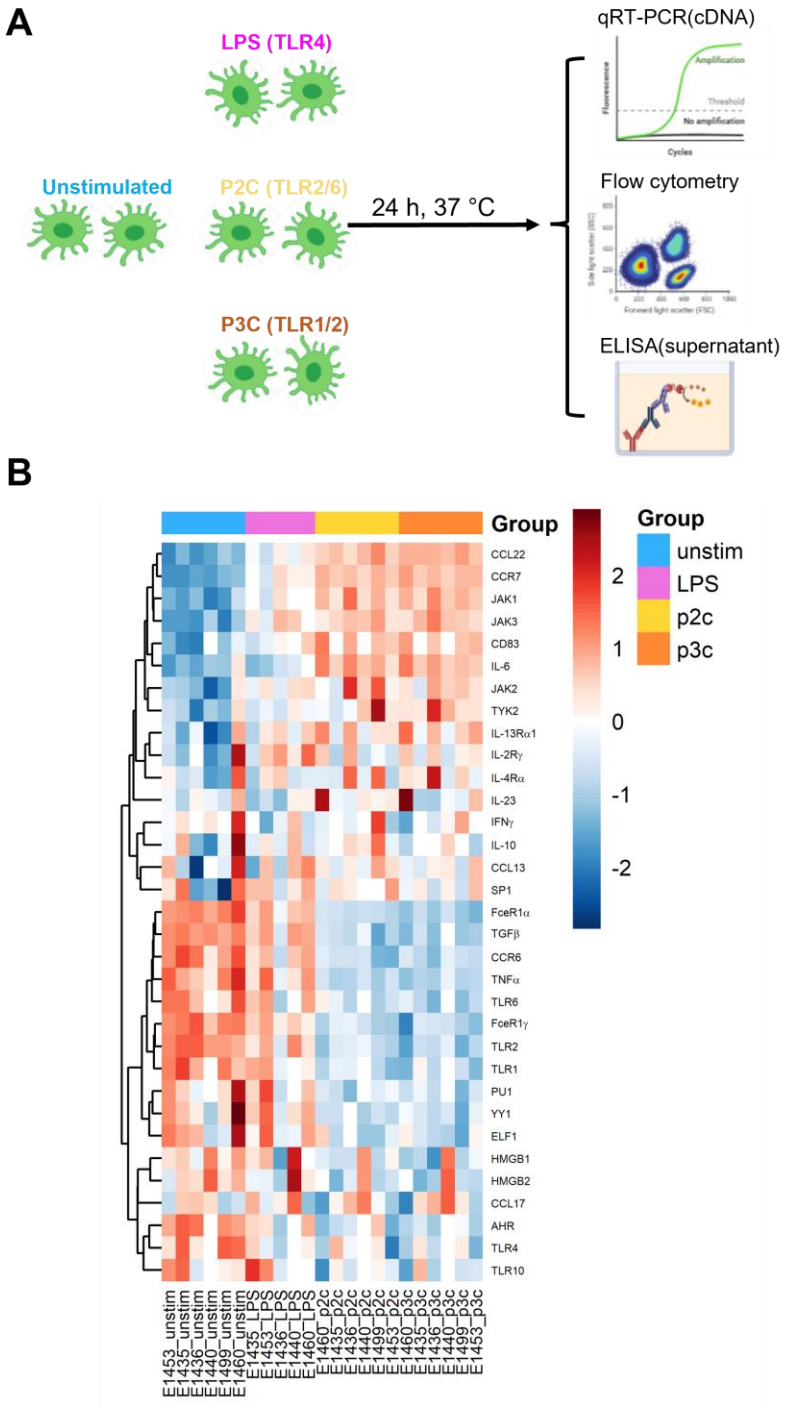

Figure 3.9 LCs strongly respond to TLRs ligation.
(A) Workflow of Study 2. *In vitro* generated day-8 LCs were exposed to LPS (TLR4), P2C (TLR2/6), P3C (TLR1/2) or sham-treated for 24h in 37°C, 5% CO_2. Day-9 cells were harvested for qRT-PCR or flow cytometry experiments. Supernatants from each condition were collected for ELISA. (B) After 24h TLR ligation, cells were analyzed via cDNA microarray analysis. Heat map visualizes differentially expressed genes among unstimulated LCs (blue), LPS stimulated LCs (pink), P2C stimulated LCs (yellow), and P3C stimulated LCs (orange). Colors represent high (red) and low (blue) expression intensity (n=6).

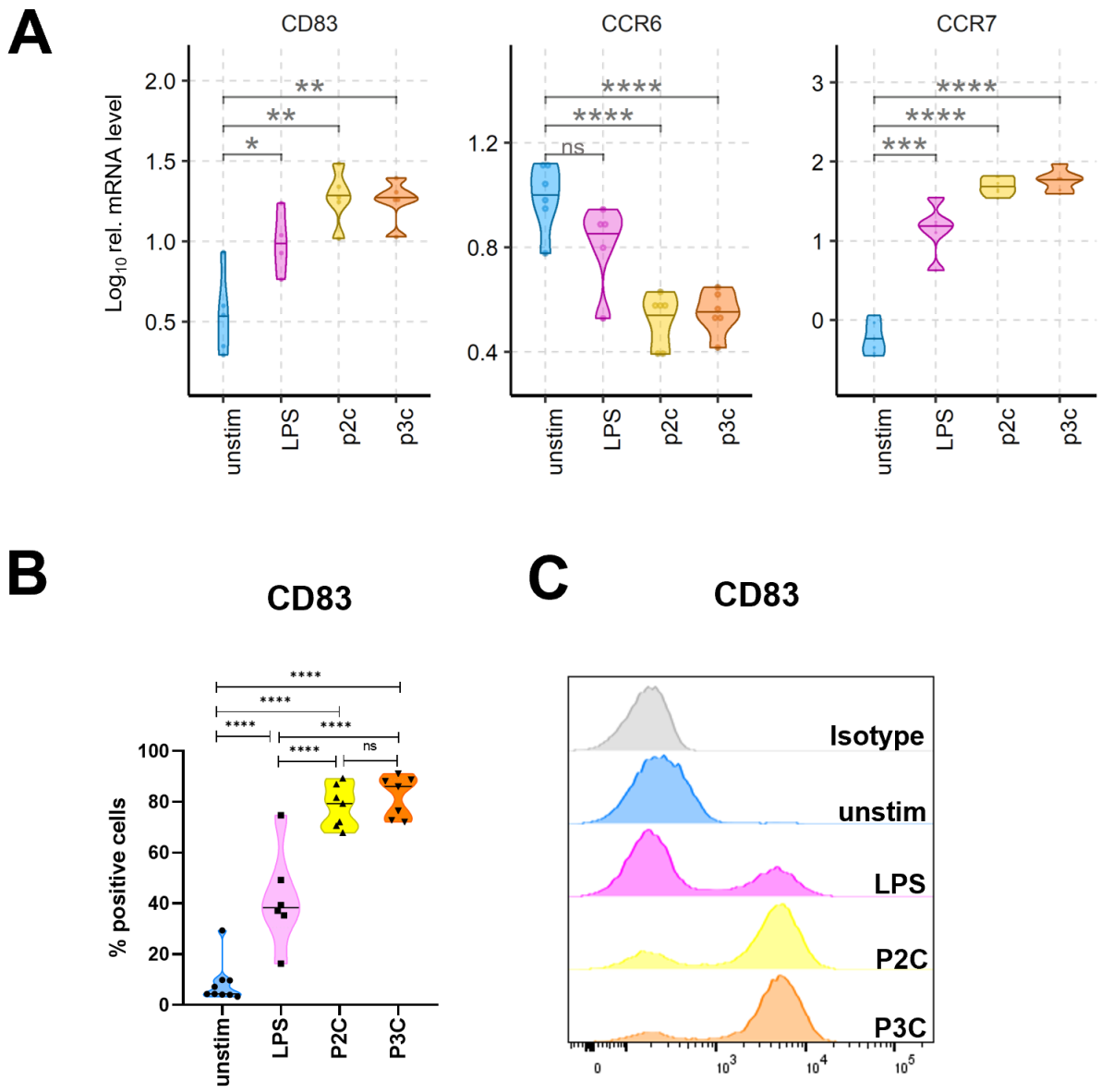

Figure 3.10 TLRs ligation induces LCs maturation.
(A) Day-9-stimulated LCs were harvested for qRT-PCR. Values were normalized to per 10^3 actin (n=6, ±SD). (B) CD83 surface expression was analyzed by flow cytometry.Violin plots shows percentage of CD83 positive cells gated on $CD1a^+CD207^+$LCs, stimulated by LPS (pink), P2C (yellow), and P3C (orange) or were sham-treated (blue). One-way-ANOVA, N=7-9, each dot represents one donor, line is median. (C) Representative histogram of CD83 expression. Isotype control was marked grey.

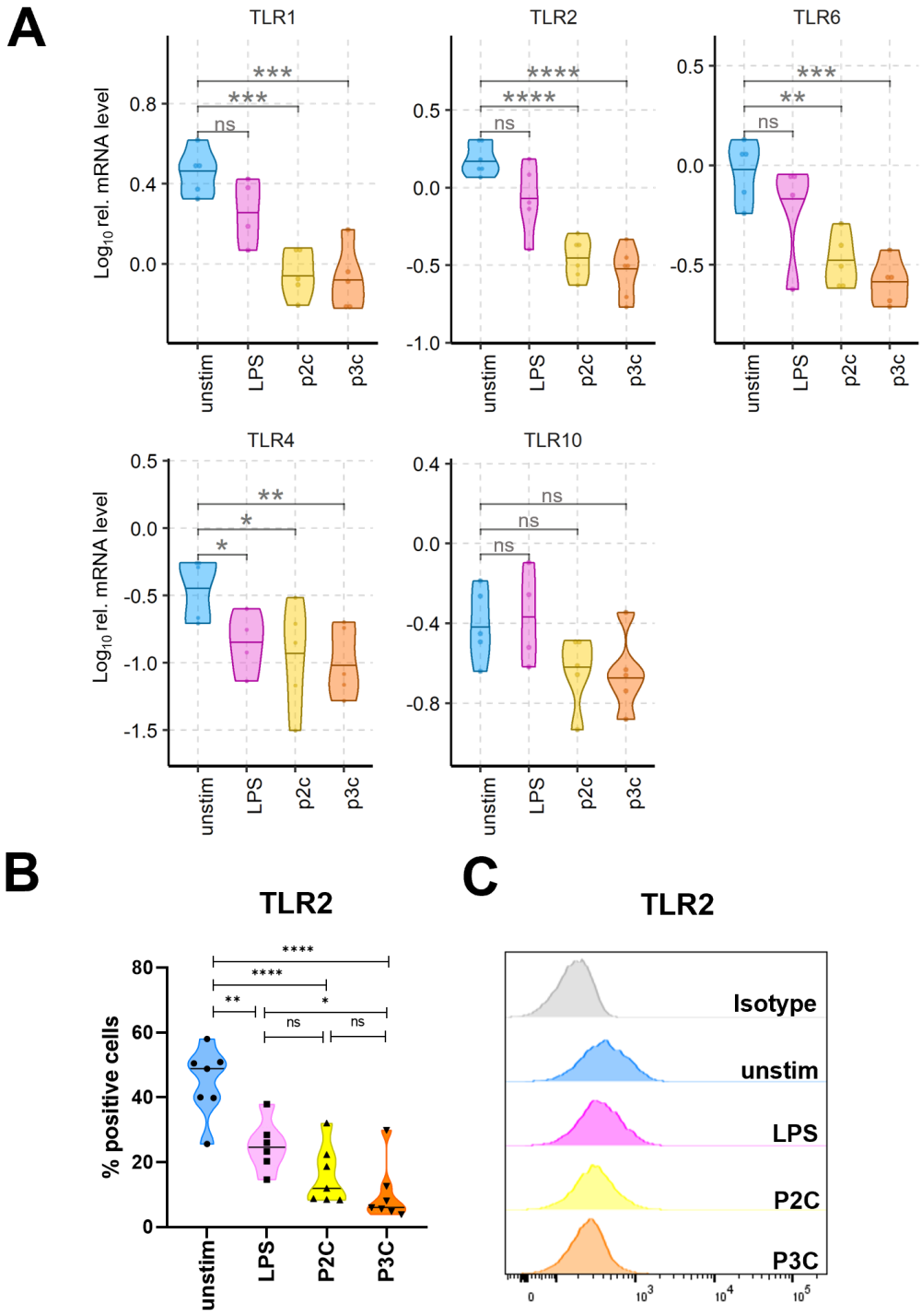

Figure 3.11 TLRs ligation downregulates TLRs on LCs.
(A) Day-9-stimulated LCs were harvested for qRT-PCR. Values were normalized to per 10^3 actin (n=6, ±SD). (B) TLR2 surface expression of day-9-stimulated LCs was confirmed via flow cytometry. Violin plots show percentage of TLR2 positive cells gated on $CD1a^+CD207^+$LCs, stimulated by LPS (pink), P2C (yellow), and P3C (orange) or were sham-treated (blue). One-way-ANOVA, N=7-9, each dot represents one donor, line is median. (C) Representative histogram of TLR2 expression. Isotype control was marked grey.

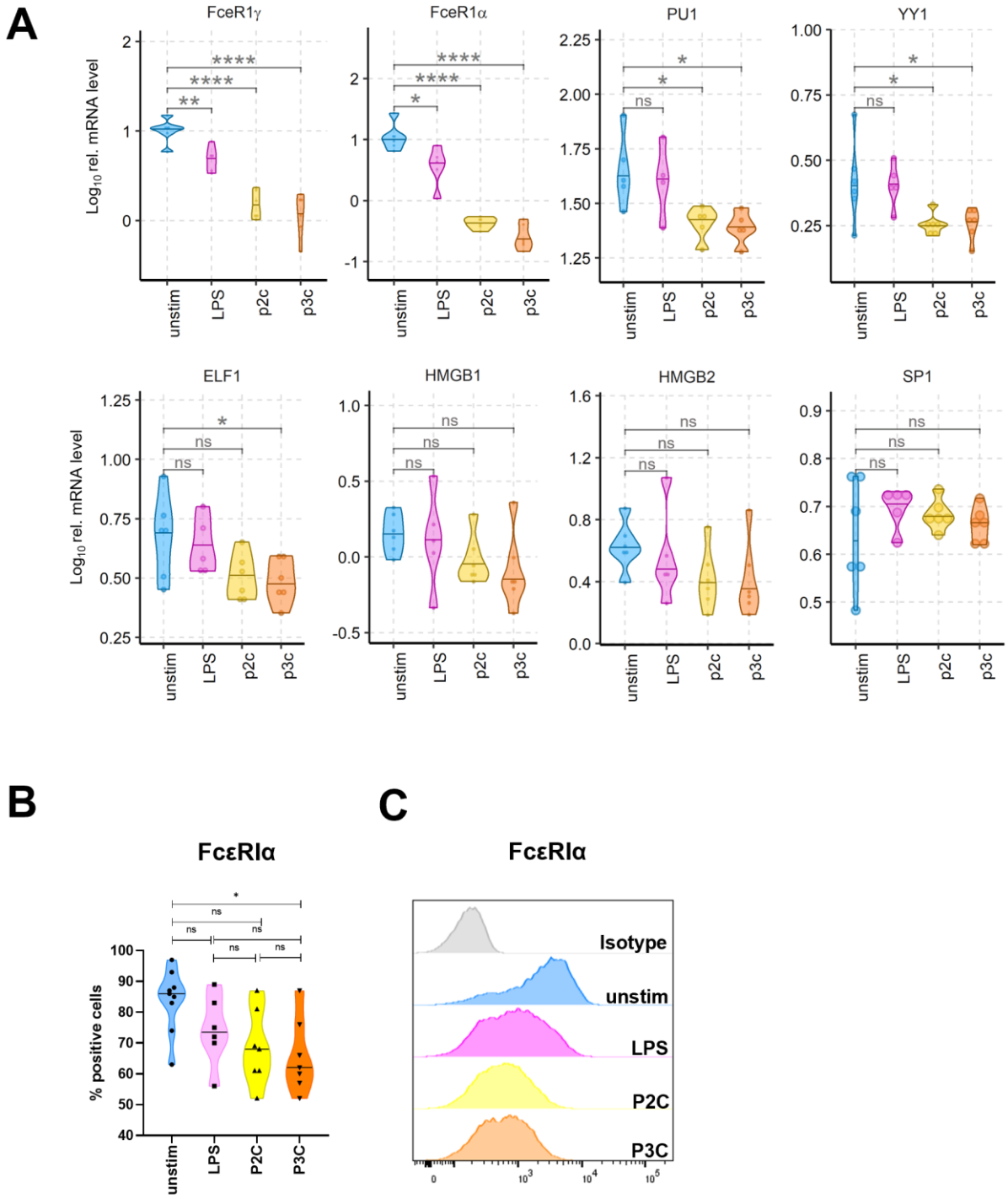

Figure 3.12 TLRs ligation downregulates FcεRI on LCs.
(A) Day-9-stimulated LCs were harvested for qRT-PCR. Values were normalized to per 10^3 actin (n=6, ±SD). (B) FcεR1α surface expression of day-9-stimulated LCs was confirmed via flow cytometry. Violin plots show percentage of FcεR1α positive cells, gated on $CD1a^+CD207^+$LCs, stimulated by LPS (pink), P2C (yellow), and P3C (orange) or were sham-treated (blue). One-way-ANOVA, N=7-9, each dot represents one donor, line is median. (C) Representative histogram of FcεR1α expression. Isotype control was marked grey.

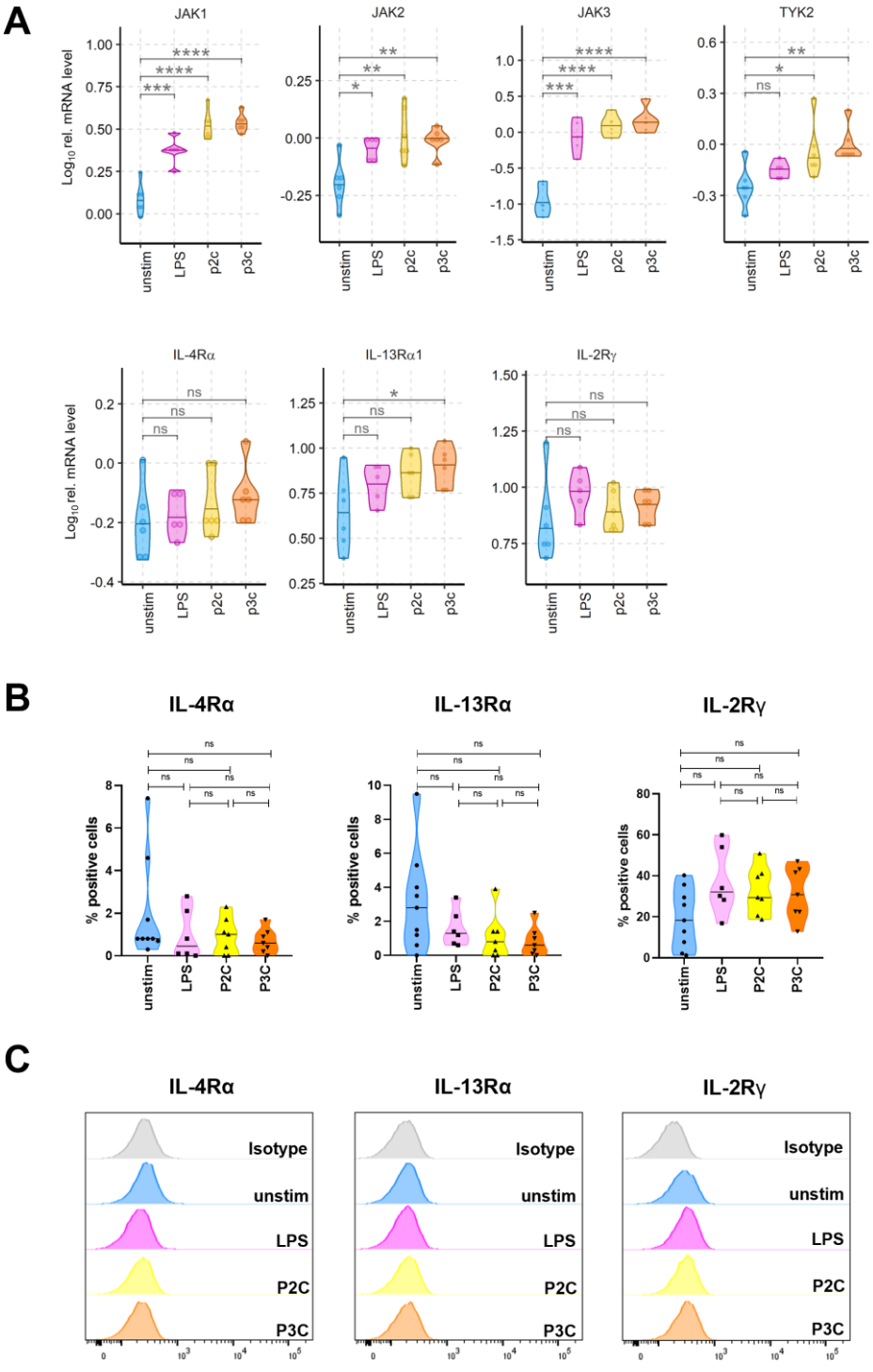

Figure 3.13 TLRs ligation upregulates JAK1 and JAK3 on LCs.
(A) Day-9-stimulated LCs were harvested for qRT-PCR. Values were normalized to per 10^3 actin (n=6, ±SD). (B) IL-4Rα, IL-13Rα1 and IL-2Rγ surface expression were further confirmed via flow cytometry. Violin plots show percentage of IL-4Rα, IL-13Rα1 and IL-2Rγ positive cells, gated on $CD1a^+CD207^+$LCs, stimulated by LPS (pink), P2C (yellow), and P3C (orange) or were sham-treated (blue). One-way-ANOVA, N=7-9, each dot represents one donor, line is median. (C) Representative histograms matching (B) Isotype control was marked grey.

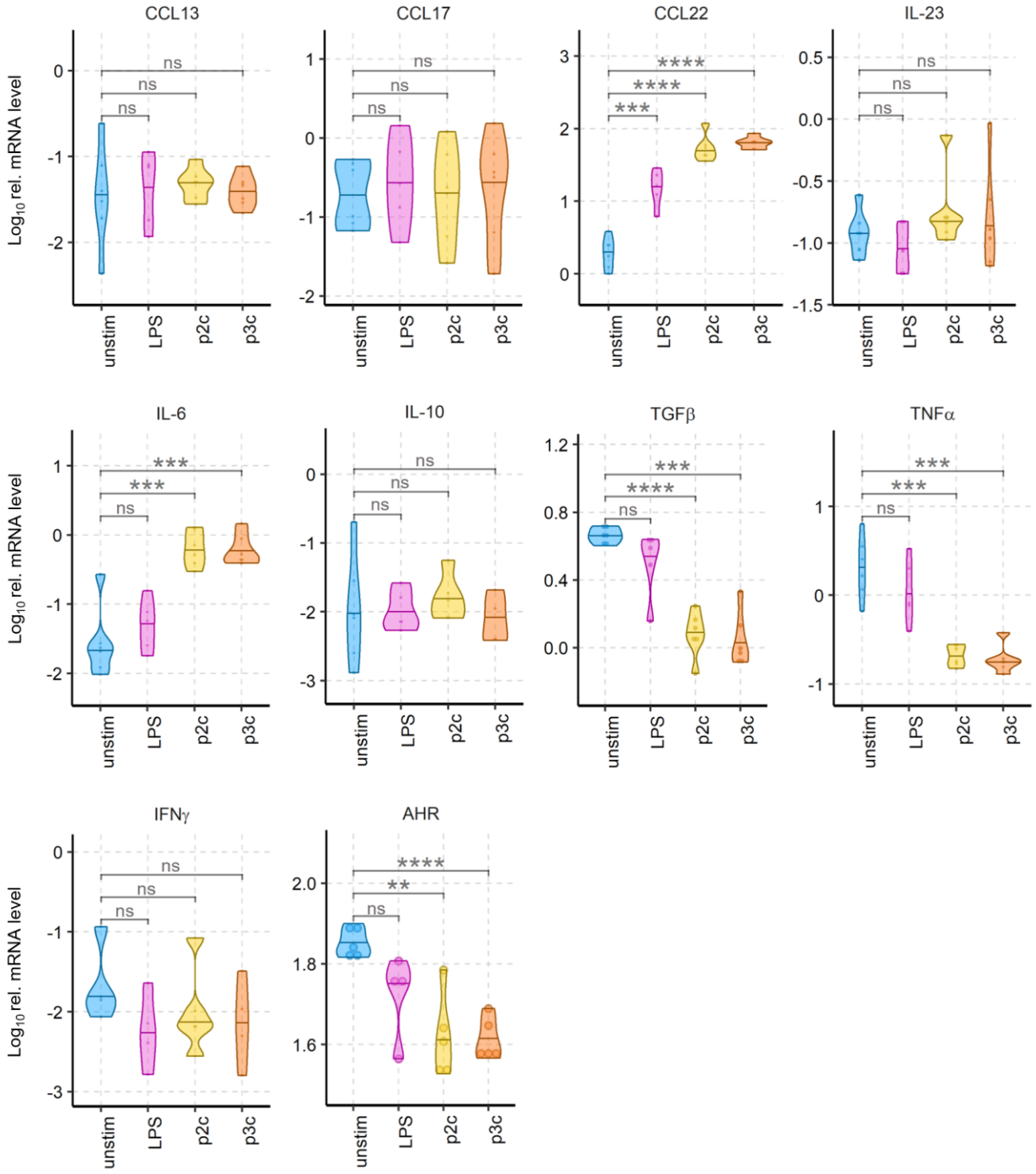

Figure 3.14 TLRs ligation instructs LCs with inflammatory gene expression profile. Day-9-stimulated LCs were harvested for qRT-PCR. Values were analyzed in R software and normalized to per 10^3 actin. One-way-ANOVA, N=6, each dot represents one donor, line is median.

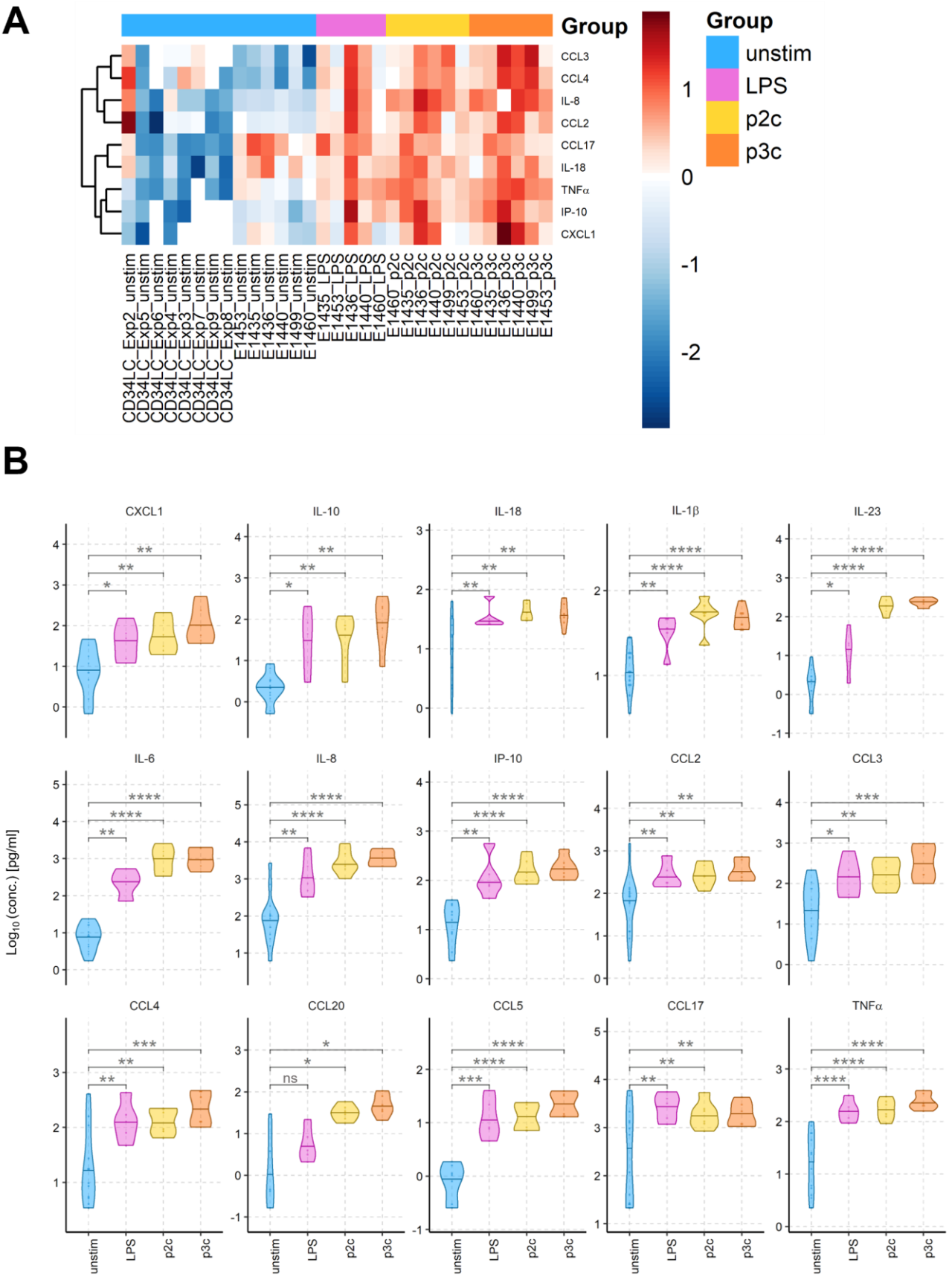
A
Group
unstim
LPS
p2c
p3c
CCL3
CCL4
IL-8
CCL2
CCL17
IL-18
TNFα
IP-10
CXCL1
1
0
-1
-2
CD34LC_Exp2_unstim
CD34LC_Exp5_unstim
CD34LC_Exp6_unstim
CD34LC_Exp4_unstim
CD34LC_Exp3_unstim
CD34LC_Exp7_unstim
CD34LC_Exp9_unstim
CD34LC_Exp8_unstim
E1453_unstim
E1435_unstim
E1436_unstim
E1440_unstim
E1499_unstim
E1460_unstim
E1435_LPS
E1453_LPS
E1436_LPS
E1440_LPS
E1460_p2c
E1435_p2c
E1436_p2c
E1440_p2c
E1499_p2c
E1453_p2c
E1460_p3c
E1435_p3c
E1436_p3c
E1440_p3c
E1499_p3c
E1453_p3c
B
CXCL1
IL-10
IL-18
IL-1β
IL-23
IL-6
IL-8
IP-10
CCL2
CCL3
CCL4
CCL20
CCL5
CCL17
TNFα
Log10 (conc.) [pg/ml]
unstim
LPS
p2c
p3c
ns

Figure 3.15 TLRs ligation triggers release of proinflammatory chemokines and inflammatory cytokines in LCs.
After 24h TLR ligation, supernatants were collected for proinflammatory chemokines and inflammatory cytokines detection using flow cytometry bead-based immunoassays. CCL11, CXCL5, CXCL9, CXCL11, IL-12p70, IFN-α2, IFN-γ, IL-17A, IL-33 are analyzed but are below detection limit. (A) Heat map visualizes differentially expressed cytokines among LCs stimulated by LPS (pink), P2C (yellow), and P3C (orange) or were sham-treated (blue). Colors represent high (red) and low (blue) expression intensity (n=6). (B) Violin plots of cytokines from (A). One-way-ANOVA, N=5-14, each dot represents one donor, line is median.

3.3 Study 3: LCs stimulated with live *S.a.* and live *S.e.*

In the first and second study, both heat-killed bacteria and TLR ligation by synthetic peptides can influence LCs significantly in their phenotype and function. However, these stimuli do not represent the real-world situation, like live microbiome interaction on human skin. Thus, in our third study, the live bacteria-host immune cell response was investigated, specifically the interaction between live *S.a.* or live *S.e.* and LCs. As it shown in Figure 3.16, in-vitro generated day-8 LCs were exposed to live *S.a.* or *S.e.* for 1h, 2h, 3h, at 37°C, 5% CO_2 for direct live imaging, followed by flow cytometry analysis of LCs phenotype. Finally, live bacteria-primed LCs were co-cultured with naïve $CD4^+$ T cells to investigate the downstream effects on the adaptive immune response. Here, again bead-based ELISA was used to analyze secreted chemokines or cytokines in the supernatants.

3.3.1 In live co-culture, *S.a.*, but not *S.e.*, leads to cell death in LCs

In vitro generated day-8 LCs were exposed to live *S.a.* for live imaging. LC reacted to the presence of *S.a.* within 10 min, maturing and activating (see Figure 3.17). However, LCs show rapid cell death, most likely due to toxins released by *S.a.*. Time-dependent death of LCs was also confirmed via flow cytometry analysis: After 1h, viability of LCs dropped to 80%, after 2h to 50% and after 3h to 20% (data not shown here).

In vitro generated day-8 LCs were also exposed to live *S.e.* as above. As shown in Figure 3.18, LCs co-cultured with *S.e.* did not show obvious signs of maturation or activation. Also, in contrast to the live *S.a. co-culture*, LCs with *S.e.* were still alive even after 130min. Viability was confirmed via flow cytometry: *S.e*. co-cultured LCs only started to die after 4h, presumably due to deficient nutrients in the medium, which live *S.e.* would be competing for (data not shown here).

Interestingly, *S.a.*- and *S.e.*-cocultured LCs display very different behaviour and morphology. LCs do internalize S.a., but not S.e. Both co-cultured LCs do migrate, but *S.a.*-LCs migrate much faster, while displaying strong attachment to the surface and dendritic protrusions, hallmarks of mesenchymal cell migration.

3.3.2 Phenotype characterization of LCs upon live bacteria stimulation

To further characterize the response of LCs to live bacteria, flow cytometry analysis was performed. *In vitro* generated day-8 LCs were exposed to live *S.e.*, live *S.a.* or sham-treated for 1h at 37°C, 5% CO_2. Cells were harvested, thoroughly washed three times, and analyzed by flow cytometry (see Figure 19). In-vitro generated unstimulated LCs are $CD207^+CD1a^+TLR2^+$ $Fc\varepsilon R1\alpha^+$LCs, the same as in Figure 3.1. Interestingly, *S.e.*-exposed LCs displayed basically the same phenotype as unstimulated LCs, except for upregulation of CCR5 and CD1b. In contrast, *S.a.*-infected LCs showed much higher expression of CD14, TLR6, CCR7, CD1c, CD209, CD324, Trop1, Trop2, CD11b, CD11c, CX3CR1, CXCR1, CD40, CD80, CD83 and HLA-DR. This fits well to our live imaging, ie., *S.a.*-infected LCs matured / activated (as evidenced by upregulation of CD40, CD80, CD83, HLA-DR and CCR7) while *S.e.*-infected LCs retained their original, more tolerogenic status.

3.3.3 Live bacteria stimulation triggers release of proinflammatory chemokines and inflammatory cytokines in LCs

To check the secretion of cytokines and chemokines in LCs upon live bacteria stimulation, the supernatants were collected. After sterile-filtration, these samples were analyzed via bead-based ELISA. As shown in Figure 20 A, live *S.a.*-primed LCs secreted high levels of IL-18, IL-1β, IP-10 (CXCL10), IFN-γ, IFN-α2, CCL20, CCL3, CCL4, IL-8, CCL2, IL-6, IL-10, CXCL1, CCL5, TNF-α, CCL17. Live *S.e.*-primed LCs also did secrete several cytokines and chemokines, but at much lower range. More interestingly, significant differences was observed between live *S.e.*-primed LCs and live *S.a.*-primed LCs in secretion of CXCL1, IFN-α2, IL-18, IL-1β, IL-6, IP-10 (CXCL10), CCL5, TNF-α after 1h stimulation; secretion of IP-10 (CXCL10) and CCL5 after 2h stimulation; secretion of CXCL1, IFN-α2, IL-10, IL-18, IL-1β, IL-6, IL-8, IP-10 (CXCL10), CCL2 and CCL4 after 3h stimulation (see Figure 20 B).

3.3.4 Live *S.a.*-primed LCs, but not *S.e.*-primed LCs, cause a strong inflammatory T-cell response

To investigate downstream T cell polarization, mixed lymphocyte reactions were performed. LCs were stimulated *in vitro* with live *S.e.* or *S.a.* for 1h. Stimulated and unstimulated LCs were washed and co-cultured with allogenic naïve CD4+ T cells. After 5 days, cells were analyzed via flow cytometry and secreted cytokines were analyzed by bead-based cytokine ELISA of culture supernatant. In response to live *S.a.*-primed LCs, T-cell underwent activation and rapid clonal expansion, as well as downregulation of CCR7 in one subset. In contrast, live *S.e.*-primed LCs do lead to activation of T-cells (as evidenced by upregulation of CD25 and downregulation of CCR7 in a subset), but these activated T-cells did not show clonal expansion (see Figure 21 A and B). Cytokine analysis showed that live *S.a.*-primed LCs induced T cells to secrete high amounts of IL-5, IL-6, IL-9 and IL-22 compared to live *S.e.* stimulation. Conversely, live *S.e.*-primed LCs induced secretion of high levels of IL-10 (see Figure 21 C). Of note, the levels of IL-17A and IL-17F were also analyzed, but in all conditions these cytokines were below detection limit (data not shown here).

Taken all together, *S.a.* induces a strong inflammatory T-cell response in an LC-dependent manner, while *S.e.*-primed LCs do not

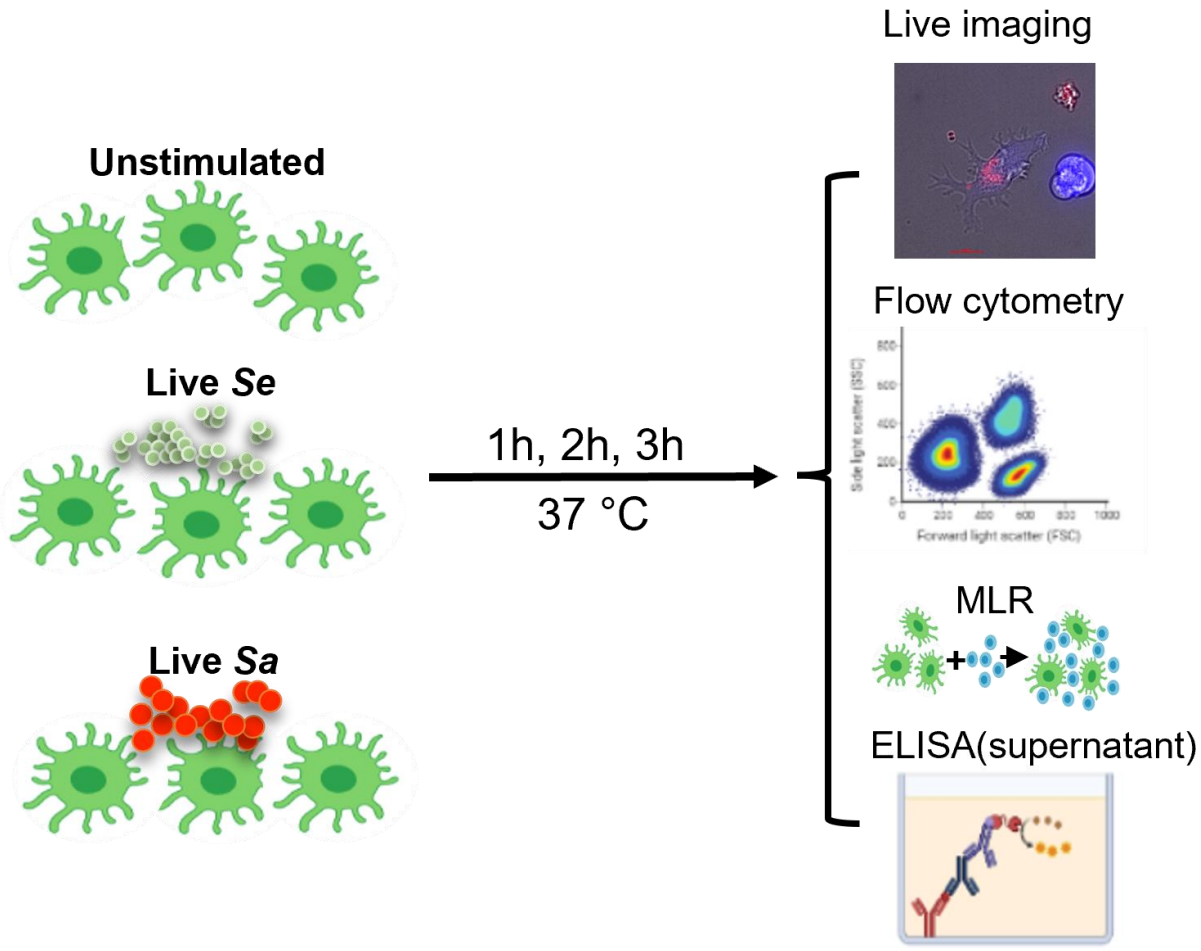

Figure 3.16 Workflow of study 3.
In vitro generated day-8 LCs were exposed to live *S.e.*, live *S.a.* or sham-treated for 1h, 2h, 3h at 37°C, 5% CO_2. Cells were harvested and stained for live imaging experiments or flow cytometry experiments. Live-bateria-primed LCs were co-cultured with allogenic naïve $CD4^+$ T cells for 5 days in a mixed lymphocyte reaction (MLR). Supernatants from MLR experiments were collected for ELISA.

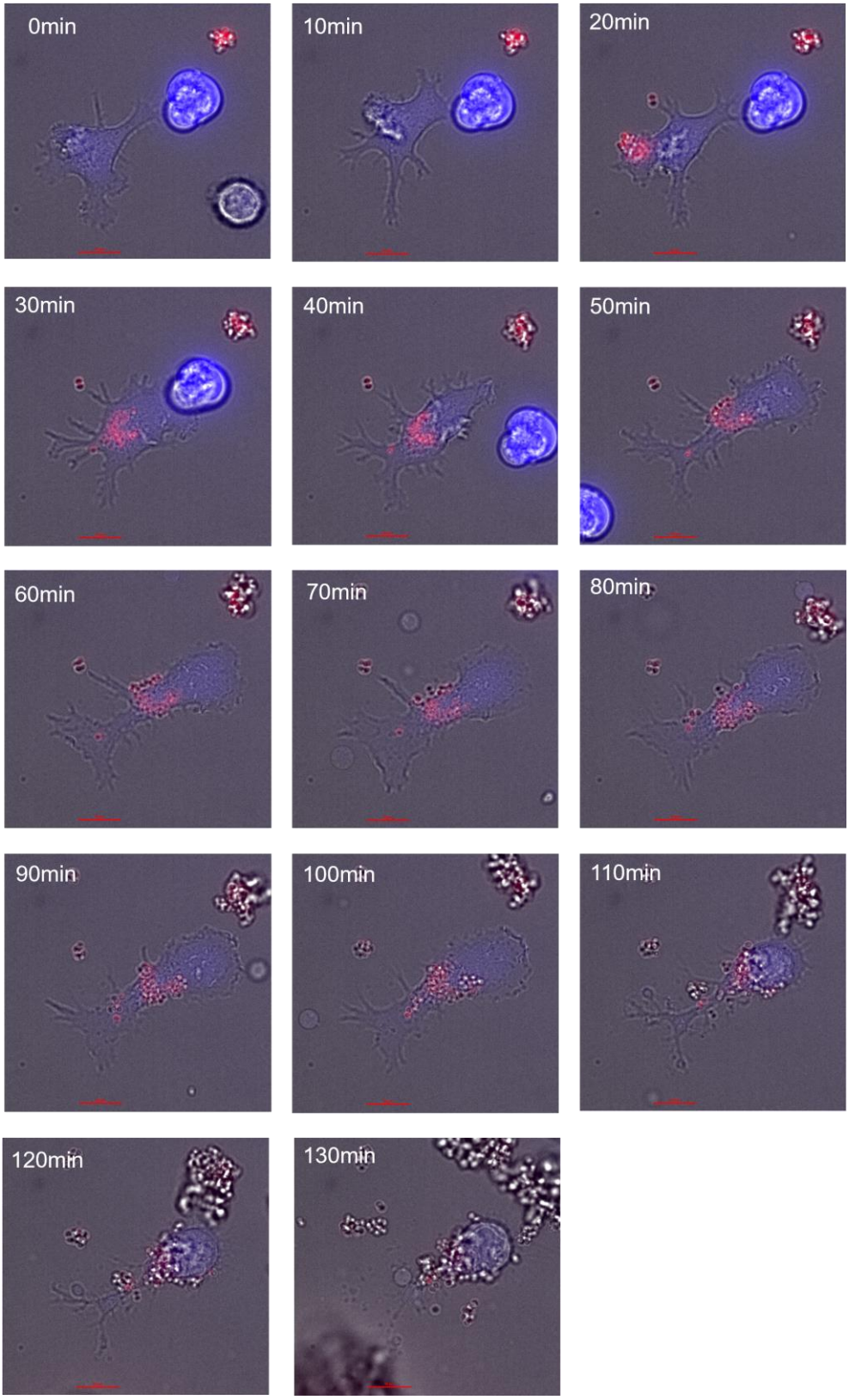

Figure 3.17 Live imaging of live *S.a.* and LCs.
In vitro generated day-8 LCs were exposed to live *S.a.* for live imaging. Blue: LCs. Red: live *S.a.*. Scale bar is 10μm.

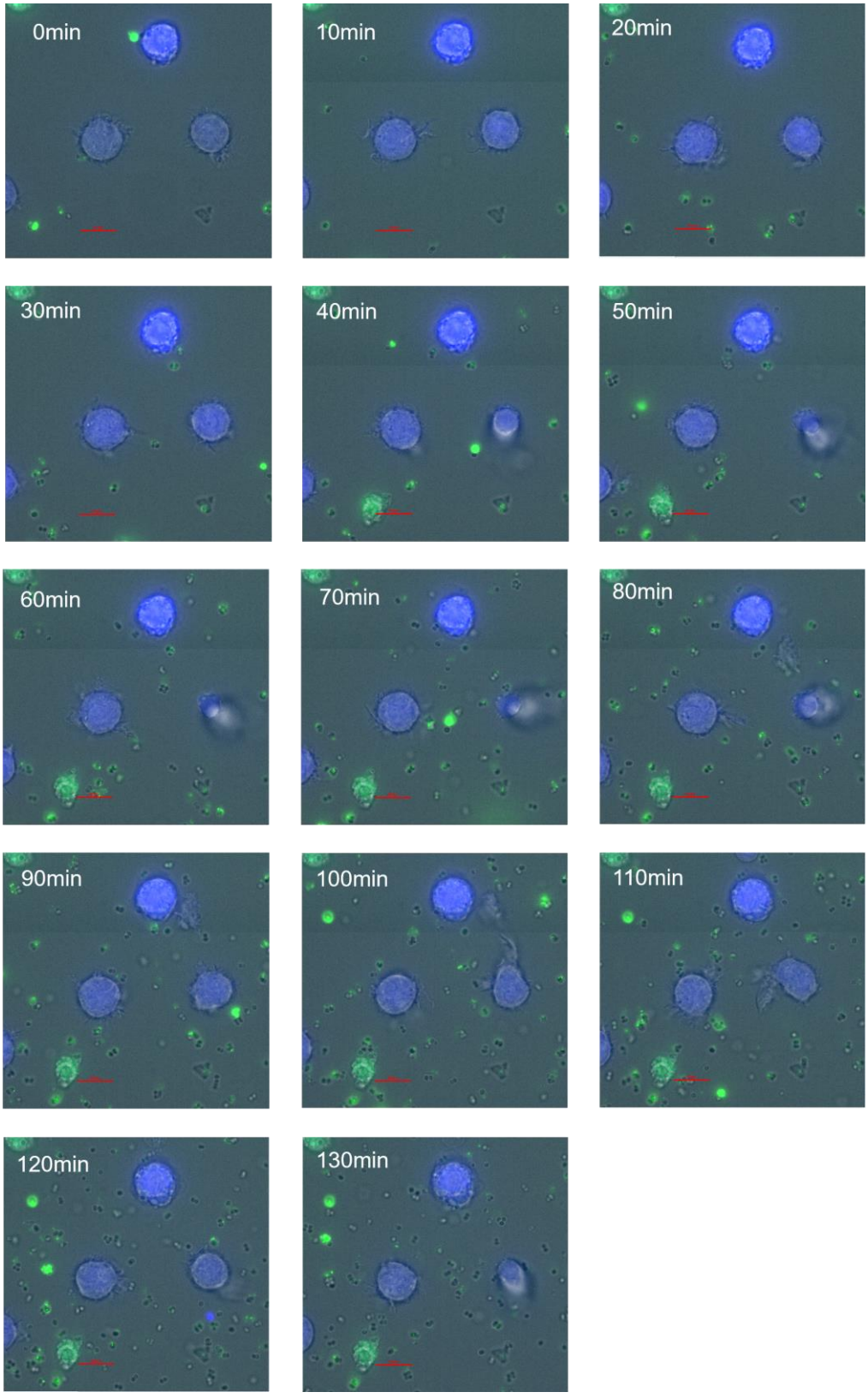

Figure 3.18 Live imaging of live *S.e.* and LCs.
In vitro generated day-8 LCs were exposed to live *S.e.* for live imaging. Blue: LCs. Green: live *S.e.*. Scale bar is 10μm.

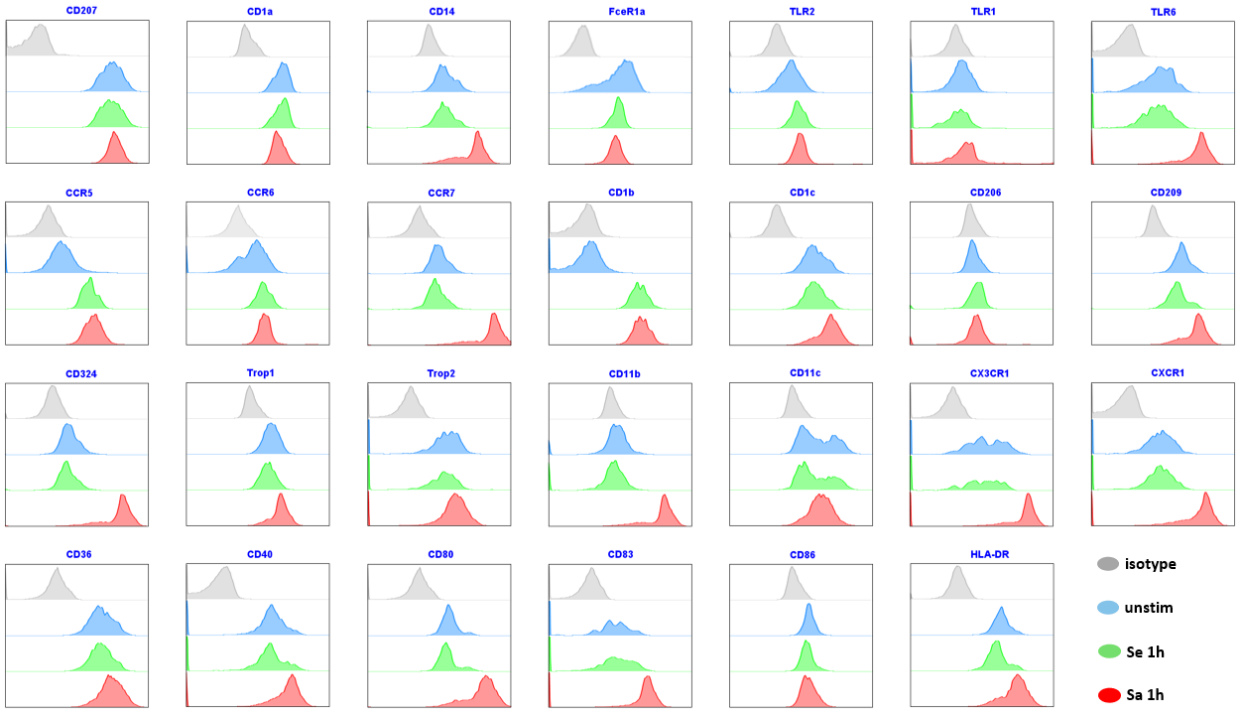

Figure 3.19 Phenotype of LCs upon live bacteria stimulation.
In vitro generated day-8 LCs were exposed to live *S.e.*, live *S.a.* or sham-treated for 1h at 37°C, 5% CO_2. Cells were harvested and analyzed via flow cytometry. Unstimulated LCs, live *S.e.*-primed LCs, live *S.a.*-primed LC marked as blue, green, red respectively. Isotype control marked as grey.

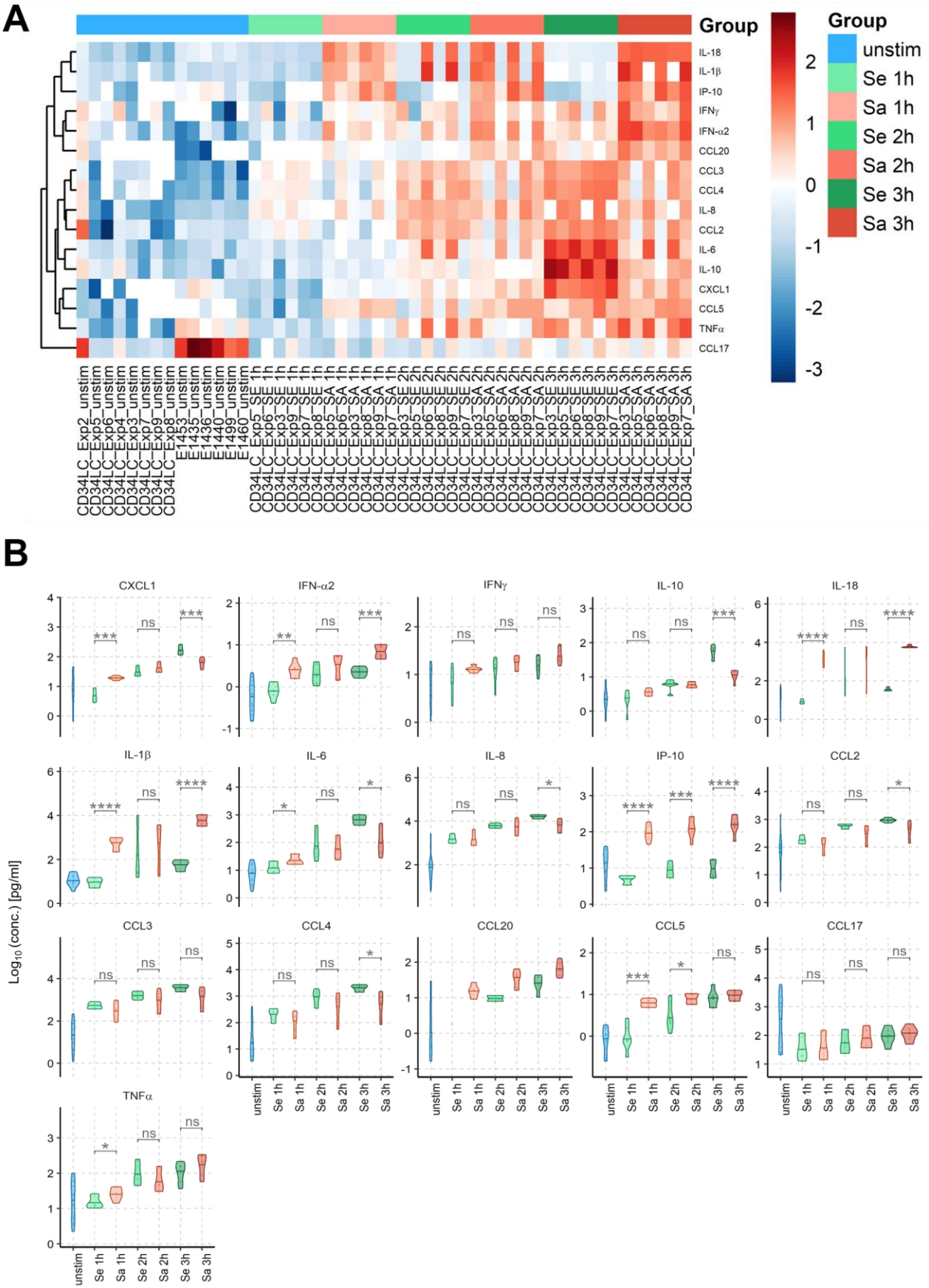
A
Group
unstim
Se 1h
Sa 1h
Se 2h
Sa 2h
Se 3h
Sa 3h
IL-18
IL-1β
IP-10
IFNγ
IFN-α2
CCL20
CCL3
CCL4
IL-8
CCL2
IL-6
IL-10
CXCL1
CCL5
TNFα
CCL17
B
Log10 (conc.) [pg/ml]
CXCL1
IFN-α2
IFNγ
IL-10
IL-18
IL-1β
IL-6
IL-8
IP-10
CCL2
CCL3
CCL4
CCL20
CCL5
CCL17
TNFα

Figure 3.20 LCs release high levels of proinflammatory chemokines and cytokines upon live bacteria stimulation.
In vitro generated day-8 LCs were exposed to live *S.e.*, live *S.a.* or sham-treated for 1h, 2h and 3h respectively at 37°C, 5% CO_2. Supernatants from each condition and time point were collected for human proinflammatory chemokines and inflammatory cytokines detection using flow cytometry bead-based ELISA. CCL3, IL-6, IL-8, IFN-α2, IFN-γ. CCL11, CXCL5, CXCL9, CXCL11, IL-12p70, IL-17A, IL-23, IL-33 are below detection and data are not shown here. (A) Heat map visualizes differentially expressed proteins in LCs stimulated by live *S.e.* (light green to dark green), live *S.a.* (light red to dark red) or sham-treated (blue). Colors represent high (red) and low (blue) expression intensity (n=6-4). (B) Violin plots corresponding to (A). One-way-ANOVA, N=5-14, each dot represents one donor, line is median.

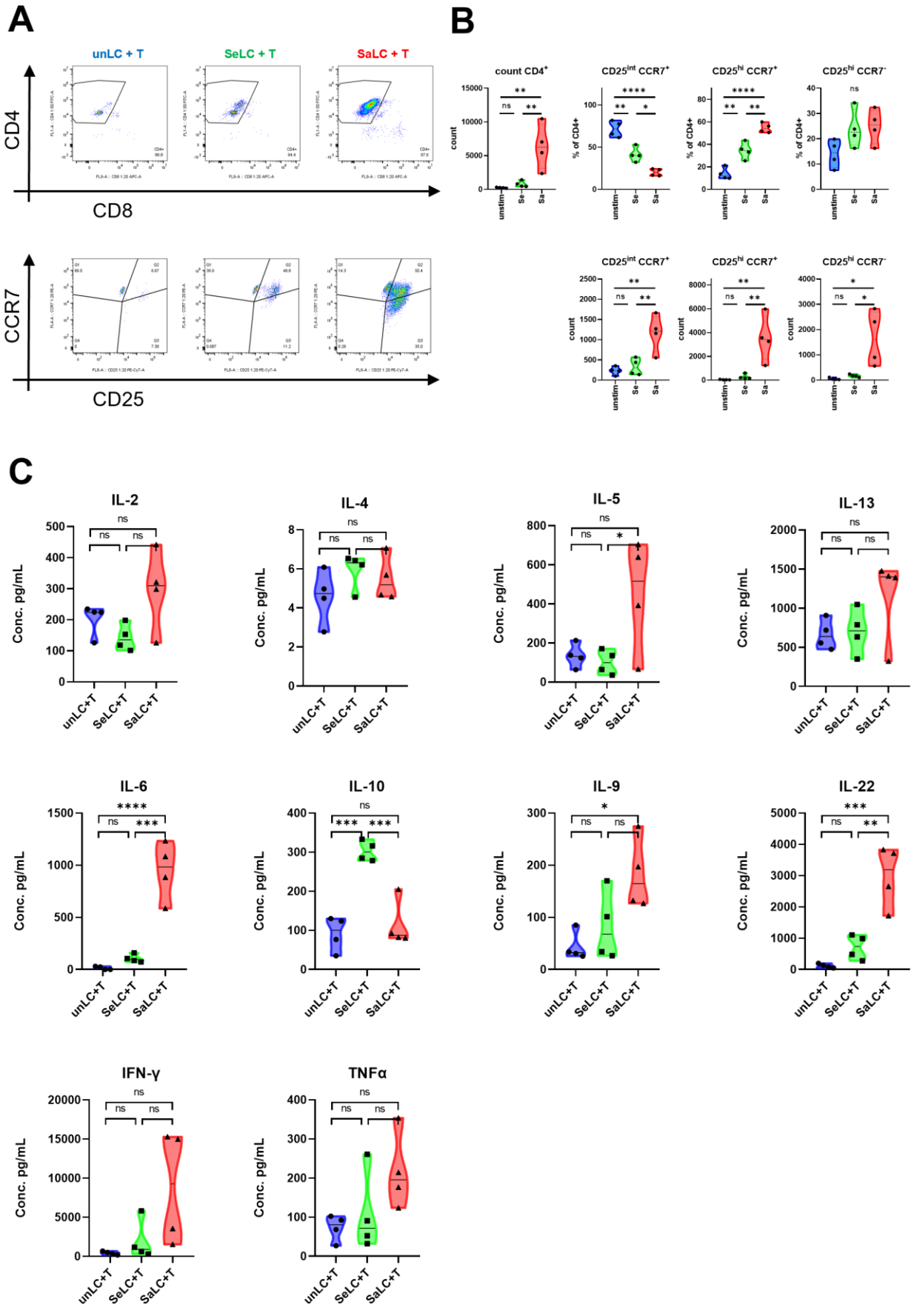
A
unLC + T
SeLC + T
SaLC + T
CD4
CD8
CCR7
CD25
B
count CD4+
CD25int CCR7+
CD25hi CCR7+
CD25hi CCR7-
count
% of CD4+
unstim
Se
Sa
C
IL-2
IL-4
IL-5
IL-13
IL-6
IL-10
IL-9
IL-22
IFN-γ
TNFα
Conc. pg/mL
unLC+T
SeLC+T
SaLC+T
ns

Figure 3.21 Live *S.e.*-primed LCs cause reduced T-cell response compared to live *S.a.* stimulation.
LCs were stimulated *in vitro* with live *S.e.* or *S.a.* for 1h. Stimulated and unstimulated LCs were washed and co-cultured with allogenic naïve $CD4^+$ T cells. After 5 days, cells were analyzed by flow cytometry and secreted cytokines were analyzed by bead-based cytokine ELISA of culture supernatant. IL-17A and IL-17F were below detection limit, data not shown here. (A) Representative FACS-plots. (B) Violin plots of flow cytometry results. (C) Violin plots of cytokine-ELISA results. N=4, each dot represents one donor. One-way-ANOVA with Sidak´s multiple comparison test, line is median.

4. Discussion

Table 4.1 Summary of three studies

Studies	**Study 1**		**Study 2**			**Study 3**					
Stimuli (Every stimuli was compared to unstimulated LC control group)	Heat-killed *S.a.*	Heat-killed *S.e.*	LPS	P2C	P3C	Live *S.a.*	Live *S.e.*	Live *S.a.*	Live *S.e.*	Live *S.a.*	Live *S.e.*
Time Points	24h		24h			1h		2h		3h	
Upregulated gene expression compared to unstimulated LCs (qRT-PCR)	CD83 CCL13 CCL22 CCR7 JAK1 JAK3 IL-4Rα IL-6 IL-10 IL-23	CD83 CCL22 CCR7 JAK1 JAK3 IL-6 IL-13Rα1 IL-23	CD83 CCL22 CCR7 JAK1 JAK2 JAK3	CD83 CCL22 CCR7 JAK1 JAK2 JAK3 TYK2 IL-6	CD83 CCL22 CCR7 JAK1 JAK2 JAK3 TYK2 IL-6 IL-13Rα1						
Downregulated gene expression compared to unstimulated LCs (qRT-PCR)	TGFβ TNFα FcεRIα FcεRIγ PU1 YY1 JAK2 AHR CCR6 TLR1 TLR2 TLR4 TLR6 TLR10	TGFβ TNFα FcεRIα FcεRIγ PU1 YY1 HMGB2 AHR CCR6 TLR1 TLR2 TLR6 TLR10	TLR4 FcεRIα FcεRIγ TNFα TLR1 TLR2 PU1 YY1	CCR6 TLR1 TLR2 TLR4 TLR6 FcεRIα FcεRIγ PU1 YY1 TGFβ TNFα AHR	CCR6 TLR1 TLR2 TLR4 TLR6 FcεRIα FcεRIγ PU1 YY1 ELF1 TGFβ TNFα AHR						
Increased expression of markers compared to unstimulated LCs (flow cytometry)	CD83	CD83	CD83	CD83	CD83	CD14 TLR6 CCR5 CCR7 CD1b CD1c CD209 CD324 Trop1 Trop2 CD11b CD11c CX3CR1 CXCR1 CD40 CD80 CD83 HLA-DR	CCR5 CD1b	CD14 TLR6 CCR5 CCR7 CD1b CD1c CD209 CD324 Trop1 Trop2 CD11b CD11c CX3CR1 CXCR1 CD40 CD80 CD83 HLA-DR	CCR5 CD1b	CD14 TLR6 CCR5 CCR7 CD1b CD1c CD209 CD324 Trop1 Trop2 CD11b CD11c CX3CR1 CXCR1 CD40 CD80 CD83 HLA-DR	CCR5 CD1b
Reduced expression of markers compared to unstimulated LCs (flow cytometry)	TLR2 FcεRIα	TLR2 FcεRIα IL-13Rα	TLR2	TLR2	TLR2 FcεRIα	FcεRIα	FcεRIα	FcεRIα	FcεRIα	FcεRIα	FcεRIα
High secretion of proinflammatory chemokines in LCs (ELISA)	CXCL1 CXCL5 CXCL9 CXCL10 CXCL11 CCL2 CCL4 CCL5 CCL11 CCL20	CXCL1 CXCL5 CXCL9 CXCL10 CXCL11 CCL2 CCL4 CCL5 CCL11 CCL20	CXCL1 CXCL10 CCL2 CCL3 CCL4 CCL5 CCL17	CXCL1 CXCL10 CCL2 CCL3 CCL4 CCL5 CCL17 CCL20	CXCL1 CXCL10 CCL2 CCL3 CCL4 CCL5 CCL17 CCL20	CXCL1 CXCL10 CCL5		CXCL1 CXCL10 CCL5	CCL2 CCL3 CCL4	CXCL1 CXCL10 CCL20 CCL5	CXCL1 CCL2 CCL3 CCL4 CCL5
Low secretion of proinflammatory chemokines in LCs (ELISA)		CCL17				CCL17	CCL17	CCL17	CCL17	CCL17	CCL17
High secretion of inflammatory cytokines in LCs (ELISA)	IFN-α2 IL-1β IL-10 IL-12p70 IL-18 TNF-α	IFN-α2 IL-1β IL-10 IL-12p70 IL-18 TNF-α	IL-1β IL-10 IL-6 IL-8 IL-18 IL-23 TNF-α	IL-1β IL-10 IL-6 IL-8 IL-18 IL-23 TNF-α	IL-1β IL-10 IL-6 IL-8 IL-18 IL-23 TNF-α	IL-18 IL-1β IL-6 IFN-α2		IL-18 IL-1β IL-6 IFN-α2 TNF-α	IL-8 IFN-α2 IL-6 TNF-α	IL-18 IL-1β IFN-γ IFN-α2 IL-8 IL-6 TNF-α	IL-8 IL-6 IL-10 IFN-α2 TNF-α
T cell proliferation (flow cytometry)						strong	weak				
Th cytokines release (ELISA from MLR assay)						IL-5 IL-6 IL-9 IL-22	IL-10				

AD is a complex and highly multifactorial disease. The skin of AD patients is heavily colonized with *S.a.*, while amounts of *S.e.* are strongly reduced. However, how these two strains of bacteria (closely related, but still one a pathogen and the other a commensal) influence human epidermal sentinel LCs is still not fully understood. Therefore, *in vitro* generated model $CD207^{+}CD1a^{+}TLR2^{+}FcεRI^{+}$LCs with immature phenotype was established. This model ideally resembled LCs in AD epidermis environments with high expression of TLR2, FcεRI and absent or low expression of CD83.

In study 1, LCs strongly responded to heat-killed bacteria stimulation by increased expression of CCL22, CCR7, IL-6, JAK1 and a lower gene expression of TGFβ, TNFα, FcεRIα, FcεRIγ, AHR, CCR6, TLR1, TLR2, TLR4, TLR6, TLR10 and CCL17. This trend was substantiated on the protein level by flow cytometry. In brief, both heat-killed *S.a.* and *S.e.* stimulation induced LCs maturation and responsed to potential chemokines for migration by upregulation of CD83, CCR7 and downregulation of CCR6. Furthermore, heat-killed bacteria stimulation downregulated TLRs, FcεRI and its related transcription factors PU1 and YY1. In addition, both heat-killed bacteria stimulation upregulated JAK1 and JAK3 but not type I or type II cytokine receptors. At last, heat-killed bacteria induced LCs significantly release increased proinflammatory chemokines such as CXCL1, CXCL5, CXCL9, IP-10 (CXCL10), CXCL11, CCL2, CCL4, CCL5, CCL11, CCL20 and inflammatory cytokines such as IFN-α2, IL-1β, IL-10, IL-12p70, IL-18 and TNF-α. Interestingly, heat-killed *S.a.*-stimulated LCs released even higher amounts of chemokines and cytokines than heat-killed *S.e.*-stimulated LCs except for CXCL5, IL-10, IL-18. Of note, CCL3, IFN-γ, IL-6, IL-8, IL-17A, IL-23 and IL-33 were below detection limits.

In study 2, LCs strongly responded to TLRs ligation by increased expression of CCL22, CCR7, JAK1, JAK3, CD83, IL-6 and reduced expression of FcεRIα, TGFβ, CCR6, TNFα, FcεRIγ, TLR1, TLR2, PU1 and YY1. This trend was confirmed on the protein level by flow cytometry. In brief, TLRs ligation induced LCs maturation and migration by upregulation of CD83, CCR7 and downregulation of CCR6. Furthermore, TLRs ligation downregulated TLRs. P2C- and P3C-stimulated LCs showed decreased expression of FcεRIα and its related transcription factors PU1 and YY1, but not LPS-stimulated LCs. P3C- stimulated LCs displayed reduced expression of ELF1. In addition, all TLRs ligation upregulated

JAK1, JAK2, JAK3. Both P2C- and P3C-stimulated LCs displayed increased expression of TYK2. P3C- stimulated LCs showed increased expression of IL-13Rα1. TLRs ligands only influenced JAK family but not type I or type II cytokine receptors. At last, TLRs ligation induced LCs significantly released high amounts of proinflammatory chemokines such as CXCL1, IP-10 (CXCL10), CCL2, CCL3, CCL4, CCL5, CCL17 and inflammatory cytokines such as IL-1β, IL-10, IL-6, IL-8, IL-18, IL-23, TNF-α. Only P2C- and P3C- stimulated LCs displayed increased secretion of CCL20. Of note, CXCL5, CXCL9, CXCL11, CCL11, IFN-α2, IFN-γ, IL-12p70, IL-17A, and IL-33 were below detection limits.

In study 3, live *S.a.* induced immunogenic LCs while live *S.e.* were less active as measured by live imaging. Phenotype of those live bacteria-stimulated LCs were further confirmed and characterized by flow cytometry. Interestingly, *S.e.*-infected LCs showed the same phenotype as unstimulated LCs except for CCR5 and CD1b. In the contrast, *S.a.*-infected LCs displayed a much higher surface expression of CD14, TLR6, CCR7, CD1c, CD209, CD324, Trop1, Trop2, CD11b, CD11c, CX3CR1, CXCR1, CD40, CD80, CD83 and HLA-DR compared to *S.e.*-infected LCs or unstimulated LCs. This finding confirmed *in vitro* live imaging observation by molecular protein level, ie., *S.a.*-infected LCs matured, activated, by the upregulation of CD40, CD80, CD83, HLA-DR and CCR7 while *S.e.*-infected LCs stayed more tolerogenic. Finally, the supernatants from infected LCs and from MLR assay were investigated by ELISA. Live *S.a.*-primed LCs released high amounts of IL-18, IL-1β, IP-10 (CXCL10), IFN-γ, IFN-α2, CCL20, CCL3, CCL4, IL-8, CCL2, IL-6, IL-10, CXCL1, CCL5, TNF-α and CCL17. Conversely, live *S.e.*-primed LCs only showed a moderate amount of production of those chemokines and cytokines in a time dependent manner. Of note, CCL11, CXCL5, CXCL9, CXCL11, IL-12p70, IL-17A, IL-23, IL-33 were below detection limits. Interestingly, strong significance between live *S.e.*-primed LCs and live *S.a.*-primed LCs was observed, with regard to the chemokines and cytokines secretion of CXCL1, IFN-α2, IL-18, IL-1β, IL-6, IP-10 (CXCL10), CCL5 and TNF-α after 1h stimulation; significant secretion of IP-10 (CXCL10) and CCL5 after 2h stimulation; and significant secretion of CXCL1, IFN-α2, IL-10, IL-18, IL-1β, IL-6, IL-8, IP-10 (CXCL10), CCL2 and CCL4 after 3h stimulation. The supernatant from MLR experiment showed that live *S.a.*-primed LCs induced T cells to secrete higher amounts of IL-5, IL-6, IL-9 and IL-22 compared to live *S.e.* stimulation. Conversely, live *S.e.*-primed

LCs induced T cells to secrete significant levels of IL-10. Of noted, IL-17A and IL-17F remained below detection limits. These data were in line with live imaging as well. In summary, live *S.e.*-primed LCs reduced T-cell response compared to live *S.a.* stimulation.

When comparing Study 1, 2 and 3, the results differed with regard to LC maturation, activation, potential for migration and T cell differentiation, depending on the different stimuli in the same LCs model. TLRs are PRRs composed of an extracellular part, which allow binding of pathogen-associated molecular patterns. TLR1, TLR2, TLR4, TLR6 and TLR10 detect extracellular pathogen-associated molecular patterns, while TLR3, TLR7, TLR8 and TLR9 are expressed on endosomal membranes and recognize nucleosides, nucleotides and oligo- and polynucleotides derived from intracellular viral and bacterial pathogens (Novak et al., 2011; Novak et al., 2010; Sun 2019). Recent research revealed that TLR4 rs11536891 polymorphism was associated with the susceptibility to AD in Chinese Han children (Shi et al., 2022). The results from the heat-killed bacteria and different TLR ligands are in line with our previous research (Allam et al., 2011; Allam et al., 2008; Herrmann et al., 2013). However, no significance was found in the production and release of chemokines and cytokines between heat-killed *S.a.*- and heat-killed *S.e.*-stimulated LCs. Conversely, live *S.a.*-infected LCs upregulated TLR6 while live *S.e.*-infected LCs did not.

A hallmark of skin LC of atopic individuals is the expression of the high-affinity receptor for IgE, FcεRI (Bieber et al., 1992a). FcεRI is a multimeric immune receptor existing in a tetrameric and a trimeric form. The tetrameric receptor consists of one α-chain for IgE binding, one β-chain with signal amplifying and stabilizing functions and two γ-chain for signal transduction. In mice and humans, the tetrameric form is expressed on mast cells and basophils. In contrast, the β-chain lacking trimeric form is restricted to human APCs like DCs or LCs. Rodents do not express FcεRI on DCs. In AD, the trimeric FcεRI shows a heterogeneous and higher expression on LCs and especially on IDECs compared to skin DC from healthy individuals. The high expression of the receptor correlated with serum IgE levels and the severity of the disease (Bieber 2007; Bieber et al., 1989a; Novak et al., 2001). Moreover, cross-linking of FcεRI on DCs can induce the production of pro-inflammatory cytokines such as TNFα, IL-1β or IL-8 and chemokines like CCL2 via the

activation of nuclear factor-κB (NF-κB) (Kraft et al., 2006; Kraft et al., 2002). FcεRI-cross linking to IDO or TLR or AHR resulted in a downregulation of FcεRI expression, thus influencing the course of AD by cross-talking of those receptors (Allam et al., 2011; Koch et al., 2017; Leib et al., 2018; Novak et al., 2011; von Bubnoff et al., 2012). In all three of our studies, we found that FcεRI was functional upon different stimuli in LCs, except for LPS or P2C stimulation.

As in other atopic diseases, the acute inflammatory reaction in AD is dominated by a Th2 immune response and its associated cytokines IL-13 while IL-4 is hardly detectable in the skin. Both cytokines decrease the production of skin barrier proteins such as filaggrin and thereby further alter the skin barrier dysfunction. JAK are a family of cytoplasmatic tyrosine kinases comprising JAK1, JAK2, JAK3, and TYK2 that can associate to type I and type II cytokine receptors as well as more than 20 other receptors for cytokines and growth factors. Each receptor recruits specific combinations of JAK dimers or trimers to the receptor and thereby determinates the signaling cascade. After ligation of a cytokine, JAK get trans-phosphorylated and concomitantly phosphorylate and thereby activate STAT6 molecules. Once activated, STAT dimers translocate into the nucleus to regulate gene transcription. Both heat-killed bacteria stimulation upregulated JAK1 and JAK3 but not type I or type II cytokine receptors. All LPS-, P2C- and P3C-stimulated LCs upregulated JAK1, JAK 2, JAK3. Both P2C- and P3C-stimulated LCs had a higher expression of TYK2. P3C- stimulated LCs had an increased expression of IL-13Rα1. In summary, heat-killed bacteria influenced JAK family and type I or type II cytokine receptors for IL-4 and IL-13 in LCs. But TLRs ligands only regulate JAK family.

With regard to proinflammatory chemokines and inflammatory cytokines, heat-killed bacteria induced LCs significantly release proinflammatory chemokines such as CXCL1, CXCL5, CXCL9, CXCL10, CXCL11, CCL2, CCL4, CCL5, CCL11, CCL20 and inflammatory cytokines such as IFN-α2, Il-1β, Il-10, IL-12p70, Il-18, TNF-α. TLRs ligation induced LCs significantly release proinflammatory chemokines such as CXCL1, CXCL10, CCL2, CCL3, CCL4, CCL5, CCL17 and inflammatory cytokines such as IL-1β, IL-6, IL-8, IL-10, IL-18, IL-23 and TNF-α. Live *S.a.*-primed LCs had a very high secretion of IL-1β, Il-6, IL-8, IL-10, IL-18, CXCL1, CXCL10, CCL2, CCL3, CCL4, CCL5, CCL17,

CCL20, IFN-γ, IFN-α2 and TNF-α. Conversely, live *S.e.*-primed LCs only had a higher amount of production in a time dependent manner compared to live *S.a.*-primed LCs. The supernatant from MLR experiment showed that live *S.a.*-primed LCs induced T cells to secrete high amount of IL-5, IL-6, IL-9 and IL-22 compared to live *S.e.* stimulation. Conversely, live *S.e.*-primed LCs induced T cells to secrete significant levels of IL-10.

The polarization of T helper (Th) cells is defined based on their distinct gene expression pattern and cytokine production profile. The master regulator of Th1 differentiation is the T-box transcription factor (T-bet), Th1 cells drive cell-mediated immunity. They are induced in response to intracellular pathogens, and they produce high levels of interferon IFN-γ and IL-2. Th2 lineage faith is regulated by GATA binding protein 3 (GATA3). Th2 cells play an important role in the activation of humoral immunity. They mediate the immune response against parasitic infection, e.g., helminths, but they are also involved in the pathophysiology of asthma and other allergic disease. Their main effector cytokines include IL-4, IL-5 and IL-13. The Th17 cells are required for the effective immune response against extracellular bacteria and fungi. They are important for the maintenance of mucosal barriers, but they have also been implicated in autoimmune and inflammatory disorders, e.g., psoriasis. Th17 cells secrete IL-17, IL-21, IL-22. Recently new finding included Th9 (producing mainly IL-9) and Th22 (IL-22). There is also a subset of Foxp3-dependent Tcells called Treg, which is important in homeostatic maintenance of the tissues. These cells prevent overshooting of inflammatory responses and subsequent immunopathology. Main mediators of immunosuppressive function of Tregs are IL-10 and TGFβ1. LCs, depending on the type of the antigen they present, can induce naïve $CD4^+$ T cells to differentiate into different effector T cells e.g., Th1, Th2 or Th17. Each T cell fate has its own transcription factor master regulator and secrets specific cytokine profile. The main finding of this thesis was that live *S.e.* was indeed able to stimulate the production of IL-10 in responding T cells, suggesting that these T cells could correspond to Treg cells. In contrast, a live *S.a.* induced the release of secretion of IL-5, IL-6, IL-9 and IL-22, suggesting the generation of Th2, Th9, and Th22 cells.

These findings are in line with clinical observations that AD patients, but not Psoriasis patients or healthy individuals, have increased serum concentration of IL-5 and IL-6

(Krupka-Olek et al., 2022). Recent studies showed that the disease-specific T-cell clusters were mostly of a Th2/Th22 sub-population in AD and Th17/Tc17 in Psoriasis, and their numbers were associated with severity scores in both diseases (Zhang et al., 2022a). This is in line with our results in figure 3.21C. The absence of IL-17 in this study also confirmed the different active inflammatory nature of AD and Psoriasis, which is known as Th17-driven disease.

Considering the current armamentarium of AD treatment, there are many options depending on the severity of the disease (Wollenberg et al., 2022). For mild to moderate forms, they include topical anti-inflammatory agents (including corticosteroids, pimecrolimus, tacrolimus) and phototherapy. Systemic therapies are used for moderate to severe forms and include immunosuppressive drugs such as ciclosporine A, targeted therapies with biologics (dupilumab and tralokinumab), and the broader approach with JAK inhibitors (baricitinib, abrocitinib and upadacitinib). The management is sometimes completed by dietary intervention, complementary medicine, psychosomatic counselling and educational interventions (Wollenberg et al., 2018a, b). Treatment of AD cases with skin infections often involves the use of antibiotics. Although administration of antibiotics is effective against *S.a.*, the resulting reduction in healthy microbiota and the emergence of drug-resistant bacteria are of concern. Therefore, alternative therapy would be preferrable to treat AD with improving the microbiota composition (Shimamori et al., 2021). Emerging microbiome-based treatments have been registered for clinical trials, which aim to restore a healthy skin microbiome in AD patients, reduce overgrowth of pathogenic drivers of AD and promote the recovery of commensals.

In macrophages it has been shown that different polarization (M0-resident, M1-activated, M2a-alternatively activated) show different migration behavior (Cui et al., 2018). M0 almost never migrate. M1 strongly adhere, stay in tissue, produce cytokines, and eat pathogens. M2a start to migrate to next lymph node to present antigen. M1 move slowly via amoeboid cell migration, M2a migrate fast via mesenchymal cell migration. Therefore, when analyzing our live-cell-imaging, *S.a.* might lead to a M2a-like polarization and downstream activation of adaptive immunity. Obviously, this needs more study; transcription factor analysis in both LCs and T Cells, in-depth analysis of cell-cell

communication and functional assays with Th and B cells. However, these analyses are beyond the scope of this project. We hope to address these questions in future works.

Live imaging and flowcytometry of LCs with live *S.a./S.e.* show clear differences. The fact that *S.e.* is not internalized by LCs means that LCs do not perceive *S.e.* as threat. But they do react: live *S.a.*-infected-LCs activate, migrate away (maybe to Lymph nodes) and lead to pro-inflammatory T cells. In contrast, *S.e.*-infected-LCs stay in the tissue, do not crawl away. Also, *S.e.*-infected-LCs make T cells produce high levels of lL-10, which is commonly seen as anti-inflammatory cytokine. Whether *S.e.*-infected-LCs can really act tolerogenically needs to be addressed in a separate follow-up study. However, the initial data is promising. If data interpretation can be confirmed or if we can unravel the exact mechanism behind this effect, it may lead to a new form of therapy. Such a study would need to focus in LC polarization and the mechanisms thereof; and a way to induce and maintain this supposed tolerogenic LC phenotype. Again, this is beyond the scope of this thesis, hopefully it will be addressed in the follow-up-studies.

In conclusion, when comparing models, it is obvious that LCs react differently to live bacteria, heat-killed bacteria and synthesized peptides. Therefore, while heat-kill bacteria and peptides may be useful for certain studies, they cannot re-capitulate the actual in-vivo situation. LCs specifically seem to react very sensitively to these differences. This needs to be taken into account when reading and comparing literature. We propose that future studies should improve on our model of live-bacteria-co-culture and aim to perform future studies with live bacteria. This will lead to data better resembling the situation in vivo and ultimately to data more relevant to the clinical situation.

Future perspectives

As AD is the port of entry for allergic sensitization and the first step of the atopic march. Hence, its prevention and appropriate treatment are essential. AD therapy has undergone a true revolution in recent years (Bieber 2022). Moreover, new insights into our understanding of the pathophysiologic complexity of AD should translate into diagnostic by biomarker discovery, therapeutic and preventive measures in the context of a precision

medicine approach, such as age- (Czarnowicki et al., 2020; Czarnowicki et al., 2019; Czarnowicki et al., 2021), endophenotype- (Koh et al., 2022), and microbiome-specific therapies (Koh et al., 2022), and cytokine or receptor-targeted therapies (Ziehfreund et al., 2022). A joint effort in the fields of genomics, immunology, bioinformatics, microbial ecology will be necessary to fully elucidate the role of microbiome in human health and diseases such as AD. This scientific approach will provide valuable information for the development of novel therapeutic strategies for AD.

5. Abstract

Atopic dermatitis (AD) is the most common chronic inflammatory skin disease worldwide. AD skin is heavily colonized with *S. aureus* (*S.a.*) and exhibits low amounts of *S. epidermidis* (*S.e.*). In this thesis, different bacteria stimuli were used to explore their impact on the biology of *in vitro* generated human Langerhans cells (LCs). In study 1, both heat-killed *S.a.* and *S.e.* stimulation induced LCs maturation and migration. Furthermore, heat-killed bacteria stimulation downregulated TLRs, FcεRI and its related transcription factors PU1 and YY1. In addition, heat-killed bacteria stimulation upregulated JAK1 and JAK3 but not type I or type II cytokine receptors. At last, heat-killed bacteria induced LCs significantly to release increased proinflammatory chemokines and inflammatory cytokines. In study 2, TLR ligation induced LC maturation and migration. Furthermore, TLR ligation downregulated TLRs. In contrast, only P2C- and P3C-stimulated LCs showed decreased expression of FcεRIα and its related transcription factors PU1 and YY1, but not LPS- stimulated LCs. P3C- stimulated LCs displayed reduced expression of ELF1. In addition, all TLR ligation only influenced JAK family members but not type I or type II cytokine receptors. At last, TLR ligation induced LCs to release high amounts of proinflammatory chemokines and inflammatory cytokines. In study 3, live *S.a.* induced immunogenic LCs while live *S.e.* induced tolerogenic LCs, as shown by live imaging, flow cytometry, MLR and bead-based ELISA. Live *S.a.*-primed LCs induced T cells to secrete higher amounts of IL-5, IL-6, IL-9 and IL-22 compared to live *S.e.* stimulation. Conversely, live *S.e.*-primed LCs induced T cells to secrete significant levels of IL-10. In conclusion, heat-killed bacteria and live bacteria differentially interacted with LCs in inducing maturation, migration, antigen presentation and T cell polarization. The lessons learned may have significant translational consequences, potentially in the therapeutic management of AD. The use of topical therapies containing microbiota-derived elements may be able to redirect the cutaneous immune response in a way that more tolerance is achieved towards environmental allergens known to be provocative factors for the disease.

6. List of figures

7. List of tables

8. References

Adam D, Arany J, Toth KF, Toth BI, Szollosi AG and Olah A. Opioidergic Signaling-A Neglected, Yet Potentially Important Player in Atopic Dermatitis. Int J Mol Sci 2022; 23

Alcantara-Hernandez M, Leylek R, Wagar LE, Engleman EG, Keler T, Marinkovich MP, Davis MM, Nolan GP and Idoyaga J. High-Dimensional Phenotypic Mapping of Human Dendritic Cells Reveals Interindividual Variation and Tissue Specialization. Immunity 2017; 47: 1037-1050 e1036

Allam JP, Duan Y, Winter J, Stojanovski G, Fronhoffs F, Wenghoefer M, Bieber T, Peng WM and Novak N. Tolerogenic T cells, Th1/Th17 cytokines and TLR2/TLR4 expressing dendritic cells predominate the microenvironment within distinct oral mucosal sites. Allergy 2011; 66: 532-539

Allam JP, Klein E, Bieber T and Novak N. Transforming growth factor-beta1 regulates the expression of the high-affinity receptor for IgE on CD34 stem cell-derived CD1a dendritic cells in vitro. J Invest Dermatol 2004; 123: 676-682

Allam JP, Peng WM, Appel T, Wenghoefer M, Niederhagen B, Bieber T, Berge S and Novak N. Toll-like receptor 4 ligation enforces tolerogenic properties of oral mucosal Langerhans cells. J Allergy Clin Immunol 2008; 121: 368-374 e361

Allam P, Niederhagen B, Bücheler M, Appel T, Betten H, Bieber T, Berg S and Novak N. Comparative analysis of nasal and oral mucosa dendritic cells. Allergy 2006; 61: 166–172

Allen CE, Merad M and McClain KL. Langerhans-Cell Histiocytosis. N Engl J Med 2018; 379: 856-868

Alves de Medeiros AK, Speeckaert R, Desmet E, Van Gele M, De Schepper S and Lambert J. JAK3 as an Emerging Target for Topical Treatment of Inflammatory Skin Diseases. PLoS One 2016; 11: e0164080

Anderson DA, 3rd, Dutertre CA, Ginhoux F and Murphy KM. Genetic models of human and mouse dendritic cell development and function. Nat Rev Immunol 2021; 21: 101-115

Anselmi G, Vaivode K, Dutertre CA, Bourdely P, Missolo-Koussou Y, Newell E, Hickman O, Wood K, Saxena A, Helft J, Ginhoux F and Guermonprez P. Engineered niches support the development of human dendritic cells in humanized mice. Nat Commun 2020; 11: 2054

Balato A, Cacciapuoti S, Di Caprio R, Marasca C, Masara A, Raimondo A and Fabbrocini G. Human Microbiome: Composition and Role in Inflammatory Skin Diseases. Arch Immunol Ther Exp (Warsz) 2019; 67: 1-18

Barbaroux JB, Kwan WH, Allam JP, Novak N, Bieber T, Fridman WH, Groves R and Mueller CG. Tumor necrosis factor-alpha- and IL-4-independent development of Langerhans cell-like dendritic cells from M-CSF-conditioned precursors. J Invest Dermatol 2006; 126: 114-120

Baurecht H, Ruhlemann MC, Rodriguez E, Thielking F, Harder I, Erkens AS, Stolzl D, Ellinghaus E, Hotze M, Lieb W, Wang S, Heinsen-Groth FA, Franke A and Weidinger S. Epidermal lipid composition, barrier integrity, and eczematous inflammation are associated with skin microbiome configuration. J Allergy Clin Immunol 2018; 141: 1668-1676 e1616

Bay L and Ring HC. Human skin microbiota in health and disease: The cutaneous communities' interplay in equilibrium and dysbiosis: The cutaneous communities' interplay in equilibrium and dysbiosis. APMIS 2021: 1-13

Berlin M, Flor-Hirsch H, Kohn E, Brik A, Keidar R, Livne A, Marom R, Ovental A, Mandel D, Lubetzky R, Factor-Litvak P, Tovbin J, Betser M, Moskovich M, Hazan A, Britzi M, Gueta I, Berkovitch M, Matok I and Hamiel U. Maternal Exposure to Polychlorinated Biphenyls and Asthma, Allergic Rhinitis and Atopic Dermatitis in the Offspring: The Environmental Health Fund Birth Cohort. Front Pharmacol 2022; 13: 802974

Bieber T. The pro- and anti-inflammatory properties of human antigen-presenting cells expressing the high affinity receptor for IgE (Fc epsilon RI). Immunobiology 2007; 212: 499-503

Bieber T. Atopic Dermatitis. N Engl J Med 2008; 358: 1483-1494.

Bieber T. How to Define Atopic Dermatitis? Dermatol Clin 2017; 35: 275-281

Bieber T. Atopic dermatitis: an expanding therapeutic pipeline for a complex disease. Nat Rev Drug Discov 2022; 21: 21-40

Bieber T, Dannenberg B, Prinz JC, Rieber EP, Stolz W, Braun-Falco O and Ring J. Occurrence of IgE-bearing epidermal Langerhans cells in atopic eczema: a study of the time course of the lesions and with regard to the IgE serum level. J Invest Dermatol 1989a; 93: 215-219

Bieber T, de la Salle H, Wollenberg A, Hakimi J, Chizzonite R, Ring J, Hanau D and de la Salle C. Human Epidermal Langerhans Cells Express the High Affinity Receptor for Immunoglobulin E (FceRI). J. Exp. Med. 1992a; 175: 1285-1290

Bieber T, Rieger A, Neuchrist C, Prinz J, Rieber E, Boltz-Nitulescu G, Scheiner O, Kraft D, Ring J and Stingl G. Induction of FceR2/CD23 on human epidermal Langerhans cells by human recombinant interleukin 4 and y interferon. J. Exp. MED. 1989b; 170: 309-314

Bieber T, Rieger A, Stingl G, Sander E, Wanek P and Strobel I. CD69, an early activation antigen on lymphocytes, is constitutively expressed by human epidermal Langerhans cells. J Invest Dermatol 1992b; 98: 771-776

Bieber T and Ring J. In vivo Modulation of the HighAffinity Receptor for IgE (FceRI) on Human Epidermal Langerhans Cells. Int Arch Allergy Immunol. 1992c; 99: 204-207

Bieber T, Simpson EL, Silverberg JI, Thaci D, Paul C, Pink AE, Kataoka Y, Chu CY, DiBonaventura M, Rojo R, Antinew J, Ionita I, Sinclair R, Forman S, Zdybski J, Biswas P,

Malhotra B, Zhang F, Valdez H and Investigators JC. Abrocitinib versus Placebo or Dupilumab for Atopic Dermatitis. N Engl J Med 2021; 384: 1101-1112

Birbeck MS, Breathnach AS and Everall JD. An Electron Microscope Study of Basal Melanocytes and High-Level Clear Cells (Langerhans Cells) in Vitiligo. Journal of Investigative Dermatology 1961; 37: 51-64

Blicharz L, Rudnicka L, Czuwara J, Waskiel-Burnat A, Goldust M, Olszewska M and Samochocki Z. The Influence of Microbiome Dysbiosis and Bacterial Biofilms on Epidermal Barrier Function in Atopic Dermatitis-An Update. Int J Mol Sci 2021; 22

Borek I, Koffel R, Feichtinger J, Spies M, Glitzner-Zeis E, Hochgerner M, Sconocchia T, Krump C, Tam-Amersdorfer C, Passegger C, Benezeder T, Tittes J, Redl A, Painsi C, Thallinger GG, Wolf P, Stary G, Sibilia M and Strobl H. BMP7 aberrantly induced in the psoriatic epidermis instructs inflammation-associated Langerhans cells. J Allergy Clin Immunol 2020; 145: 1194-1207 e1111

Byrd A, Deming C, Cassidy S, Harrison O, Ng W, Conlan S, Belkaid Y, Segre J and Kong H. Staphylococcus aureus and Staphylococcus epidermidis strain diversity underlying pediatric atopic dermatitis. Sci. Transl. Med. 2017; 9, eaal4651

Cau L, Williams MR, Butcher AM, Nakatsuji T, Kavanaugh JS, Cheng JY, Shafiq F, Higbee K, Hata TR, Horswill AR and Gallo RL. Staphylococcus epidermidis protease EcpA can be a deleterious component of the skin microbiome in atopic dermatitis. J Allergy Clin Immunol 2020

Clausen BE, Romani N and Stoitzner P. Meeting Report of the 16th International Langerhans Cell Workshop: Recent Developments in Langerhans Cell and Skin Dendritic Cell Biology and their Therapeutic Application. J Invest Dermatol 2020; 140: 1315-1319

Clausen BE and Stoitzner P. Functional Specialization of Skin Dendritic Cell Subsets in Regulating T Cell Responses. Front Immunol 2015; 6: 534

Clausen ML, Agner T, Lilje B, Edslev SM, Johannesen TB and Andersen PS. Association of Disease Severity With Skin Microbiome and Filaggrin Gene Mutations in Adult Atopic Dermatitis. JAMA Dermatol 2018; 154: 293-300

Collin M and Bigley V. Human dendritic cell subsets: an update. Immunology 2018; 154: 3-20

Collin M, Bigley V, Haniffa M and Hambleton S. Human dendritic cell deficiency: the missing ID? Nat Rev Immunol 2011; 11: 575-583

Cui K, Ardell CL, Podolnikova NP and Yakubenko VP. Distinct Migratory Properties of M1, M2, and Resident Macrophages Are Regulated by alphaDbeta2 and alphaMbeta2 Integrin-Mediated Adhesion. Front Immunol 2018; 9: 2650

Czarnowicki T, He H, Canter T, Han J, Lefferdink R, Erickson T, Rangel S, Kameyama N, Kim HJ, Pavel AB, Estrada Y, Krueger JG, Paller AS and Guttman-Yassky E. Evolution of pathologic T-cell subsets in patients with atopic dermatitis from infancy to adulthood. J Allergy Clin Immunol 2020; 145: 215-228

Czarnowicki T, He H, Krueger JG and Guttman-Yassky E. Atopic dermatitis endotypes and implications for targeted therapeutics. J Allergy Clin Immunol 2019; 143: 1-11

Czarnowicki T, Kim HJ, Villani AP, Glickman J, Duca ED, Han J, Pavel AB, Lee BH, Rahman AH, Merad M, Krueger JG and Guttman-Yassky E. High-dimensional analysis defines multicytokine T-cell subsets and supports a role for IL-21 in atopic dermatitis. Allergy 2021; 76: 3080-3093

de Jong A and Ogg G. CD1a function in human skin disease. Mol Immunol 2021; 130: 14-19

de Lusignan S, Alexander H, Broderick C, Dennis J, McGovern A, Feeney C and Flohr C. Atopic dermatitis and risk of autoimmune conditions: population-based cohort study. J Allergy Clin Immunol 2022

Deckers J, Hammad H and Hoste E. Langerhans Cells: Sensing the Environment in Health and Disease. Front Immunol 2018; 9: 93

Di Domenico EG, Cavallo I, Capitanio B, Ascenzioni F, Pimpinelli F, Morrone A and Ensoli F. Staphylococcus aureus and the Cutaneous Microbiota Biofilms in the Pathogenesis of Atopic Dermatitis. Microorganisms 2019; 7

Doebel T, Voisin B and Nagao K. Langerhans Cells - The Macrophage in Dendritic Cell Clothing. Trends Immunol 2017; 38: 817-828

Feuillie C, Vitry P, McAleer MA, Kezic S, Irvine AD, Geoghegan JA and Dufrene YF. Adhesion of Staphylococcus aureus to Corneocytes from Atopic Dermatitis Patients Is Controlled by Natural Moisturizing Factor Levels. mBio 2018; 9

Fleury OM, McAleer MA, Feuillie C, Formosa-Dague C, Sansevere E, Bennett DE, Towell AM, McLean WHI, Kezic S, Robinson DA, Fallon PG, Foster TJ, Dufrene YF, Irvine AD and Geoghegan JA. Clumping Factor B Promotes Adherence of Staphylococcus aureus to Corneocytes in Atopic Dermatitis. Infect Immun 2017; 85

Flores GE, Seité S, Zelenkova H, Aguilar L, Henley JB, Martin R and Fierer N. Microbiome of Affected and Unaffected Skin of Patients With Atopic Dermatitis Before and After Emollient Treatment. Journal of Drugs in Dermatology 2014; 13: 611-618

Folster-Holst R. The role of the skin microbiome in atopic dermatitis - correlations and consequences. J Dtsch Dermatol Ges 2022

Fyhrquist N, Muirhead G, Prast-Nielsen S, Jeanmougin M, Olah P, Skoog T, Jules-Clement G, Feld M, Barrientos-Somarribas M, Sinkko H, van den Bogaard EH, Zeeuwen P, Rikken G, Schalkwijk J, Niehues H, Daubener W, Eller SK, Alexander H, Pennino D, Suomela S, Tessas I, Lybeck E, Baran AM, Darban H, Gangwar RS, Gerstel U, Jahn K, Karisola P, Yan L, Hansmann B, Katayama S, Meller S, Bylesjo M, Hupe P, Levi-Schaffer F, Greco D, Ranki A, Schroder JM, Barker J, Kere J, Tsoka S, Lauerma A, Soumelis V,

Nestle FO, Homey B, Andersson B and Alenius H. Microbe-host interplay in atopic dermatitis and psoriasis. Nat Commun 2019; 10: 4703

Geoghegan JA, Irvine AD and Foster TJ. Staphylococcus aureus and Atopic Dermatitis: A Complex and Evolving Relationship. Trends Microbiol 2018; 26: 484-497

Gonzalez T, Stevens ML, Baatyrbek Kyzy A, Alarcon R, He H, Kroner JW, Spagna D, Grashel B, Sidler E, Martin LJ, Biagini Myers JM, Khurana Hershey GK and Herr AB. Biofilm propensity of Staphylococcus aureus skin isolates is associated with increased atopic dermatitis severity and barrier dysfunction in the MPAACH pediatric cohort. Allergy 2021; 76: 302-313

Gough P, Khalid MB, Hartono S and Myles IA. Microbial manipulation in atopic dermatitis. Clin Transl Med 2022; 12: e828

Hendriks A, van Dalen R, Ali S, Gerlach D, van der Marel GA, Fuchsberger FF, Aerts PC, de Haas CJC, Peschel A, Rademacher C, van Strijp JAG, Codee JDC and van Sorge NM. Impact of Glycan Linkage to Staphylococcus aureus Wall Teichoic Acid on Langerin Recognition and Langerhans Cell Activation. ACS Infect Dis 2021; 7: 624-635

Herrmann N, Koch S, Leib N, Bedorf J, Wilms H, Schnautz S, Fimmers R and Bieber T. TLR2 down-regulates FcepsilonRI and its transcription factor PU.1 in human Langerhans cells. Allergy 2013; 68: 621-628

Hoeffel G, Wang Y, Greter M, See P, Teo P, Malleret B, Leboeuf M, Low D, Oller G, Almeida F, Choy SH, Grisotto M, Renia L, Conway SJ, Stanley ER, Chan JK, Ng LG, Samokhvalov IM, Merad M and Ginhoux F. Adult Langerhans cells derive predominantly from embryonic fetal liver monocytes with a minor contribution of yolk sac-derived macrophages. J Exp Med 2012; 209: 1167-1181

Hülpüsch C, Weins AB, Traidl-Hoffmann C and Reiger M. A new era of atopic eczema research: Advances and highlights. Allergy 2021; 76: 3408-3421

Hwang J, Jaros J and Shi VY. Staphylococcus aureus in Atopic Dermatitis: Past, Present, and Future. Dermatitis 2020; 31: 247-258

Iijima N, Thompson JM and Iwasaki A. Dendritic cells and macrophages in the genitourinary tract. Mucosal Immunol 2008; 1: 451-459

Iwamoto K, Moriwaki M, Niitsu Y, Saino M, Takahagi S, Hisatsune J, Sugai M and Hide M. Staphylococcus aureus from atopic dermatitis skin alters cytokine production triggered by monocyte-derived Langerhans cell. J Dermatol Sci 2017; 88: 271-279

Iwamoto K, Numm TJ, Koch S, Herrmann N, Leib N and Bieber T. Langerhans and inflammatory dendritic epidermal cells in atopic dermatitis are tolerized toward TLR2 activation. Allergy 2018; 73: 2205-2213

Iwase T, Uehara Y, Shinji H, Tajima A, Seo H, Takada K, Agata T and Mizunoe Y. Staphylococcus epidermidis Esp inhibits Staphylococcus aureus biofilm formation and nasal colonization. Nature 2010; 465: 346-349

Janek D, Zipperer A, Kulik A, Krismer B and Peschel A. High Frequency and Diversity of Antimicrobial Activities Produced by Nasal Staphylococcus Strains against Bacterial Competitors. PLoS Pathog 2016; 12: e1005812

Joubert IA, Otto M, Strunk T and Currie AJ. Look Who's Talking: Host and Pathogen Drivers of Staphylococcus epidermidis Virulence in Neonatal Sepsis. Int J Mol Sci 2022; 23

Kanitakis J, Petruzzo P and Dubernard JM. Turnover of Epidermal Langerhans' Cells. N Engl J Med 2004; 351: 2661-2662

Kaplan DH. In vivo function of Langerhans cells and dermal dendritic cells. Trends Immunol 2010a; 31: 446-451

Kaplan DH. Langerhans cells: not your average dendritic cell. Trends Immunol 2010b; 31: 437

Kaplan DH. Ontogeny and function of murine epidermal Langerhans cells. Nat Immunol 2017; 18: 1068-1075

Kaplan DH, Jenison MC, Saeland S, Shlomchik WD and Shlomchik MJ. Epidermal langerhans cell-deficient mice develop enhanced contact hypersensitivity. Immunity 2005; 23: 611-620

Kaplan DH, Kissenpfennig A and Clausen BE. Insights into Langerhans cell function from Langerhans cell ablation models. Eur J Immunol 2008; 38: 2369-2376

Kashem SW, Haniffa M and Kaplan DH. Antigen-Presenting Cells in the Skin. Annu Rev Immunol 2017; 35: 469-499

Kim BS, Howell MD, Sun K, Papp K, Nasir A, Kuligowski ME and Investigators IS. Treatment of atopic dermatitis with ruxolitinib cream (JAK1/JAK2 inhibitor) or triamcinolone cream. J Allergy Clin Immunol 2020; 145: 572-582

Kim MJ, Im MA, Lee JS, Mun JY, Kim DH, Gu A and Kim IS. Effect of S100A8 and S100A9 on expressions of cytokine and skin barrier protein in human keratinocytes. Mol Med Rep 2019; 20: 2476-2483

Klaeschen AS, Numm TJ, Herrmann N, Leib N, Maintz L, Sakai T, Wenzel J and Bieber T. JAK1/2 inhibition impairs the development and function of inflammatory dendritic epidermal cells in atopic dermatitis. J Allergy Clin Immunol 2020

Klufa J, Bauer T, Hanson B, Herbold C, Starkl P, Lichtenberger B, Srutkova D, Schulz D, Vujic I, Mohr T, Rappersberger K, Bodenmiller B, Kozakova H, Knapp S, Loy A and Sibilia M. Hair eruption initiates and commensal skin microbiota aggravate adverse events of anti-EGFR therapy. Sci Transl Med 2019; 11

Koch S, Kohl K, Klein E, von Bubnoff D and Bieber T. Skin homing of Langerhans cell precursors: adhesion, chemotaxis, and migration. J Allergy Clin Immunol 2006; 117: 163-168

Koch S, Stroisch TJ, Vorac J, Herrmann N, Leib N, Schnautz S, Kirins H, Forster I, Weighardt H and Bieber T. AhR mediates an anti-inflammatory feedback mechanism in human Langerhans cells involving FcepsilonRI and IDO. Allergy 2017; 72: 1686-1693

Koh LF, Ong RY and Common JE. Skin microbiome of atopic dermatitis. Allergol Int 2022; 71: 31-39

Kohl K, Klein E, Koch S, Schnautz S and Bieber T. Migration and differentiation of Langerhans cell precursors. Eur J Cell Biol 2004; 83: 805-811

Kohl K, Schnautz S, Pesch M, Klein E, Aumailley M, Bieber T and Koch S. Subpopulations of human dendritic cells display a distinct phenotype and bind differentially to proteins of the extracellular matrix. Eur J Cell Biol 2007; 86: 719-730

Kong HH, Oh J, Deming C, Conlan S, Grice EA, Beatson MA, Nomicos E, Polley EC, Komarow HD, Program NCS, Murray PR, Turner ML and Segre JA. Temporal shifts in the skin microbiome associated with disease flares and treatment in children with atopic dermatitis. Genome Res 2012; 22: 850-859

Kraft S and Novak N. Fc receptors as determinants of allergic reactions. Trends Immunol 2006; 27: 88-95

Kraft S, Wessendorf JH, Haberstok J, Novak N, Wollenberg A and Bieber T. Enhanced expression and activity of protein-tyrosine kinases establishes a functional signaling pathway only in FcepsilonRIhigh Langerhans cells from atopic individuals. J Invest Dermatol 2002; 119: 804-811

Krupka-Olek M, Bozek A and Kawczyk-Krupka A. The Immunological and Allergen Profiles of Patients with Atopic Dermatitis or Psoriasis. Medicina (Kaunas) 2022; 58

Krysko O, Teufelberger A, Van Nevel S, Krysko DV and Bachert C. Protease/antiprotease network in allergy: The role of Staphylococcus aureus protease-like proteins. Allergy 2019; 74: 2077-2086

Langerhans P. Ueber die Nerven der menschlichen Haut. Archiv f. pathol. Anat. 1868: 325-337

Leech JM, Dhariwala MO, Lowe MM, Chu K, Merana GR, Cornuot C, Weckel A, Ma JM, Leitner EG, Gonzalez JR, Vasquez KS, Diep BA and Scharschmidt TC. Toxin-Triggered Interleukin-1 Receptor Signaling Enables Early-Life Discrimination of Pathogenic versus Commensal Skin Bacteria. Cell Host Microbe 2019; 26: 795-809 e795

Leib N, Herrmann N, Koch S, Stroisch TJ, Schnautz S, Wilms H and Bieber T. MicroRNA-155 mediates downregulation of the high-affinity receptor for IgE through Toll-like receptor signaling. J Allergy Clin Immunol 2018; 141: 425-429 e426

Leyden J, Marples R and Kligman A. Staphylococcus aureus in the lesions of atopic dermatitis. Br J Dermatol 1974; 90: 525–530

Linehan JL, Harrison OJ, Han SJ, Byrd AL, Vujkovic-Cvijin I, Villarino AV, Sen SK, Shaik J, Smelkinson M, Tamoutounour S, Collins N, Bouladoux N, Dzutsev A, Rosshart SP, Arbuckle JH, Wang CR, Kristie TM, Rehermann B, Trinchieri G, Brenchley JM, O'Shea JJ and Belkaid Y. Non-classical Immunity Controls Microbiota Impact on Skin Immunity and Tissue Repair. Cell 2018; 172: 784-796 e718

Liu X, Zhu R, Luo Y, Wang S, Zhao Y, Qiu Z, Zhang Y, Liu X, Yao X, Li X and Li W. Distinct human Langerhans cell subsets orchestrate reciprocal functions and require different developmental regulation. Immunity 2021

Luger T, Romero WA, Gruben D, Smith TW, Cha A and Neary MP. Clinical and Humanistic Burden of Atopic Dermatitis in Europe: Analyses of the National Health and Wellness Survey. Dermatol Ther (Heidelb) 2022; 12: 949-969

Lundberg K, Albrekt AS, Nelissen I, Santegoets S, de Gruijl TD, Gibbs S and Lindstedt M. Transcriptional profiling of human dendritic cell populations and models--unique profiles of in vitro dendritic cells and implications on functionality and applicability. PLoS One 2013; 8: e52875

Lutz MB, Strobl H, Schuler G and Romani N. GM-CSF Monocyte-Derived Cells and Langerhans Cells As Part of the Dendritic Cell Family. Front Immunol 2017; 8: 1388

Magnifico I, Petronio Petronio G, Venditti N, Cutuli MA, Pietrangelo L, Vergalito F, Mangano K, Zella D and Di Marco R. Atopic Dermatitis as a Multifactorial Skin Disorder. Can the Analysis of Pathophysiological Targets Represent the Winning Therapeutic Strategy? Pharmaceuticals (Basel) 2020; 13

Meylan P, Lang C, Mermoud S, Johannsen A, Norrenberg S, Hohl D, Vial Y, Prod'hom G, Greub G, Kypriotou M and Christen-Zaech S. Skin Colonization by Staphylococcus aureus Precedes the Clinical Diagnosis of Atopic Dermatitis in Infancy. J Invest Dermatol 2017; 137: 2497-2504

Mnich ME, van Dalen R and van Sorge NM. C-Type Lectin Receptors in Host Defense Against Bacterial Pathogens. Front Cell Infect Microbiol 2020; 10: 309

Mohr N, Augustin M, Zeervi L, Bieber T, Werfel T, Wollenberg A and Langenbruch A. Determinants of costs and benefits in atopic dermatitis routine care in Germany. J Eur Acad Dermatol Venereol 2022

Moriwaki M, Iwamoto K, Niitsu Y, Matsushima A, Yanase Y, Hisatsune J, Sugai M and Hide M. Staphylococcus aureus from atopic dermatitis skin accumulates in the lysosomes of keratinocytes with induction of IL-1alpha secretion via TLR9. Allergy 2019; 74: 560-571

Naik S. One Size Does Not Fit All: Diversifying Immune Function in the Skin. J Immunol 2022; 208: 227-234

Naik S, Bouladoux N, Linehan JL, Han SJ, Harrison OJ, Wilhelm C, Conlan S, Himmelfarb S, Byrd AL, Deming C, Quinones M, Brenchley JM, Kong HH, Tussiwand R, Murphy KM, Merad M, Segre JA and Belkaid Y. Commensal-dendritic-cell interaction specifies a unique protective skin immune signature. Nature 2015; 520: 104-108

Nakatsuji T, Chen T, Narala S, Chun K, Two A, Yun T, Shafiq F, Kotol P, Bouslimani A, Melnik A, Latif H, Kim J, Lockhart A, Artis K, David G, Taylor P, Streib J, Dorrestein P, Grier A, Gill S, Zengler K, Hata T, Leung D and Gallo R. Antimicrobials from human skin commensal bacteria protect against Staphylococcus aureus and are deficient in atopic dermatitis. Sci. Transl. Med. 2017; 9, eaah4680

Nakatsuji T, Chen TH, Butcher AM, Trzoss LL, Nam SJ, Shirakawa KT, Zhou W, Oh J, Otto M, Fenical W and Gallo RL. A commensal strain of Staphylococcus epidermidis protects against skin neoplasia. Science Advances 2018; 4

Nakatsuji T, Chen TH, Two AM, Chun KA, Narala S, Geha RS, Hata TR and Gallo RL. Staphylococcus aureus Exploits Epidermal Barrier Defects in Atopic Dermatitis to Trigger Cytokine Expression. J Invest Dermatol 2016; 136: 2192-2200

Nakatsuji T and Gallo RL. The role of the skin microbiome in atopic dermatitis. Ann Allergy Asthma Immunol 2019; 122: 263-269

Nguyen TH, Park MD and Otto M. Host Response to Staphylococcus epidermidis Colonization and Infections. Front Cell Infect Microbiol 2017; 7: 90

Novak N and Bieber T. FcεRI- Toll- Like Receptor Interaction in Atopic Dermatitis. 2011

Novak N, Bieber T and Peng WM. The immunoglobulin E-Toll-like receptor network. Int Arch Allergy Immunol 2010; 151: 1-7

Novak N, Kraft S and Bieber T. IgE receptors. Current Opinion in Immunology. 2001; 13: 721–726

Novak N, Valenta R, Bohle B, Laffer S, Haberstok J, Kraft S and Bieber T. FcepsilonRI engagement of Langerhans cell-like dendritic cells and inflammatory dendritic epidermal cell-like dendritic cells induces chemotactic signals and different T-cell phenotypes in vitro. J Allergy Clin Immunol 2004; 113: 949-957

Ostman S, Rask C, Wold AE, Hultkrantz S and Telemo E. Impaired regulatory T cell function in germ-free mice. Eur J Immunol 2006; 36: 2336-2346

Otsuka M, Egawa G and Kabashima K. Uncovering the Mysteries of Langerhans Cells, Inflammatory Dendritic Epidermal Cells, and Monocyte-Derived Langerhans Cell-Like Cells in the Epidermis. Front Immunol 2018; 9: 1768

Paller AS, Kong HH, Seed P, Naik S, Scharschmidt TC, Gallo RL, Luger T and Irvine AD. The microbiome in patients with atopic dermatitis. J Allergy Clin Immunol 2019; 143: 26-35

Peng W, Benfadal S, Yu C, Wenzel J, Oldenburg J and Novak N. JAK1/2 inhibitor but not IL-4 receptor alpha antibody suppresses allergen-mediated activation of human basophils in vitro. Allergy 2022

Peng W, Kwiek B, Yu C, Garbi N, Allam JP, Oldenburg J and Novak N. Infiltration and Clustering of Major Histocompatibility Complex II(+) Antigen-Presenting Cells in the Skin of Patients with Atopic Dermatitis. J Invest Dermatol 2020

Renert-Yuval Y, Thyssen JP, Bissonnette R, Bieber T, Kabashima K, Hijnen D and Guttman-Yassky E. Biomarkers in atopic dermatitis - a review on behalf of the international eczema council. J Allergy Clin Immunol 2021

Ring J. A brave new world with emerging treatment options for atopic eczema. J Eur Acad Dermatol Venereol 2022; 36: 632

Romani N, Clausen BE and Stoitzner P. Langerhans cells and more: langerin-expressing dendritic cell subsets in the skin. Immunol Rev 2010; 234: 120-141

Scharschmidt TC. Establishing Tolerance to Commensal Skin Bacteria: Timing Is Everything. Dermatol Clin 2017; 35: 1-9

Schuler G and Steinman R. Murine epidermal Langerhans cells mature into potent immunostimulatory dendritic cells in vitro. J. Exp. Med. 1985; 161: 526-546

Schuster C, Vaculik C, Fiala C, Meindl S, Brandt O, Imhof M, Stingl G, Eppel W and Elbe-Burger A. HLA-DR+ leukocytes acquire CD1 antigens in embryonic and fetal human skin and contain functional antigen-presenting cells. J Exp Med 2009; 206: 169-181

Shi J, He L, Tao R, Zheng H, Li W, Huang S, Li Y and Shang S. TLR4 polymorphisms as potential predictors of atopic dermatitis in Chinese Han children. J Clin Lab Anal 2022: e24385

Shima K, Inoue T, Uehara Y, Iwamura M, Fukagawa S, Kuwano T, Tanida K, Takada N, Saito-Abe M, Yamamoto-Hanada K, Ohya Y and Murase T. Non-invasive transcriptomic analysis using mRNAs in skin surface lipids obtained from children with mild-to-moderate atopic dermatitis. J Eur Acad Dermatol Venereol 2022

Shimamori Y, Pramono AK, Kitao T, Suzuki T, Aizawa SI, Kubori T, Nagai H, Takeda S and Ando H. Isolation and Characterization of a Novel Phage SaGU1 that Infects Staphylococcus aureus Clinical Isolates from Patients with Atopic Dermatitis. Curr Microbiol 2021; 78: 1267-1276

Silverberg NB. Typical and atypical clinical appearance of atopic dermatitis. Clin Dermatol 2017; 35: 354-359

Simpson EL, Bissonnette R, Paller AS, King B, Silverberg JI, Reich K, Thyssen JP, Doll H, Sun L, DeLozier AM, Nunes FP and Eichenfield LF. The Validated Investigator Global Assessment for Atopic Dermatitis (vIGA-AD): A Clinical Outcome Measure for the Severity of Atopic Dermatitis. Br J Dermatol 2022

Simpson EL, Villarreal M, Jepson B, Rafaels N, David G, Hanifin J, Taylor P, Boguniewicz M, Yoshida T, De Benedetto A, Barnes KC, Leung DYM and Beck LA. Patients with Atopic Dermatitis Colonized with Staphylococcus aureus Have a Distinct Phenotype and Endotype. J Invest Dermatol 2018; 138: 2224-2233

Sirobhushanam S, Parsa N, Reed TJ, Berthier CC, Sarkar MK, Hile GA, Tsoi LC, Banfield J, Dobry C, Horswill AR, Gudjonsson JE and Kahlenberg JM. Staphylococcus aureus Colonization Is Increased on Lupus Skin Lesions and Is Promoted by IFN-Mediated Barrier Disruption. J Invest Dermatol 2020; 140: 1066-1074 e1064

Steinman RM and Cohn ZA. Identification of a novel cell type in peripheral lymphoid organs of mice. The journal of experimental medicine 1973; 137: 1142-1162

Stoitzner P, Holzmann S, McLellan AD, Ivarsson L, Stossel H, Kapp M, Kammerer U, Douillard P, Kampgen E, Koch F, Saeland S and Romani N. Visualization and characterization of migratory Langerhans cells in murine skin and lymph nodes by antibodies against Langerin/CD207. J Invest Dermatol 2003; 120: 266-274

Strobl H, Krump C and Borek I. Micro-environmental signals directing human epidermal Langerhans cell differentiation. Semin Cell Dev Biol 2019; 86: 36-43

Sun L. The Role of Toll-Like Receptors in Skin Host Defense, Psoriasis, and Atopic Dermatitis. 2019

Sun Z, Huang S, Zhu P, Yue F, Zhao H, Yang M, Niu Y, Jing G, Su X, Li H, Callewaert C, Knight R, Liu J, Smith E, Wei K and Xu J. A Microbiome-Based Index for Assessing Skin Health and Treatment Effects for Atopic Dermatitis in Children. mSystems 2019; 4

Thyssen JP, Vestergaard C, Deleuran M, de Bruin-Weller MS, Bieber T, Taieb A, Seneschal J, Cork MJ, Paul C, Flohr C, Weidinger S, Trzeciak M, Werfel T, Heratizadeh A, Barbarot S, Darsow U, Simon D, Torrelo A, Chernyshov PV, Stalder JF, Gelmetti C, Szalai Z, Svensson A, von Kobyletzki LB, De Raeve L, Folster-Holst R, Cristen-Zaech S, Hijnen D, Gieler U, Ring J and Wollenberg A. European Task Force on Atopic Dermatitis

(ETFAD): treatment targets and treatable traits in atopic dermatitis. J Eur Acad Dermatol Venereol 2020; 34: e839-e842

Tokura Y and Hayano S. Subtypes of atopic dermatitis: From phenotype to endotype. Allergol Int 2022; 71: 14-24

Traisaeng S, Herr DR, Kao HJ, Chuang TH and Huang CM. A Derivative of Butyric Acid, the Fermentation Metabolite of Staphylococcus epidermidis, Inhibits the Growth of a Staphylococcus aureus Strain Isolated from Atopic Dermatitis Patients. Toxins (Basel) 2019; 11

Tsakok T, Woolf R, Smith CH, Weidinger S and Flohr C. Atopic dermatitis: the skin barrier and beyond. Br J Dermatol 2019; 180: 464-474

Uebele J, Habenicht K, Ticha O and Bekeredjian-Ding I. Staphylococcus aureus Protein A Induces Human Regulatory T Cells Through Interaction With Antigen-Presenting Cells. Front Immunol 2020; 11: 581713

Valladeau J, Ravel O, Dezutter-Dambuyant C, Moore K, Kleijmeer M, Liu Y, Duvert-Frances V, Vincent C, Schmitt D, Davoust J, Caux C, Lebecque S and S. S. Langerin, a Novel C-Type Lectin Specific to Langerhans Cells, Is an Endocytic Receptor that Induces the Formation of Birbeck Granules. Immunity. 2000; 12: 71–81

Vandecandelaere I, Depuydt P, Nelis HJ and Coenye T. Protease production by Staphylococcus epidermidis and its effect on Staphylococcus aureus biofilms. Pathog Dis 2014; 70: 321-331

Verollet C, Charriere GM, Labrousse A, Cougoule C, Le Cabec V and Maridonneau-Parini I. Extracellular proteolysis in macrophage migration: losing grip for a breakthrough. Eur J Immunol 2011; 41: 2805-2813

von Bubnoff D, Bausinger H, Matz H, Koch S, Hacker G, Takikawa O, Bieber T, Hanau D and de la Salle H. Human epidermal langerhans cells express the immunoregulatory enzyme indoleamine 2,3-dioxygenase. J Invest Dermatol 2004; 123: 298-304

von Bubnoff D and Bieber T. The indoleamine 2,3-dioxygenase (IDO) pathway controls allergy. Allergy 2012; 67: 718-725

Von Bubnoff D, Scheler M, Wilms H, Fimmers R and Bieber T. Identification of IDO-positive and IDO-negative human dendritic cells after activation by various proinflammatory stimuli. J Immunol 2011; 186: 6701-6709

Weil C, Sugerman PB, Chodick G, Liang H, Wang H, Calimlim BM, Dorfman A, Shalev V, Ben Amitai D and Leshem YA. Epidemiology and Economic Burden of Atopic Dermatitis: Real-World Retrospective Data from a Large Nationwide Israeli Healthcare Provider Database. Adv Ther 2022

Williams MR, Costa SK, Zaramela LS, Khalil S, Todd DA, Winter HL, Sanford JA, O'Neill AM, Liggins MC, Nakatsuji T, Cech NB, Cheung AL, Zengler K, Horswill AR and Gallo RL. Quorum sensing between bacterial species on the skin protects against epidermal injury in atopic dermatitis. Sci. Transl. Med. 2019; 11(490): 1-12

Wollenberg A, Barbarot S, Bieber T, Christen-Zaech S, Deleuran M, Fink-Wagner A, Gieler U, Girolomoni G, Lau S, Muraro A, Czarnecka-Operacz M, Schäfer T, Schmid-Grendelmeier P, Simon D, Szalai Z, Szepietowski JC, Taieb A, Torrelo A, Werfel T and Ring J. Consensus-based European guidelines for treatment of atopic eczema (atopic dermatitis) in adults and children: part I. JEADV 2018a; 32: 657–682

Wollenberg A, Barbarot S, Bieber T, Christen-Zaech S, Deleuran M, Fink-Wagner A, Gieler U, Girolomoni G, Lau S, Muraro A, Czarnecka-Operacz M, Schäfer T, Schmid-Grendelmeier P, Simon D, Szalai Z, Szepietowski JC, Taieb A, Torrelo A, Werfel T and Ring J. Consensus ‐ based European guidelines for treatment of atopic eczema (atopic dermatitis) in adults and children: part II. JEADV 2018b; 32: 850–878

Wollenberg A, Kinberger M, Arents B, Aszodi N, Avila Valle G, Barbarot S, Bieber T, Brough HA, Calzavara Pinton P, Christen-Zach S, Deleuran M, Dittmann M, Dressler C, Fink-Wagner AH, Fosse N, Gaspar K, Gerbens L, Gieler U, Girolomoni G, Gregoriou S, Mortz CG, Nast A, Nygaard U, Redding M, Rehbinder EM, Ring J, Rossi M, Serra-Baldrich E, Simon D, Szalai ZZ, Szepietowski JC, Torrelo A, Werfel T and Flohr C. European guideline (EuroGuiDerm) on atopic eczema - part II: non-systemic treatments and treatment recommendations for special AE patient populations. J Eur Acad Dermatol Venereol 2022; 36: 1904-1926

Wollenberg A, Kraft S, Hanau D and Bieber T. Immunomorphological and ultrastructural characterization of Langerhans cells and a novel, inflammatory dendritic epidermal cell (IDEC) population in lesional skin of atopic eczema. J Invest Dermatol 1996; 106: 446-453

Wu X, Briseno CG, Durai V, Albring JC, Haldar M, Bagadia P, Kim KW, Randolph GJ, Murphy TL and Murphy KM. Mafb lineage tracing to distinguish macrophages from other immune lineages reveals dual identity of Langerhans cells. J Exp Med 2016; 213: 2553-2565

Yasmin N, Bauer T, Modak M, Wagner K, Schuster C, Koffel R, Seyerl M, Stockl J, Elbe-Burger A, Graf D and Strobl H. Identification of bone morphogenetic protein 7 (BMP7) as an instructive factor for human epidermal Langerhans cell differentiation. J Exp Med 2013; 210: 2597-2610

Ye C, Gu H, Li M, Chen R, Xiao X and Zou Y. Air Pollution and Weather Conditions Are Associated with Daily Outpatient Visits of Atopic Dermatitis in Shanghai, China. Dermatology 2022: 1-11

Yoshida K, Kubo A, Fujita H, Yokouchi M, Ishii K, Kawasaki H, Nomura T, Shimizu H, Kouyama K, Ebihara T, Nagao K and Amagai M. Distinct behavior of human Langerhans cells and inflammatory dendritic epidermal cells at tight junctions in patients with atopic dermatitis. J Allergy Clin Immunol 2014; 134: 856-864

Yoshida T, Beck LA and De Benedetto A. Skin barrier defects in atopic dermatitis: From old idea to new opportunity. Allergol Int 2022; 71: 3-13

Zhang B, Roesner LM, Traidl S, Koeken V, Xu CJ, Werfel T and Li Y. Single-cell profiles reveal distinctive immune response in atopic dermatitis in contrast to psoriasis. Allergy 2022a

Zhang DJ, Hao F, Qian T and Cheng HX. Expression of Helper and Regulatory T Cells in Atopic Dermatitis: A Meta-Analysis. Front Pediatr 2022b; 10: 777992

Ziehfreund S, Tizek L, Hangel N, Fritzsche MC, Weidinger S, Smith C, Bryce PJ, Greco D, van den Bogaard EH, Flohr C, Rastrick J, Eyerich S, Buyx A, Conrad C, Eyerich K and Zink A. Requirements and expectations of high-quality biomarkers for atopic dermatitis and psoriasis in 2021 - a two-round Delphi survey among international experts. J Eur Acad Dermatol Venereol 2022

9. Acknowledgements

I would like to express my gratitude to my supervisor Professor Thomas Bieber, for choosing me to join his research group. He entrusted me with this project and gave me space and encouragement to develop and test my ideas and motivated me to challenge myself every step of the way.

I would like to cordially thank my co-supervisor Professor Peter Wolf, for accepting me as his PhD exchange student. He kindly supported my project with research samples, research fundings and great scientific discussions. He motived me to be an independent researcher and encouraged me to always try new techniques.

I would like to say thank you to all the members of the Department of Dermatology both in Bonn and Graz. Thank our technician Sylvia Schnautz and postdoc Dr. Nicole Leib to teach me all the techniques when I started PhD in Bonn. Thank lab manager Dr. Jörg Weßendorf for his trust and organization. Special thanks to our senior data scientist Dr. Natalie Bordag for helping out with data analysis. I want to thank all our postdocs Dr. Andrea Teufelberger, Dr. Nicole Golob-Schwarzl, Dr. Theresa Benezeder, Dr. Patra Vijaykumar for their thoughtful and scientific discussions. Thank our PhD students Aaroh Joshi and Saptaswa Dey, our lab manager Isabella Perchthaler for all the support and enjoyable and friendly environment in the lab.

I would also like to thank all the members from Professor Herbert Strobl´s lab. Thank Christina Passegger and Elke Schwarzenberger for providing me stem cells for research. Thank Dr. Izabela Borek for her inspiring words and friendship.

Last but not least, I want to thank my family for endless support and love, I can never get this far without you. Special thanks to Dr. Mathias Hochgerner for encouraging me to be a brave, strong and independent woman in science.